The Black Dog Prospect, Québec, Canada: a Rare Example of Archean Tourmaline Breccia-Hosted Au-Cu Mineralization

By

Philippe Drouin

Department of Earth and Planetary Sciences

McGill University, Montreal, Qc, Canada

December 2019

A thesis submitted to the Faculty of Graduate Studies and Research in fulfillments of the requirements for the degree of Masters of Science

Abstract

The Black Dog Au-Cu prospect occurs in a two km-long tourmaline alteration zone in a mafic volcanic sequence of the Urban-Barry greenstone belt, Abitibi region, Québec. This zone is two to three meters thick for most of its length but reaches over 30 meters in thickness at Black Dog, where tourmaline is present both as an alteration phase and as the cement of a magmatic-hydrothermal breccia. The tourmaline breccia has roughly equivalent proportions of tourmaline matrix and quartz and tourmaline-altered clasts. The Au-Cu mineralization occurs in a sulfide breccia that cuts the tourmaline breccia. In decreasing order of abundance, the main sulfide minerals are pyrite, chalcopyrite, sphalerite, cobaltite, arsenopyrite and pyrrhotite. Gold occurs mainly as electrum and is associated with hessite, matildite, native silver and Bi-telluride minerals. This mineralization is generally intergrown with chalcopyrite and occurs in contact with pyrite and arsenopyrite grains in the sulfide veins.

The gold mineralization is hosted by weakly foliated, basaltic rocks that have been altered mainly to tourmaline, quartz and sericite. The early tourmaline (Type A tourmaline) is dominantly dravite, whereas in the subsequent stages (Types B and C), schorl is predominant. Late stage tourmaline (type C) has elevated concentrations of ore-related elements, including Co, Zn, Cu, Ag and Bi. Principal component analyses applied to bulk rock compositions demonstrate that concentrations of these metals correlate strongly with that of gold.

Many features of the Black Dog prospect are unusual for the Abitibi greenstone belt, where the vast majority of the ore deposits belong to the orogenic gold and volcanogenic massive sulfide classes. In contrast to Black Dog, the orogenic deposits are characterized by limited abundances

of sulfide minerals, magmatic-hydrothermal breccias are absent, and the ores are usually associated with quartz/carbonate (and more rarely tourmaline) veins.

Temperatures estimated from sulfur isotope compositions of pyrite, chalcopyrite and sphalerite range between 400 and 600°C (± ~50°C) and average 496°C for six sample pairs (±26°). This relatively high temperature of formation and the narrow range of sulfur isotope compositions ($\delta_{34}S$ from +1.7 to +3.6 ‰ on sulfide minerals, corresponding to +1.4 to +2.4‰ H_2S) suggest that the fluids, which produced the mineralization, were dominantly magmatic. Typical orogenic Au deposits generally are depleted in Cu and have a wider range of sulfur isotope values, possibly reflecting multiple sources of sulfur. They also display lower mineralization temperatures.

The timing relationships indicate that tourmaline alteration and mineralization took place after the main deformation event had started. Tourmaline veins cutting foliation, foliated clasts in the breccia, and the sub-vertical orientation of the breccia pipe, which also cuts the regional foliation, are strong evidence for the crystallization of tourmaline during the late stages of regional deformation.

It is proposed that magmatic fluids emanating from a calc-alkaline intrusion at depth were responsible for the alteration and mineralization observed at Black Dog. This depositional model is analogous to that postulated for the Au-Cu-bearing tourmaline breccias associated with porphyry copper deposits in Phanerozoic rocks.

Sommaire

L'indice aurifère et cuprifère Black Dog est situé sur une zone d'altération à tourmaline longue de deux kilomètres dans une séquence volcanique de la ceinture de roches vertes d'Urban-Barry, Abitibi, Québec. Cette zone mesure de deux à trois mètres d'épaisseur sur la majorité de sa longueur mais atteint plus de 30 mètres d'épaisseur à Black Dog où la tourmaline est présente à la fois en tant que minéral d'altération et ciment d'une brèche à tourmaline magmatique-hydrothermal. Cette brèche à tourmaline comporte des proportions environ équivalentes de matrice de tourmaline et de clastes altérés à tourmaline et quartz. La minéralisation aurifère et cuprifère se présente dans une brèche à sulfures qui recoupe la brèche à tourmaline. En ordre décroissant d'abondance, les sulfures principaux sont la pyrite, la chalcopyrite, la sphalérite, la cobaltite, l'arsénopyrite et la pyrrhotite. L'or est présent principalement sous la forme d'électrum et est associé avec de la hessite, de la matildite, de l'argent natif et des des tellurures de bismuth. Cette minéralisation est généralement présente en intercroissance à l'intérieur des grains de chalcopyrite et aux contacts avec la pyrite ou d'arsénopyrite.

La minéralisation aurifère est contenue dans des roches basaltiques faiblement foliées altérées principalement à tourmaline, quartz et séricite. La tourmaline précoce (de Type A) est principalement dravitique alors que les épisodes subséquents (de Types B et C) appartiennent à la famille du schorl. La tourmaline tardive (de Type C) contient des proportions élevées d'éléments reliés au minerai et incluent le cobalt, le zinc, le cuivre, l'argent et le bismuth. Une analyse en composante principale a démontré que la concentration de ces éléments sont fortement corrélés avec l'or.

Plusieurs caractéristiques de Black Dog sont inusuelles pour la ceinture de roches vertes de l'Abitbi, où la vaste majorité des gisements appartiennent aux catégories de l'or orogénique et des sulfures massifs volcanogènes. Contrairement à Black Dog, les gisements de type orogénique sont caractérisés par une abondance limitée de sulfures, ne présentent pas de brèches hydrothermales et le minerai est habituellement relié à des veinules de quartz et carbonate et plus rarement de tourmaline.

Les températures de dépositions estimées d'après la composition isotopique de la pyrite, la chalcopyrite et la sphalérite à Black Dog ont donné une fenêtre allant de 400 à 600 ºC (± ~50°C) et une moyenne de 496 ºC pour six paires d'échantillons (±26°). Ces températures de formation relativement élevées et l'intervalle étroit des compositions isotopiques ($\delta_{34}S$ de +1.7 à +3.6 ‰ sur les sulfures, correspondant à +1.4 à +2.4‰ H_2S) suggèrent que les fluides ayant mené à la minéralisation était majoritairement magmatiques. Les gisements orogéniques typiques sont généralement pauvres en cuivre et présente un plus large intervalle de compositions isotopiques, possiblement dû à de multiples sources de soufre. Ils présentent également des températures de formation plus basses.

Les relations temporelles à Black Dog indiquent que l'altération à tourmaline et la minéralisation ont été mises en place après le début de l'épisode de déformation principal. Les veines de tourmaline qui recoupent la foliation, les clastes foliés dans la brèche et l'orientation sub-verticale de la cheminée de brèche qui recoupe également la foliation régionale sont des preuves tangibles d'une origine tardi-tectonique de la tourmaline.

Il est suggéré que des fluides magmatiques émanant d'une intrusion calc-alcaline en profondeur furent responsables pour l'altération et la minéralisation observée à Black Dog. Ce modèle de

déposition est analogue à ceux présentés pour les brèches à tourmaline aurifères et cuprifères associées aux porphyres de cuivre communs dans les roches phanérozoïques.

Contribution of Authors

This thesis is divided in three chapters. Chapter 1 is an introduction to the geological context of the area and to the subject of this research, Chapter 2 is a stand-alone manuscript for publication and will be submitted to a peer-reviewed journal and Chapter 3 presents the conclusions drawn from this study. Philippe Drouin is the first author on this paper and shares authorship with Anthony E. Williams-Jones and James R. Clark. Field work and sampling was performed by Philippe Drouin and Anthony E. Williams-Jones. Sample preparation, petrography, geochemical analyses, EMP and LA-ICP-MS were carried out by Philippe Drouin with guidance from Anthony E. Williams-Jones and James R. Clark. This thesis was written by Philippe Drouin based on recommendations and corrections provided by Anthony E. Williams-Jones and James R. Clark.

Acknowledgments

In order of appearance, I would first like to thank Jean-Philippe Desrochers who suggested that Black Dog could be the subject of a Masters project in 2016 and has since helped me significantly in my career and personal development. I would also like to thank the "Fond de Recherche du Québec – Nature et Technologies" whose financial support was essential for this project.

I am greatly thankful to my supervisor Anthony E. Williams-Jones whose impressive knowledge, open-mindedness, patience and benevolence inspired me to produce interesting and relevant research and keep fighting through the difficulties of graduate studies. James R. Clark also played a major role in the realization of this project in providing insightful conversations, advice, edits and corrections.

I would also like to thank Osisko Mining who provided funding for the field work, chemical analyses, EMP and LA-ICP-MS analyses and isotope analyses. Louis Grenier and Isabelle Roy were very responsive and helpful in coordinating visits, expenses and information transmission.

The McGill University Electron Microprobe Laboratory and Laser Ablation laboratories and the Queen's Facility for Isotope Research (QFIR) provided very generous access to their staff and reliable data.

Duncan McLeish, Emily Laycock, Édouard C. Lavoie, Vincent Van Hinsberg, Rebecca Paisley, Roman Hanes, Pierre-Hughes Lamirande, Antoine Ouellet and many others were a great help on a wide variety of academic and technical topics, including the local geology of the Lac aux Loutres area, porphyry copper deposits, LA-ICP-MS data handling and metamorphism.

Table of Contents

Table of Figures

List of Tables

List of Appendixes

Chapter I: Introduction

1.1 Introduction

Ore-bearing tourmaline breccias are common close to the copper porphyries of the Andes, the North American Cordillera and other convergent margin environments (Sillitoe et al., 1971; Sillitoe, 1985; Warnaars et al., 1985; Williams et al., 1999; Skewes et al., 2003; Mlynarczyk, 2005; Sillitoe, 2010; Garrido et al., 2010 and Ochoa-Landin et al., 2016). These breccias are generally pipe-shaped and are characterized by a tourmaline-dominated matrix that hosts silicified and angular clasts of variable sizes. The ore in tourmaline breccias in those environments is contained in sulfide breccias that cut through the tourmaline breccia and are generally concentrated at its margins (Corbett et al., 1997). Common minerals include pyrite, chalcopyrite, sphalerite and traces of other sulfide minerals and gold is present as electrum and is in close association with the sulfides. While such occurrences are common in the vicinity of Phanerozoic copper porphyries, they have not been reported in greenstone belts where orogenic gold and volcanogenic massive sulfides are the predominant types of deposits.

1.2 The Abitibi Greenstone Belt Environment

The Archean Abitibi Greenstone Belt is located in Eastern Canada and is one of the best preserved greenstone belts in the world. It is host to many world-class orogenic and VMS deposits with a total endowment of more than 200 Moz of gold and around 775 Mt of Cu, Zn and Pb (Monecke et al., 2017). The VMS deposits were emplaced in a submarine volcanic environment between 2795 and 2695 Ma. Following this volcanism, large volumes of sedimentary rocks comprising the Porcupine assemblage were deposited between 2690 and 2685 Ma (Thurston et al., 2008). These rocks and the earlier volcanic succession were deformed prior to 2679. This was succeeded by deposition of Timiskaming sedimentary rocks in extensional basins between 2679 and 2669 Ma, locally accompanied by alkaline volcanism. Crustal shortening after 2669 Ma generated the Porcupine-Destor and Larder Lake-Cadillac fault zones

which, together with adjacent second and third order faults, controlled the emplacement of a large number of orogenic gold deposits in the southern volcanic zone (Monecke et al., 2017). In addition to the orogenic gold deposits, there are also deposits like the Canadian Malartic and Windfall deposits that are interpreted to be intrusion-related (Helt et al., 2014; Hardie et al., 2018). This relatively new deposit type for the Abitibi has led to intense exploration for further deposits of this type.

Tourmaline Hill, which hosts the Black Dog prospect, is a narrow topographical high in an area of otherwise low relief near the Windfall Lake intrusion-related gold deposit (Hardie et al., 2018); Windfall lies 14 km northeast of Black Dog, and is currently undergoing exploration, with indicated geological resources of 1.769 million Moz gold at an average grade of 7.85 g/t Au (Hardie et al., 2018). Black Dog is also close to the Barry mine (3.5 km to the northeast), an orogenic vein-type deposit with estimated resources of 309 500 oz gold at an average grade of 1.25 g/t Au (Kitney et al., 2011). The gold mineralization at Windfall occurs in close spatial association with a swarm of quartz porphyritic calc-alkaline dykes (Hardie, et al., 2018), which have undergone strong silica, sericite and local tourmaline alteration; the gold is hosted mainly by pyrite and tourmaline-pyrite stringers. Both Tourmaline Hill and Windfall Lake are underlain by volcano-sedimentary rock units of the Macho Formation of the Urban-Barry greenstone belt (Figure 1).

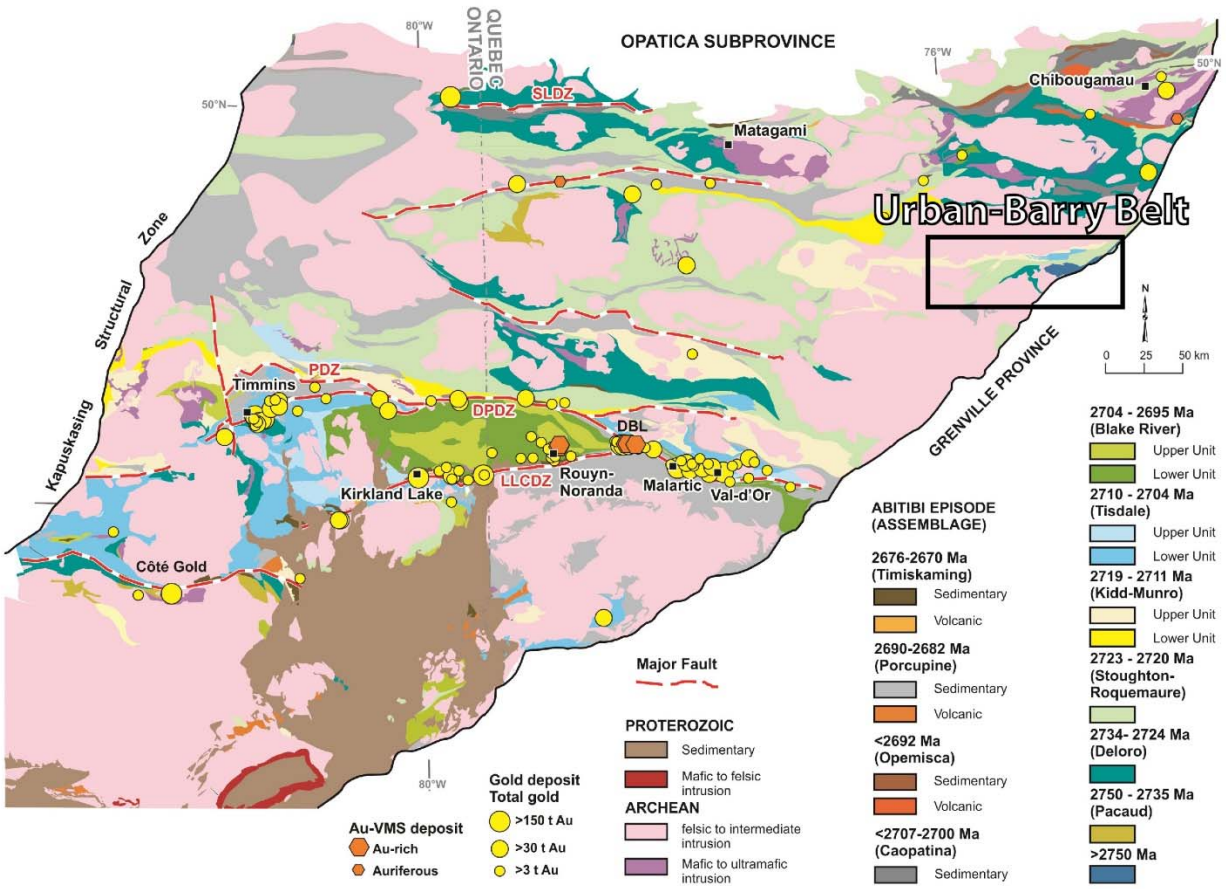

Figure 1: The gold and base metal deposits of the Abitibi, modified from Castongay (2019)

The Macho Formation comprises much of the Urban-Barry greenstone belt. It is dominantly composed of basalt with rare felsic to intermediate dykes and felsic volcanic rocks. The Tourmaline Hill units are part of the Amac 5 member, which was earlier classified as comprising tuffs and sedimentary rocks. They are now interpreted as per the results of this research to be altered basalt based on their relatively high Ti/Zr ratios. The Amac 1 member containing the tourmaline-rich rocks of Black Dog is surrounded by thick sequences of aphyric basalts of the Amac1 member. The Windfall rhyolites have been dated at 2716.9 ± 1.2 Ma, whereas the gold-bearing dykes have been dated at 2697 ± 0.9 Ma at Windfall and 2697 ± 0.6 Ma at the Barry lake

mine (zircon U-Pb; Bandyayera et al., 2002). The Macho Formation rocks have yielded ages of 2707 ± 3.2 and 2727 ± 1.0 Ma (zircon U-Pb; Bandyayera et al., 2004).

Tourmaline Hill is oriented parallel to the regional foliation, has a length of over 2 km and a maximum width of 100m, and has the Black Dog deposit at its center. From the outside to its core, the rocks of Tourmaline Hill vary from a weakly sericite- and tourmaline-altered basalt to a rock consisting almost entirely of quartz and tourmaline. At the center there is a tourmaline breccia with around 50% silicified angular clasts.

The Urban-Barry greenstone belt experienced two main deformation events. The first is manifested by a steeply dipping E-W trending foliation and is overprinted by a second event observed as a foliation at around 50º with a dip of around 50º. The Masère Fault, one of the main faults of the Urban Barry greenstone belt, passes through Tourmaline Hill and appears to have been part of the second event with regard to its orientation and dip. The Macho formation, comprising most of the Urban-Barry greenstone belt appears to have gone under upper greenschist metamorphism conditions (Rhéaume et al., 2006). There is no evidence that mineralization and alteration assemblages were affected by the regional metamorphism, although these assemblages are stable at conditions corresponding to those of the metamorphism.

1.3 Tourmaline Breccias Related to Copper Porphyry Deposits

Ore-bearing tourmaline breccias are common in the vicinity of porphyry copper deposits in late Paleozoic and younger subduction-related continental arcs. They are most common in the Andes and the North American Cordillera (Sillitoe et al., 1971; Sillitoe, 1985; Warnaars et al., 1985; Corbett et al., 1997; Williams et al., 1999; Skewes et al., 2003; Mlynarczyk, 2005; Sillitoe, 2010; Garrido et al., 2010 and Ochoa-Landin et al., 2016) but also occur in other continental arcs (Clark, 1965; Fletcher, 1977; Demiral et al., 2009 and Baksheeva et al., 2010). The oldest known

mineralized tourmaline breccia is the breccia that hosts the Proterozoic Ylöjärvi Cu-W deposit, Finland (Clark, A. H. et al., 1965).

Tourmaline breccias related to porphyry copper deposits comprise angular, silicified lithic clasts of highly variable size, cemented by tourmaline that ranges in composition from dravite to schorl. They generally take the form of pipes that cut the main porphyry intrusion or occur at the contact between the porphyries and their host-rocks. In some cases, however, tourmaline breccias are hosted entirely in volcanic or sedimentary rocks and their relationship with intrusions is unclear. Ore-bearing tourmaline breccias typically contain chalcopyrite + pyrite ± sphalerite filling late fractures (Sillitoe, 1985 and Corbett et al., 1997). Gold occurs as electrum in the sulfide-rich portions of the breccias. Although ore-bearing tourmaline breccias occur commonly in association with Phanerozoic porphyry deposits, there have been no reports of such breccias in Archean greenstone belts, possibly because only a small number of porphyry deposits have been identified in this setting.

1.4 Overview of Previous work

The Black Dog property comprises the Tourmaline Hill and Souart properties. In 1950, Nubar Mines Ltd. sunk a 44 meter deep shaft and developed 135 meters of drifts and crosscuts at Black Dog. Since then, numerous exploration surveys have been conducted by a variety of companies including Glenelm Developers Limited, Goldmaster Mines Ltd., Shell Canada Limited, Tut Exploration, Société de Développement de la Baie-James and Oasis Resources Inc. In 1985, Oasis Resources Inc. drilled 37 holes and subsequent resource modelling indicated 47 505 tons resource grading 5.39 g/t (Hardie, 2018). Osisko Mining carried out further drilling between 2016 to 2018. The best hole on the property returned 6.14 g/t Au and 34.1 g/t Ag over 14.4 meters. Although these are potentially economic gold and silver grades, the mineralization was

considered to be too irregular to justify exploitation and no further resource modelling was performed on the property.

1.5 Objectives

The Black Dog prospect is very different from the other gold deposits in the Abitibi Greenstone Belt. Instead, it is similar in many respects to the ore-bearing tourmaline breccias of the Andes. The occurrence of fracture filling sulfides within 50 meter wide zones of tourmaline breccia containing angular silicified clasts is a common feature of many of the copper porphyries of Peru, Argentina and Chile, but with the exception of the Black Dog property, is unknown in the Abitibi and other Archean greenstone belts. The overarching objective of this thesis is therefore to understand the genesis of this unusual type of Archean gold mineralization. The following are questions that will be addressed to meet this objective:

1) What was the nature of the rock subjected to tourmaline alteration and brecciation and what is the relationship between this alteration and the gold-bearing sulfide mineralization?
2) What were the physicochemical conditions of the alteration and mineralization, including temperature and pressure and compositional parameters?
3) What were the processes that led to deposition of the ore minerals?
4) What was the source of the fluids and what were the drivers for the hydrothermal system that produced the alteration and mineralization?

The first question was addressed by careful examination of the host rock, alteration and ore mineralogy and textures, the timing relationships between the host rock, tourmaline breccia and fracture-filling sulfides.

The second question was tackled using calculations based on results of sulfur isotope and mineral and whole rock chemical analyses in conjunction with observations of the relationship between the ore minerals and the alteration or host-rock minerals.

Answers to the third and fourth questions developed by addressing the first two questions and also in part by considering possible relationships of the mineralization to intrusion-related Windfall Lake deposit and the orogenic Barry deposit.

1.6 Methods

Field work was conducted over the summers of 2016 and 2017. Over five thousand channel and drill core samples were analyzed for major and trace element contents using XRF and LA-ICP-MS techniques during exploration of the prospect by Osisko Mining Ltd. Representative samples of the different rock types, both mineralized and unmineralized, were examined in polished thin sections using a combination of optical microscopy (Olympus BX51) and scanning electron microscopy (SEM; Hitachi SU5000) to identify the minerals, determine their relative proportions and evaluate textural relationships. The SEM is equipped with an energy dispersive spectrometer (EDS) for semi-quantitative analyses and was used to facilitate mineral identification and prepare element maps of tourmaline and the ore minerals. Phase quantification was conducted using a JEOL 8900L electron microprobe (EMP) equipped with five wavelength dispersive spectrometers (WDS) and a Cameca SXFive-FE EMP. The beam diameter was 5 μm, the acceleration voltage 20 kV, and the current 8 nA. Results of analyses were compared to those for a NIST 610 standard glass. The level 3 data method of Henry et al. (2011) was used for element site allocation in tourmaline. Trace element concentrations in tourmaline and in quartz were analyzed using a New Wave 213 mm ND-YAG laser ablation system coupled to a Thermo Scientific iCAP Q inductively coupled plasma mass spectrometer (LA-ICP-MS). Analyses were

performed in traverse mode (40 μm wide) with an ablation rate of 5 μm per second at 10 Hz and 60% energy output. This included a 15 second dwell time between traverses. The average energy was ~8 joules. A NIST SRM 610 glass was used as a standard for the trace elements in both tourmaline and quartz. Sodium, which had been analyzed previously with the electron microprobe, was used as the internal standard for tourmaline analyses; Si was used for quartz. Sulfur isotope analyses of pyrite, chalcopyrite and sphalerite were conducted at Queen's University using a Delta Plus XP Stable Isotope Ratio Mass Spectrometer (IRMS) to retrieve S^{32} and S^{34} values relative to the Vienna-Canyon El Diablo Troilite (VCDT) standard with a 0.1 per mil error. The sulfide minerals were extracted using a microdrill and clean separates were selected manually under a binocular microscope. Mineral pairs in textural equilibrium were used to calculate temperatures of mineralization.

1.7 Thesis Organization

This thesis is organized in three chapters, an introduction, a stand-alone manuscript and a general conclusion. The introduction contains a review of the literature pertinent to the project, a geological environment description and a description of the objectives, methods and thesis organization. The stand-alone manuscript of the second chapter examines the geology and genesis of the Black Dog prospect and its affinity to other deposits in the region and the copper porphyry-related ore-bearing tourmaline breccias in the Andes. The final chapter presents a summary of the results and conclusions relating to the genesis of the Black Dog prospect, and places the research in the broader context of the metallogeny of the Abitibi greenstone belt.

References

Clark, A. H. (1965) The Mineralogy and Geochemistry of the Ylöjärvi Cu-W Deposit, Southwest Finland: Mackinawite-Pyrrhotite-Troilite Assemblages, Comptes Rendus de la Société Géologique de la Finlande, vol. 38, pp. 331-342.

Corbett, G. J., Leach, T. M. (1997) South West Pacific Rim Gold-Copper Systems: Structure, Alteration and Mineralization, Short Course Manual, 282 pp.

Garrido, M. M., Gómez, M. C., Fernández, M. L., (2010) Brecha de Turmalina del Pórfido de Cobre-Oro San Jorge, Mendoza: Alteración, Mineralización y Origen de los Fluidos. Revista de la Asociación Geológica Argentina, vol. 67, pp. 47-57.

Hardie C., et al. (2018) Preliminary Economic Assessment of the Windfall Lake Project, Lebel-sur-Quévillon, Québec, Canada. NI43-101 Technical Report, Osisko Mining Inc., August 2018, 826 p.

Helt, K. M., Williams-Jones, A. E., Clark, J. R. (2014) Constraints on the Genesis of the Archean Oxidized, Intrusion-Related Canadian Malartic Gold Deposit, Quebec, Canada. Economic Geology, vol. 109, pp. 713-735

Kitney, E. K., Olivo, G., R., David, D. D., Desrochers, J. P., Tessier, A. (2011) The Barry Gold Deposit, Abitibi Subprovince, Canada: A Greenstone Belt-Hosted Gold Deposit Coeval with Late Archean Deformation and Magmatism. Economic Geology, vol. 106, pp. 1129-1154.

Mlynarczyk, M. S. J. (2005) Constraints on the genesis of lode-style tin mineralization: Evidence from the San Rafael tin-copper deposit, Peru. PhD Thesis, McGill University.

Monecke, T., Mercier-Langevin, P., Dubé, B., Frieman, B. M. (2017) Geology of the Abitibi Greenstone Belt. Reviews of Economic Geology, vol. 19, pp. 7-49.

Ochoa-Landin, L. H., Valencia-Morena, M., Valmus, T. (2016) Geology and Geochemistry of the Suaqui Verde Deposit: A Contribution to the Knowledge of the Laramide Porphyry Copper Mineralization in South Central Sonora, Mexico. Ore Geology Reviews, vol. 81, *in progress*.

Bandyayera, D., Rhéaume, P., Doyon, J., Sharma, N. M. (2004) Géologie de la région du lac Hébert (32G/03) - RG 2003-07, Ministère des Ressources naturelles et de la Faune, Québec.

Rhéaume, P., Bandyayera, D. (2006) Révision stratigraphique de la Ceinture d'Urban-Barry. Ressources Naturelles et Faune, RP 2006-08.

Sillitoe, R. H., Sawkins, F. J. (1971) Geologic, Mineralogic and Fluid Inclusion Studies Relating to the Origin of Copper-bearing Breccia Pipes, Chile. Economic Geology, vol. 66, pp. 1028-1041.

Sillitoe, R. H. (1985) Ore-Related Breccias in Volcanoplutonic Arcs. Economic Geology, vol. 80, pp. 1467-1514.

Sillitoe, R. H., (2010) Porphyry Copper Systems. Economic Geology, v.105, pp. 3-41.

Skewes, M. A., Holmgren, C., Stern, C.R. (2003) The Donoso Copper-Rich, Tourmaline-Bearing Breccia Pipe in Central Chile: Petrologic, Fluid Inclusion and Stable Isotope Evidence for an Origin from Magmatic Fluids. Mineralium Deposita, vol. 38, pp. 2-21.

Thurston, P.C., Ayer, J.A., Goutier, J., Hamilton, M.A. (2008) Depositional Gaps in Abitibi Greenstone Belt Stratigraphy: A Key to Exploration for Syngenetic Mineralization. Economic Geology, vol. 103, pp. 1097–1134.

Warnaars, F. W., Holmgren, D., C., Barassi, F. S. (1985) Porphyry Copper and Tourmaline Breccia at Los Bronces, Chile. Economic Geology, vol. 80, pp. 1544-1565.

Williams, W. C., Meissl, E., Madrid, J., De Machuca, B. C. (1999) The San Jorge, Porphyry Copper Deposit, Mendoza, Argentina: a Combination of Orthomagmatic and Hydrothermal Mineralization. Ore Geology Reviews, vol. 14, pp. 185-201.

Chapter II: The Black Dog Prospect, Québec, Canada: a Rare Example of Archean Tourmaline Breccia-Hosted Au-Cu Mineralization

Philippe Drouin [(1)], Anthony E. Williams-Jones [(1)], James R. Clark [(1)]

(1) Department of Earth and Planetary Sciences, McGill University, 3450, University Street, Montreal, Québec, Canada, H3A 2A7

Abstract

The Black Dog Au-Cu prospect occurs in a two km-long tourmaline alteration zone in a mafic volcanic sequence of the Urban-Barry greenstone belt, Abitibi region. This zone is two to three meters thick for most of its length but reaches over 30 meters in thickness at Black Dog, where tourmaline is present both as an alteration phase and as the cement of a magmatic-hydrothermal breccia. The tourmaline breccia has roughly equivalent proportions of tourmaline matrix and quartz- and tourmaline-altered clasts. The Au-Cu mineralization occurs in a sulfide breccia that cuts the tourmaline breccia. In decreasing order of abundance, the main sulfide minerals are pyrite, chalcopyrite, sphalerite, cobaltite, arsenopyrite and pyrrhotite. Gold occurs mainly as electrum and is associated with hessite, matildite, native silver and Bi-telluride minerals. This mineralization generally occurs at the contacts of pyrite or arsenopyrite grains in the sulfide matrix or veins.

The mineralization is hosted by weakly foliated, basaltic rocks that have been altered to tourmaline, quartz and sericite. The early tourmaline (Type A) is dominantly dravitic, whereas in the subsequent stages (Types B and C), schorl is predominant. Late stage tourmaline (Type C) has elevated concentrations of ore-related elements, including Co, Zn, Cu, Ag and Bi. Principal component analyses applied to bulk rock compositions demonstrate that these metals correlate strongly with gold.

Many features of the Black Dog prospect are unusual for the Abitibi greenstone belt, where the vast majority of the ore deposits belong to the orogenic gold and volcanogenic massive sulfide classes. In contrast to Black Dog, the orogenic deposits are characterized by limited abundances of sulfide minerals, magmatic-hydrothermal breccias are absent, and the ores are usually

associated with quartz/carbonate and tourmaline veins where tourmaline is only present as veinlets and is not a major constituent of the rock.

Temperatures estimated from sulfur isotope compositions of pyrite, chalcopyrite and sphalerite at Black Dog range between 400 and 600°C (± ~50°C) and average 496°C on six sample pairs (±26°). This relatively high temperature of formation and the narrow range of sulfur isotope compositions ($\delta^{34}S$ from +1.7 to +3.6 ‰ for sulfide minerals, corresponding to +1.4 to +2.4‰ H_2S) suggest that the mineralizing fluids were dominantly magmatic. Orogenic Au deposits are generally depleted in Cu and have a wider range of sulfur isotope values than at Black Dog, possibly reflecting multiple sources of sulfur. They also are interpreted to have formed at lower temperature.

The timing relationships at Black Dog indicate that tourmaline alteration and mineralization took place after the main deformation event had begun. Tourmaline veins that cut the foliation, foliated clasts in the breccia, and the sub-vertical orientation of the breccia pipe (which cuts the regional foliation), are strong evidence for the emplacement of the veins and breccia pipe at a late stage of deformation.

We propose that magmatic fluids emanating from a calc-alkaline intrusion at depth were responsible for the alteration and mineralization observed at Black Dog. This model is analogous to that postulated for the Au-Cu-bearing tourmaline breccias associated with porphyry copper deposits in Phanerozoic rocks.

2.1 Introduction

Tourmaline breccias occur commonly in the vicinity of porphyry copper deposits in late Paleozoic and younger subduction-related continental arcs, and in some cases contain high concentrations of gold and copper. Ore-bearing tourmaline breccias are most common in the

Andes and the American Cordillera (Sillitoe et al., 1971; Sillitoe, 1985; Warnaars et al., 1985; Corbett et al., 1997; Williams et al., 1999; Skewes et al., 2003; Mlynarczyk, 2005; Sillitoe, 2010; Garrido et al., 2010 and Ochoa-Landin et al., 2016) but also occur in other continental arcs (Clark, 1965; Fletcher, 1977; Demiral et al., 2009 and Baksheeva et al., 2010). The oldest known mineralized tourmaline breccia is the breccia that hosts the Proterozoic Ylöjärvi Cu-W deposit in Finland dated at around 1850 Ma (Himmi et al., 1979).

Tourmaline breccias related to porphyry copper deposits comprise angular, silicified lithic clasts of highly variable size, cemented by tourmaline that ranges in composition from dravite to schorl. They generally take the form of pipes that cut the main porphyry intrusion or occur at the contact between the porphyries and their host-rocks. In some cases, however, tourmaline breccias are hosted entirely in volcanic or sedimentary rocks and their relationship with intrusions is unknown. Ore-bearing tourmaline breccias typically contain chalcopyrite + pyrite ± sphalerite filling late fractures (Sillitoe, 1985 and Corbett et al., 1997). Gold occurs as electrum in the sulfide-rich portions of the breccias. Although ore-bearing tourmaline breccias occur commonly in association with Phanerozoic porphyry deposits, there have been no reports of such breccias in Archean greenstone belts, possibly because only a small number of porphyry deposits have been identified in this setting.

In this paper, we describe and interpret the genesis of a tourmaline breccia-hosted gold deposit in the Abitibi greenstone belt of Canada, namely the Black Dog prospect, which displays features similar to the ore-bearing tourmaline breccias associated with Andean porphyry copper deposits. The Black Dog breccia consists of angular silicified fragments of basalt cemented by fine-grained tourmaline and is surrounded by a halo in which basalt was subjected to tourmaline alteration and silicification. The gold mineralization takes the form of electrum and occurs in

sulfide veins that cut the sub-vertical breccia body. A genetic model is proposed for the prospect involving the exsolution of fluids from a cooling, calc-alkaline intrusion related to the Kenoran orogeny that brecciated the host rocks by hydrofracturing, and evolved from early tourmaline to late sulfide saturation, crystallizing tourmaline and depositing chalcopyrite, sphalerite, pyrite and electrum, respectively.

2.2 Geological Setting

Tourmaline Hill, which hosts the Black Dog prospect, is a narrow topographical high in an area of otherwise low relief near the Windfall Lake intrusion-related gold deposit (Hardie et al., 2018); Windfall lies 14 km northeast of Black Dog, and is currently undergoing exploration, with resources to date comprising 1.769 million Moz gold at an average grade of 7.85 g/t Au (Hardie et al., 2018). Black Dog is also close to the Barry mine (3.5 km to the northeast), an orogenic vein-type deposit with estimated resources of 309 500 oz gold at an average grade of 1.25 g/t Au (Kitney et al., 2011). The gold mineralization at Windfall occurs in close spatial association with a swarm of quartz porphyritic calc-alkaline dykes (Hardie, et al., 2018), which have undergone strong silica, sericite and local tourmaline alteration; the gold is hosted mainly by pyrite and tourmaline-pyrite stringers. Both Tourmaline Hill and Windfall Lake are underlain by volcano-sedimentary rock units of the Macho Formation of the Urban-Barry greenstone belt, which forms part of the Northern Volcanic Zone of the Abitibi greenstone belt (Figure 2). The contact between the Northern (2730-2710 Ma) and Southern Volcanic (2705-2698 Ma) Zones, which are host to many world class orogenic and gold-rich VMS deposits, is marked by the Porcupine-Destor fault zone (Card et al., 1998). The Southern Volcanic Zone is responsible for most of the production of precious and base metals in the Superior Province (Spooner et al., 1993).

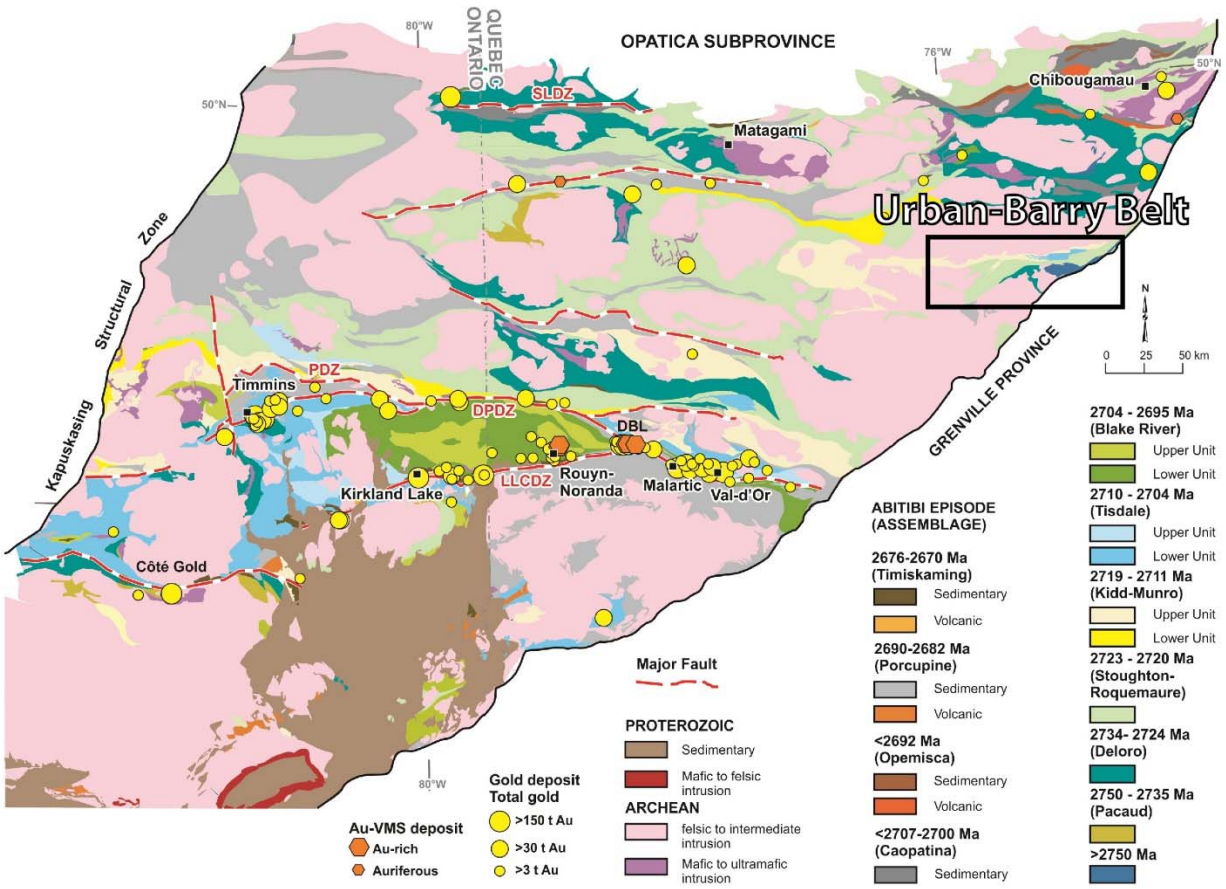

Figure 2: The gold and base metal deposits of the Abitibi, modified from Castongay (2019)

The Macho Formation constitutes most of the Urban-Barry greenstone belt (Figure 3). It comprises ~95% basalt, with the remainder consisting mostly of felsic to intermediate dykes and some rare felsic volcanic rocks, all belonging to the Windfall member. The brecciated rocks of Tourmaline Hill form part of the Amac 5 member, which historically was considered to comprise tuffs and sedimentary rocks. On the basis of relatively high Ti/Zr ratios (see below), we now interpret the brecciated rocks to be altered basalts. The tourmaline-rich rocks of the Black Dog prospect are bounded by thick sequences of aphyric basalts of the Amac1 member. The Windfall rhyolites have been dated at 2716.9 ± 2 Ma, whereas the mineralization-bearing dykes have been dated at 2697 ± 0.9 Ma at Windfall and 2697 ± 0.6 Ma at the Barry Lake mine (zircon U-Pb;

Bandyayera et al., 2002). The Macho Formation rocks yielded ages of 2707 ± 3.2 and 2727 ± 1.0 Ma (zircon U-Pb; Bandyayera et al., 2004).

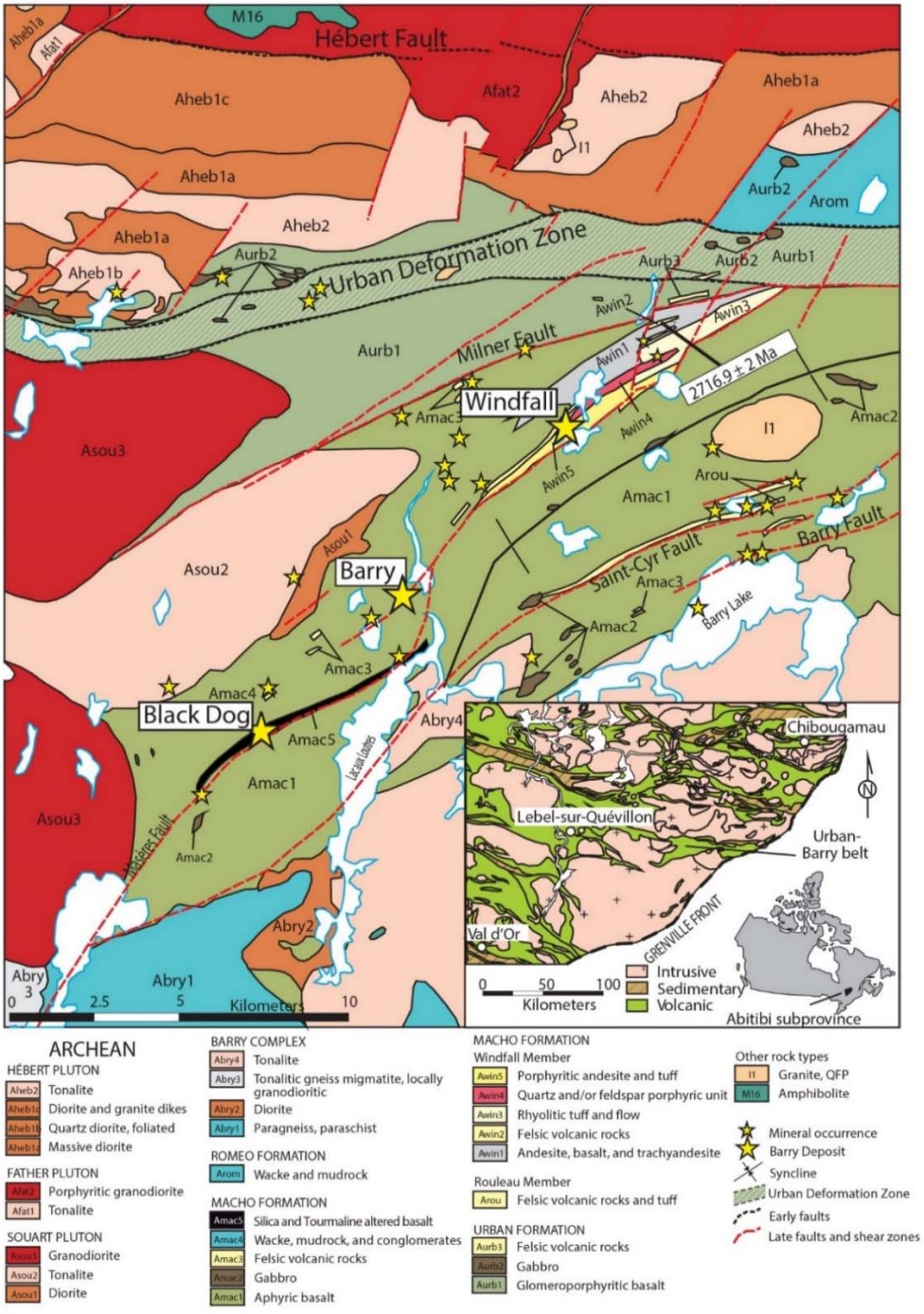

Figure 3: A geological Map of the Urban-Barry greenstone belt, modified from Kitney et al. (2011)

The tourmaline alteration at Tourmaline Hill is in a zone elongated parallel to the regional foliation and extends laterally for more than 2 km, reaching a width of 100 m at Black Dog. At its margins, the zone is evident as a weakly to moderately tourmaline-altered basalt with ptygmatic tourmaline veinlets, whereas in its core, at least 50 vol.% of the rock consists of tourmaline and much of the remainder of quartz; tourmaline and quartz. These minerals replaced all the primary minerals and/or cemented breccias, obliterating most of the textures of the precursor basalt.

Two main deformation trends are observed in the Urban-Barry greenstone belt. The main regional foliation trends NE-SW (045 to 055°) with a dip of 40 to 60°. It is locally overprinted by a weak second, more steeply dipping E-W foliation. Brittle deformation is evident in the Urban Deformation Zone and a number of sub-parallel subsidiary structures (Masère, Milner, Saint-Cyr and Barry faults). One of them, the Masère fault, passes through Tourmaline Hill. The regional metamorphic grade in the area reached upper greenschist facies (Rhéaume et al., 2006). Regional metamorphism in the Abitibi can be bracketed between 2677 and 2643 Ma (Powell, 1995).

2.3 Sampling and analytical methods

Over five thousand channel and drill core samples were analyzed for major and trace element contents using XRF and LA-ICP-MS techniques during exploration of the prospect by Osisko Mining Ltd. Representative samples of the different rock types, both mineralized and unmineralized, were examined in polished thin section using a combination of optical microscopy (Olympus BX51) and scanning electron microscopy (SEM; Hitachi SU5000) to identify the minerals, determine their relative proportions and evaluate textural relationships. The SEM is equipped with an energy dispersive spectrometer (EDS) for semi-quantitative analyses and was used to facilitate mineral identification and prepare element maps of tourmaline and the

ore minerals. Phase quantification was conducted using a JEOL 8900L electron microprobe (EMP) equipped with five wavelength dispersive spectrometers (WDS) and a Cameca SXFive-FE EMP. The beam size was 5 μm, the acceleration voltage 20 kV, and the current was of 8 nA. Results of analyses were compared to those for a NIST 610 standard glass. The level 3 data method of Henry et al. (2011) was used for element site allocation in tourmaline. Trace element concentrations in tourmaline and in quartz were analyzed using a New Wave 213 mm ND-YAG laser ablation system coupled to a Thermo Scientific iCAP Q inductively coupled plasma mass spectrometer (LA-ICP-MS). Analyses were performed in traverse mode (40 μm wide) with an ablation rate of 5 μm per second at 10 Hz and 60% energy output. The well time between traverses was 15 seconds. The average energy was ~8 joules. A NIST SRM 610 glass was used as a standard for the trace elements in both tourmaline and quartz. Sodium, which had been analyzed previously with the electron microprobe, was used as the internal standard for tourmaline; Si was used for quartz. Sulfur isotope analyses of pyrite, chalcopyrite and sphalerite were conducted at Queens University using a Delta Plus XP Stable Isotope Ratio Mass Spectrometer (IRMS) to retrieve S^{32} and S^{34} values relative to the Vienna-Canyon El Diablo Troilite (VCDT) standard with a 0.1 per mil error. The sulfide minerals were extracted using a microdrill and clean separates were selected manually under a binocular microscope. Mineral pairs in textural equilibrium were used to calculate temperatures of mineralization.

2.4 Local Geology

The rocks containing the tourmaline breccias that host the Black Dog Au-Cu prospect consist almost exclusively of basalts of the Macho Formation that have undergone upper greenschist facies metamorphism. Pillows are rarely observed, and the rock is weakly to moderately foliated. The main rock-forming minerals are hornblende, quartz, biotite and chlorite, which are

accompanied by minor to trace amounts of calcite, muscovite, epidote and pyrite. Locally, there are meter-wide layers containing up to 2 vol.% garnet. The foliation strikes ~ 060°/45°E and is parallel to the primary layering. A geological map of the Black Dog main trench, superimposed on an aerial photograph is presented in Figure 44.

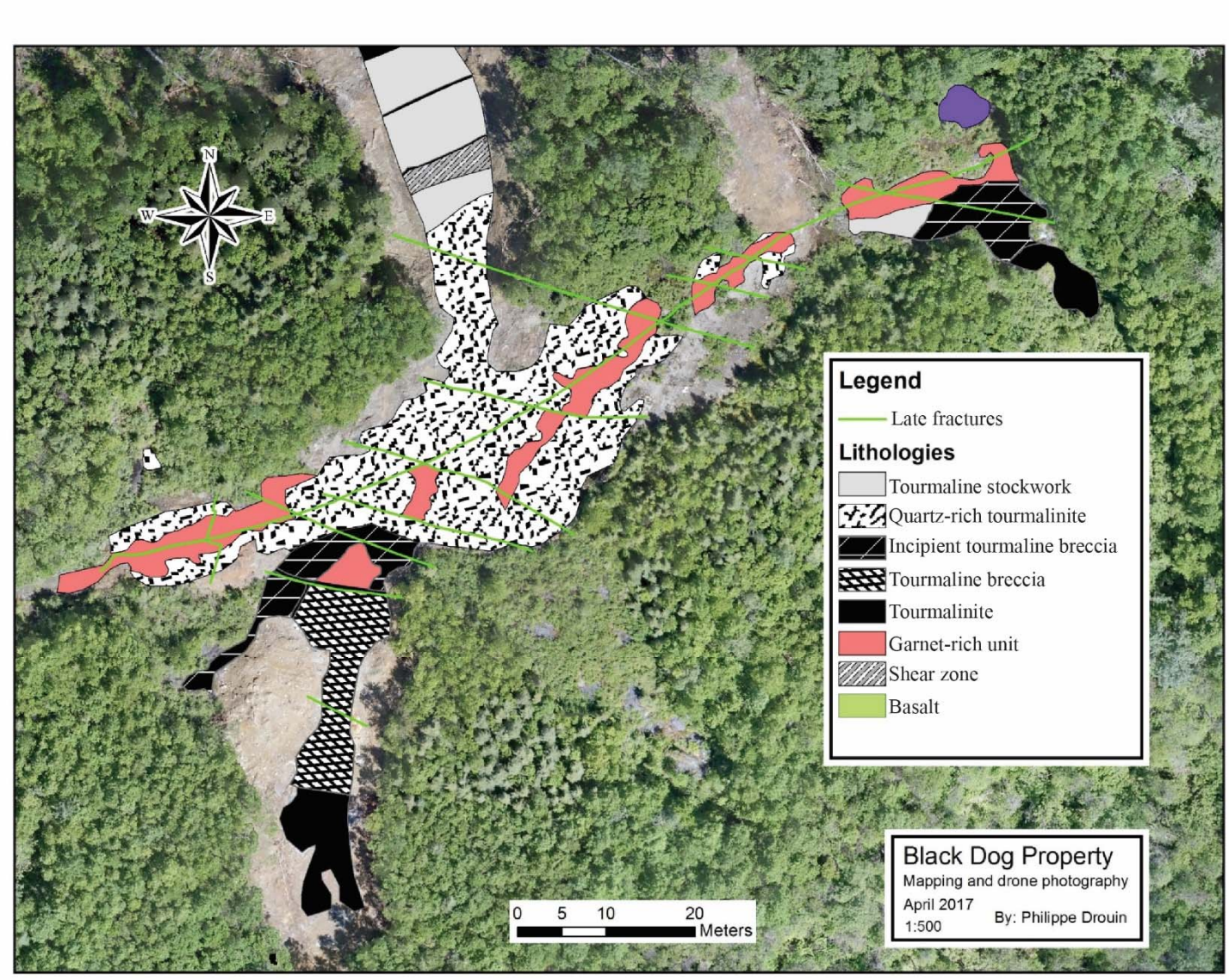

Figure 4: A geological map of the main Black Dog trench

The concentrations of relatively immobile elements, such as Ti, Zr, Nb and Y, indicate that the tourmaline-bearing rocks and the adjacent less-altered host rocks are basalts and that they formed in a continental arc setting (Figure 5). The altered rocks that comprise the Black Dog prospect have been subdivided into five units, namely (1) tourmaline stockwork, (2) tourmalinite, (3) tourmaline breccia, (4) sulfide breccia, and (5) garnet-rich unit.

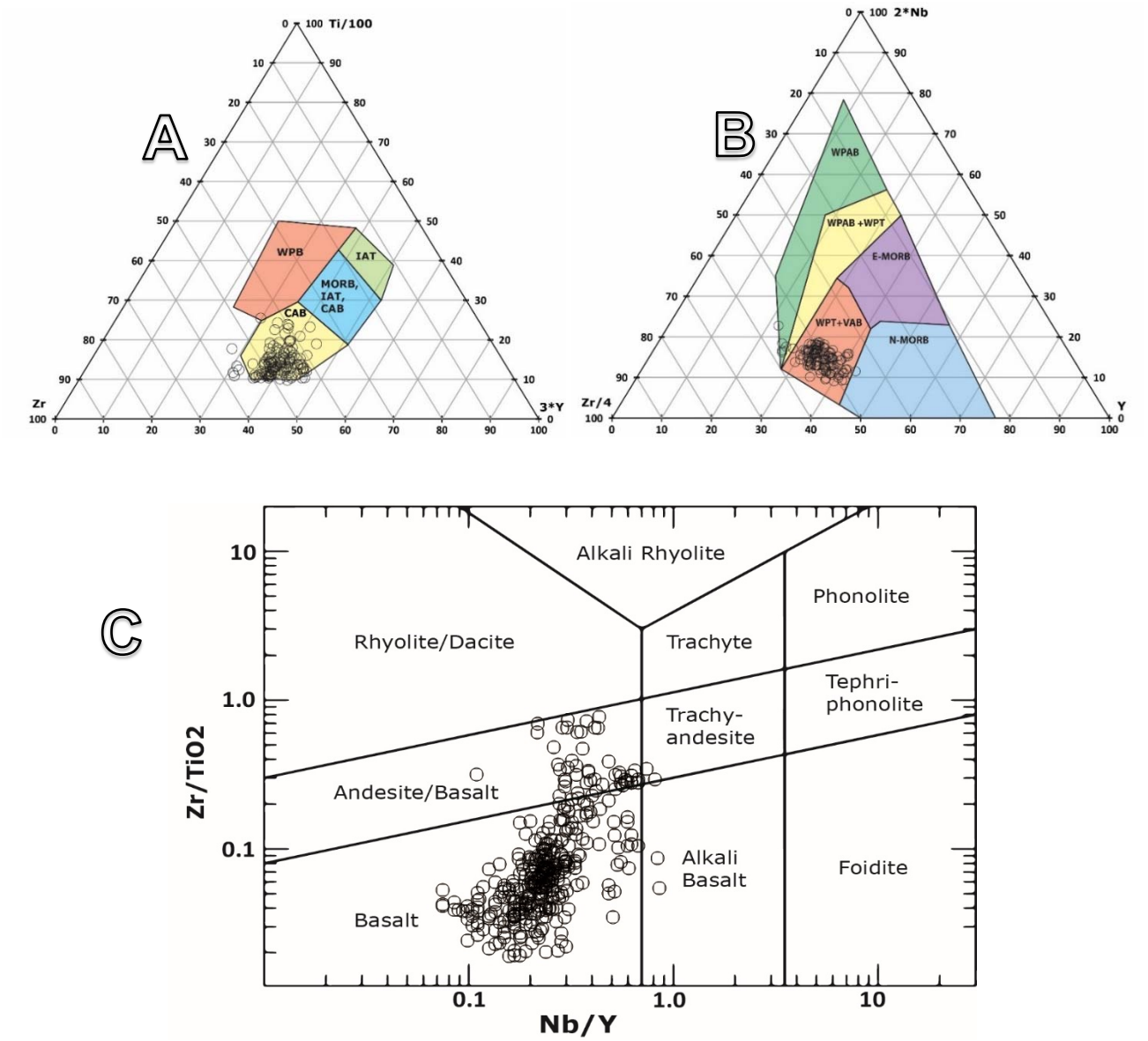

Figure 5: a) Zr, Ti and Y immobile elements tectonic environment classification diagram where host rock samples plot in the calc-alkali basalt area. From Pearce and Cann (1973). b) Zr, Nb

and Y immobile elements tectonic environment classification diagram where host rock samples plot in the volcanic arc basalt and within plate tholeiites. From Meschede (1986). c) Zr/TiO2 vs. Nb/Y ratios immobile elements rock type classification diagram where host rock samples mostly plot in the basalt and andesite/basalt area. From Pearce (1996).

Tourmaline stockwork

The tourmaline stockwork is hosted by basalt that has been altered to quartz, sericite and tourmaline, and consists of a complex network of ptygmatic veins and veinlets 0.1 to 2 cm in width that cross-cut foliation, and masses of tourmaline ranging from 0.5 to 2 cm in diameter (Figure 6). Most of the primary mineralogy has been replaced by tourmaline, quartz and sericite leaving behind minor remnants of biotite and amphibole. The larger veins are zoned outwards from a core of fine-grained quartz and tourmaline, through a quartz-rich outer layer to a tourmaline-rich rim. In general, the boundaries of both the veins and veinlets are diffuse. This unit developed mainly along the margins of the tourmalinite with which its contacts are gradational. Tourmaline comprises ~3% of the rock and generally occurs as very fine-grained aggregates and fans within the veins/veinlets and in the first few centimeters of the adjacent rock. Traces of chlorite, magnetite, garnet, biotite, epidote, apatite, rutile, ilmenite and chalcopyrite, as well as disseminated pyrite occur in the altered rock. This unit contains 50 ppb Au on average.

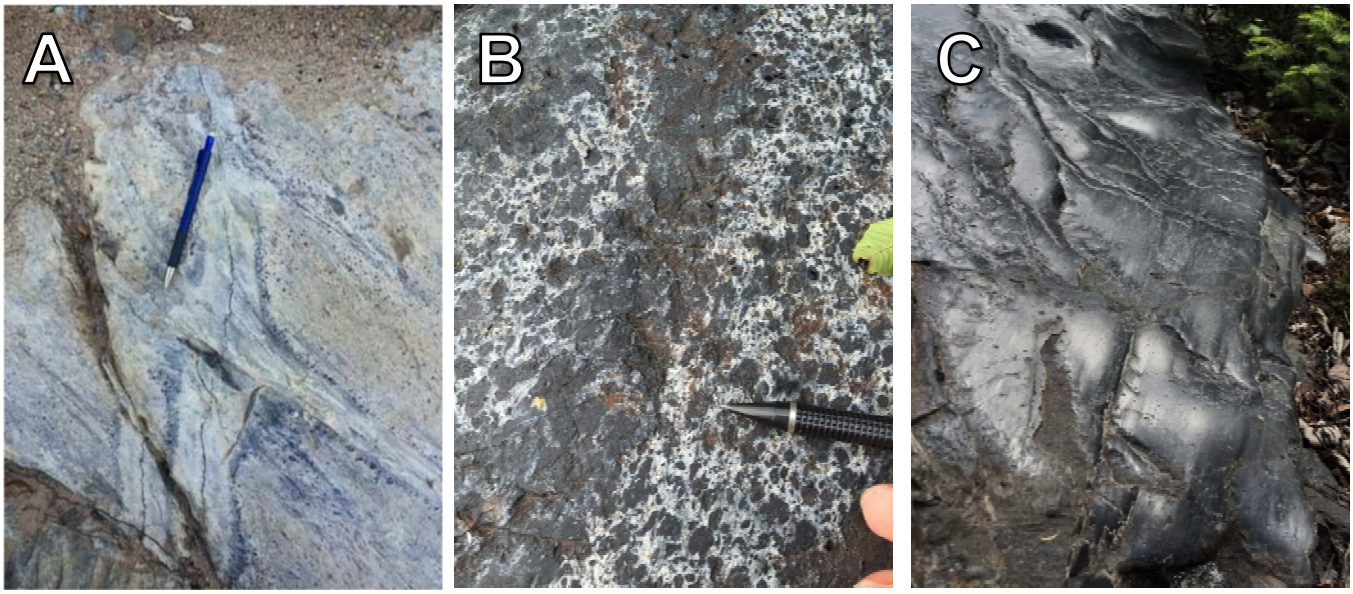

Figure 6: Major geological units at Black Dog. A) Tourmaline veinlets cutting altered basalt. The veinlets have zoned alteration envelopes, comprising proximal (0 to 3 cm) quartz-rich haloes and distal (3 cm +) tourmaline-rich haloes. Beyond the alteration envelopes, the rock consists mainly of sericite with minor silica and tourmaline. B)Tourmalinite with black tourmaline pods in a pervasively silicified rock. C) Massive tourmalinite containing ~ 70% tourmaline with the remainder of the rock being quartz.

Tourmalinite

Tourmalinite is composed mainly of tourmaline and quartz in the proportions ~ 30 to 60 vol.% and ~ 40 to 70%, respectively, in the quartz-rich tourmaline or ~ 60 to 90 vol.% and ~ 10 to 40 vol.% respectively in the tourmalinite. The tourmaline and quartz are accompanied by minor proportions of sericite and chalcopyrite and traces of pyrite. Tourmalinite occurs locally as a fine-grained rock comprising evenly distributed black tourmaline as ellipsoidal masses in a white quartz matrix (Figure 5b), whereas elsewhere it is a very fine-grained massive rock containing uniformly distributed tourmaline and quartz (Figure 6c). This unit is commonly cut by tourmaline-sulfide lenses reaching 20 cm in length and 2 cm in thickness containing 5% pyrite, with garnet masses at their margins. These lenses also contain variable proportions of quartz, and

display crack and seal textures manifested by alternating layers of quartz and tourmaline. The average Au content of the unit is 150 ppb.

Tourmaline breccia

The tourmaline breccia is composed of white, angular, quartz- and sericite-altered clasts in a black tourmaline matrix (Figure 7a) and b)). Although much of the material in this breccia is hydrothermal in origin, the remnant clasts are considered to originally have been of basaltic composition. The clasts range from 2 mm to over a meter in diameter and constitute 20 to 70 vol.% of the rock. The breccia is generally matrix-supported and commonly displays a jigsaw texture. Some larger clasts display strong layering manifested by alternating tourmaline- and quartz-rich zones (Fig. 6b). The matrix consists of 95% fine-grained tourmaline, 4% quartz and 1% pyrite. In outcrop, the breccia forms a sheet-like body ~25 m thick that extends along strike for ~ 100 m. It has been intersected by drilling to a depth of at least 700 m and has an elongated lens shape. Its orientation is sub-vertical and it cuts through the regional foliation. The unit is oriented ~ 060°/45°E and there is no preferential orientation of the clasts. The contacts with the adjacent silicified and sericite altered basalt are gradational. The tourmaline breccia grades into the stockwork unit described above, in which the fractures that became the veins/veinlets served to separate blocks of silicified and sericite altered rock. The average Au content of the unit is 350 ppb.

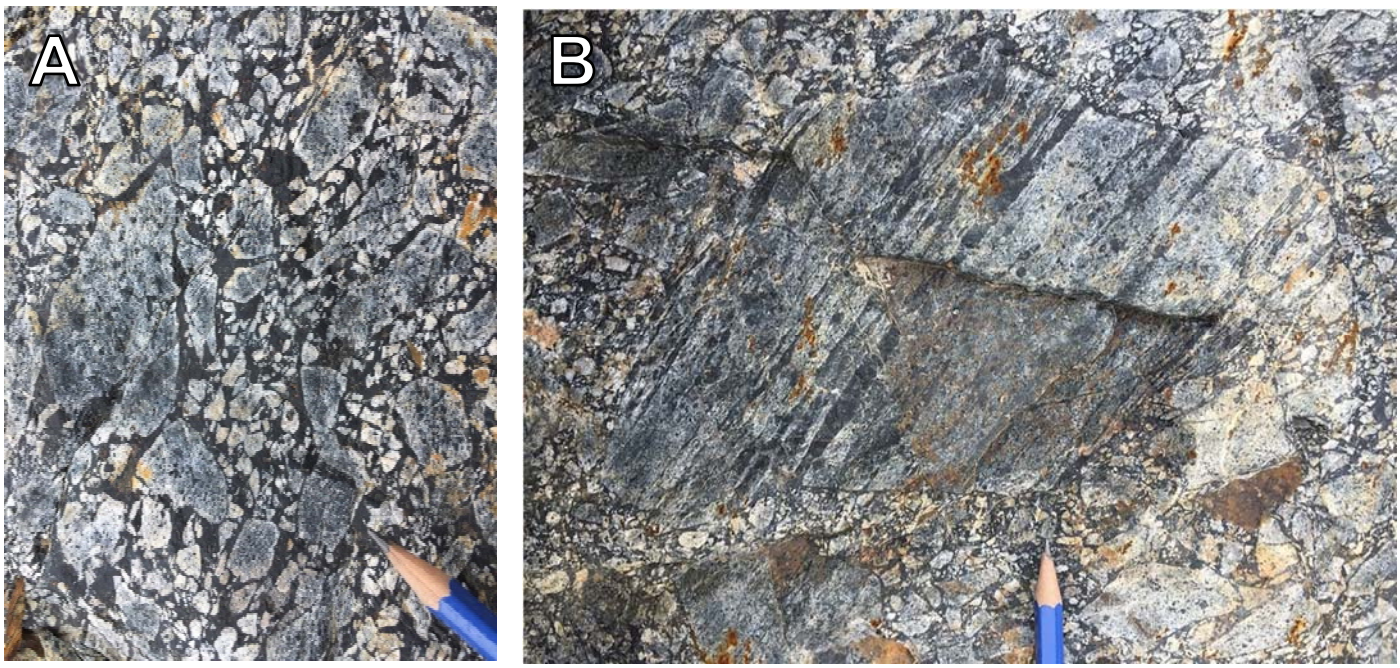

Figure 7: Examples of tourmaline breccia units. A) Tourmaline breccia which displaying a local jigsaw texture and contains angular fragments that have been strongly silicified,. B) Tourmaline breccia with a large, 25 cm diameter clast that contains pre-existing linear structures that were replaced preferentially by tourmaline or quartz.

Sulfide breccia

The sulfide breccia is characterized by irregular sulfide-rich veins either lining the contact of the tourmaline breccia and the tourmalinite units or cross-cutting the tourmaline breccia unit (Figure 8). This unit is adjacent to the tourmaline breccia unit in drill core and is sub-vertical. The tourmaline-rich clasts are angular and compose ~ 30 vol.% of the rock. Sulfide minerals make up 70% vol.% of the rock on average. Pyrite and chalcopyrite generally constitute at least 90 vol.% of the sulfides. Locally, however, there is up to 50 vol.% sphalerite and there are traces of wolframite. Gold concentrations reach 26 g/t as electrum grains (5 to 50 µm in diameter) that are mainly in contact with chalcopyrite and pyrite, or chalcopyrite and arsenopyrite. Pyrite and cobaltite occur as disseminated grains in tourmalinite (Figure 9b and d), whereas chalcopyrite,

arsenopyrite and sphalerite are concentrated in the matrix or in veins (Figure 9d). Sphalerite commonly displays “chalcopyrite disease” (Figs. 8 b and d). This unit averages 4 ppm Au and 4.7 wt.% Cu.

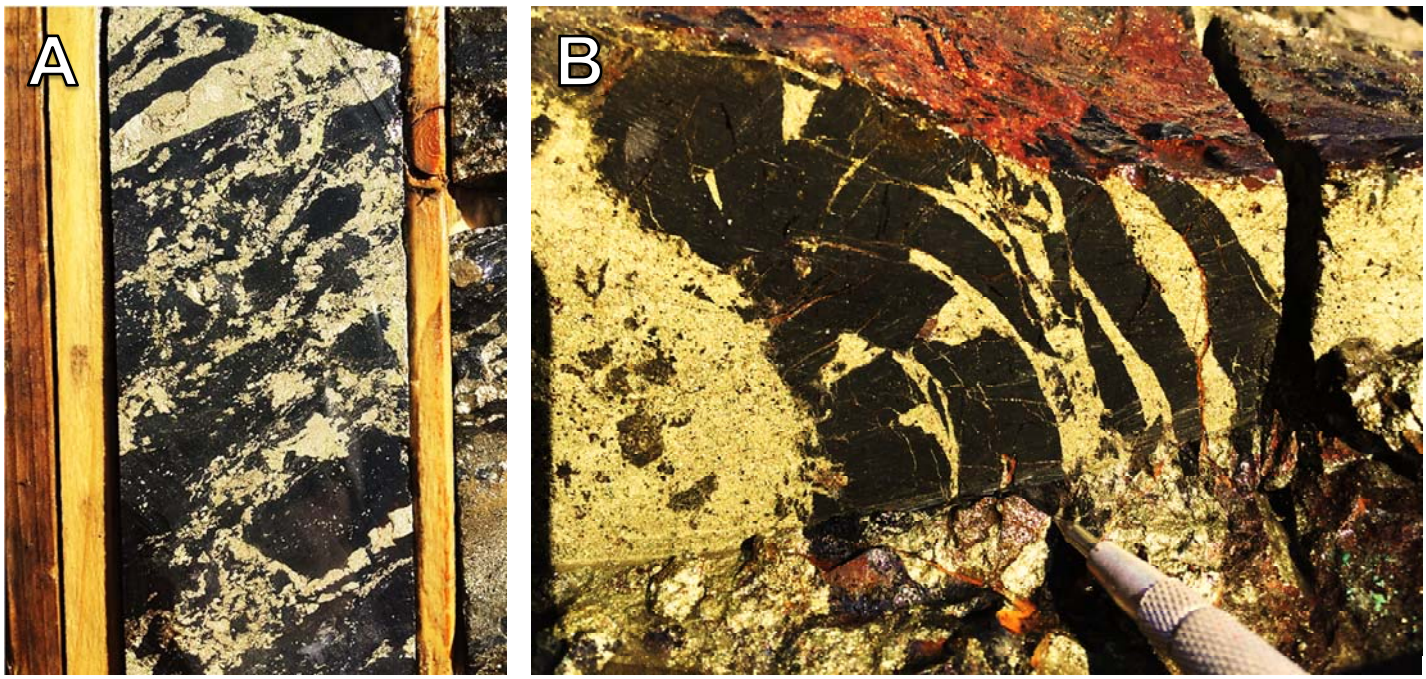

Figure 8: Sulfide breccia unit in drill core and outcrop. A) Sulfide breccia unit in drill core, containing tourmaline-rich clasts in a sulfide (mainly pyrite) matrix. The pyrite cross-cuts tourmaline; replacement depositional textures are also observable. B) Sulfide breccia comprised in outcrop comprised of tourmaline clasts in a chalcopyrite dominated matrix with minor sphalerite. The sulfide breccia presents a cross-cutting relationship with the tourmaline breccia.

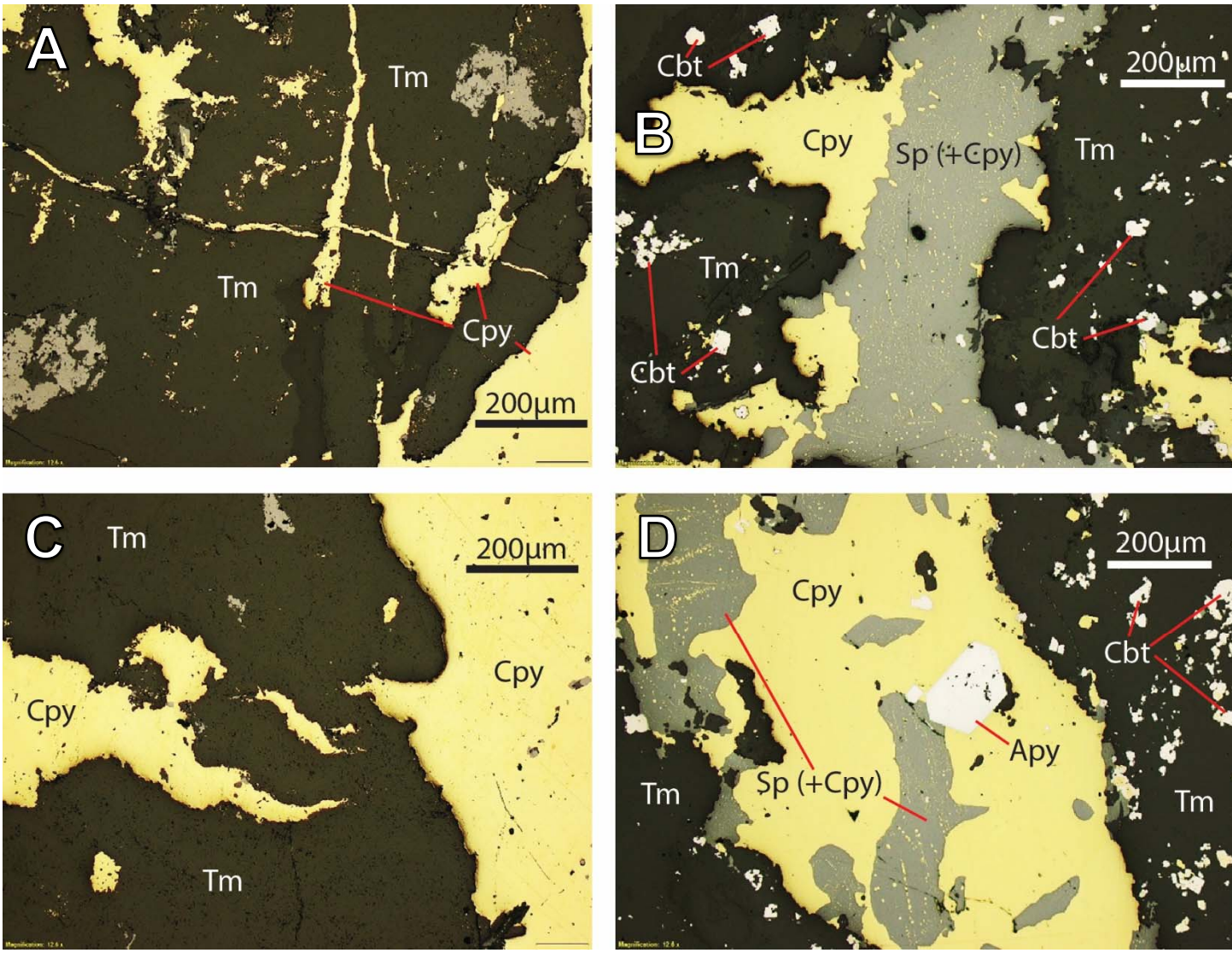

Figure 9: Reflected light images of the sulfide breccia, showing cross-cutting relationships between tourmaline and sulfides. A) Chalcopyrite ± sphalerite cuts microcrystalline tourmaline. B) ~2 vol.% cobaltite occurs locally in tourmaline. D) arsenopyrite accompanied by chalcopyrite + sphalerite, and cobaltite in the surrounding tourmaline. Apy = arsenopyrite, Cbt = cobaltite, Cpy = chalcopyrite, Sp = sphalerite, Tm = tourmaline.

Garnet-rich unit

The garnet-rich unit is an altered, medium grey basalt with 5 to 20 vol.% disseminated, coarse-grained garnet and contains 150 ppb Au on average. It also contains 20 vol.% quartz, 5 vol.%

sericite and 5 vol.% tourmaline, as well as traces of ilmenite, pyrite and biotite. Most occurrences of this unit are as irregular domains within the tourmalinite unit.

Mineralization in the sulfide breccia

The minerals associated with potentially economic concentrations of Au (as electrum) at Black Dog comprise tourmaline, pyrite, chalcopyrite, sphalerite, arsenopyrite, cobaltite, quartz, muscovite, hessite, matildite and bismuth tellurides. They are found in the sulfide breccia unit, which cross-cuts the tourmaline breccia unit and is preferentially located at its margins or as a network inside the breccia. Pyrite occurs as grains 1 to 5 mm in diameter, and constitutes 40 vol.% on average of the sulfide breccia unit; pyrite is also present as inclusions in tourmaline and locally replaced tourmaline. Cobaltite and arsenopyrite are finely disseminated among tourmaline and chalcopyrite in proportions ranging from 0.5 to 5 vol.% (avg. 2 vol.%) of the rock (Figure 9b and d). Chalcopyrite comprises ~ 20 vol.% of the sulfide breccia and, with sphalerite, fills fractures in pyrite and tourmaline (Figure 9a to d). Traces of electrum, hessite, matildite and bismuth tellurides occur along the margins of pyrite or arsenopyrite crystals and are intergrown with chalcopyrite (Figure 10b and c), and more rarely, occur as inclusions in chalcopyrite (Figure 10a).

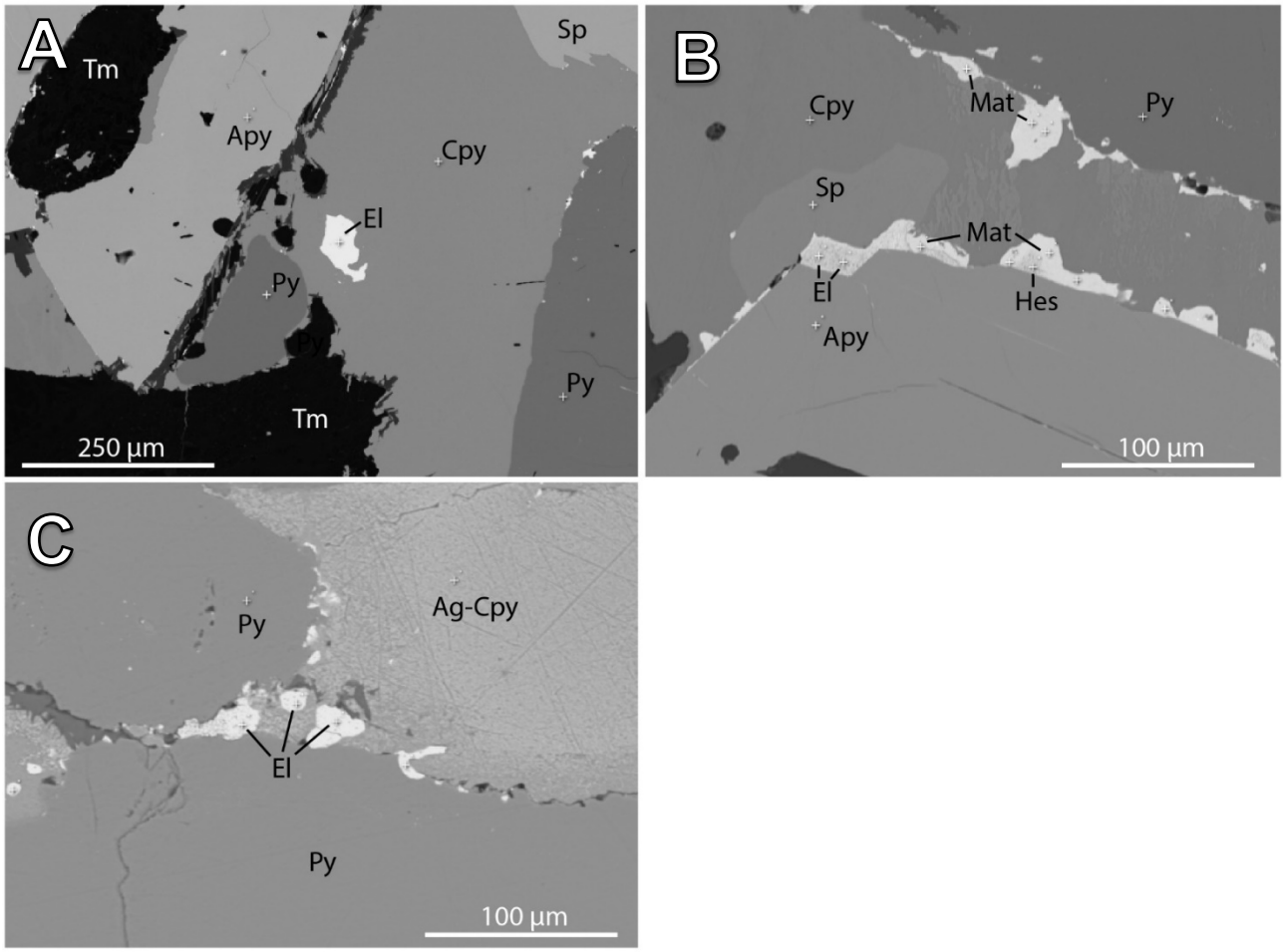

Figure 10: Backscattered electron images of electrum and associated phases. A) A large electrum grain in chalcopyrite, in close spatial association with arsenopyrite, pyrite and sphalerite. B) Several electrum grains in association with matildite and hessite in chalcopyrite and associated sphalerite, pyrite and arsenopyrite. C) Electrum grains in chalcopyrite and adjacent pyrite. Chalcopyrite locally contains up to 2 wt% Ag. Apy = arsenopyrite, Cpy = chalcopyrite, El = electrum, Hes = hessite, Mat = matildite, Py = pyrite, Sp = sphalerite, Tm = tourmaline, Ag-Cpy = Ag-rich chalcopyrite (up to ~1% Ag).

The gold to silver mass ratio in electrum varies from 0.7 to 2 and averages ~ 1.2, though in some large (200 µm) grains in chalcopyrite the ratio reaches 8; the electrum grains typically have a diameter in the range 5 to 50 µm (avg. 15 µm). Locally, the sulfide paragenesis is suggested by pyrite crystals have been overgrown sequentially by arsenopyrite, followed by cobaltite and

chalcopyrite (Figure 11). However, arsenopyrite may also occur as inclusions in pyrite (Figure 11) suggesting that their crystallization may have been concurrent. The Au-Ag mineralization clearly post-dated pyrite and arsenopyrite and was either synchronous with chalcopyrite crystallization or pre-dated the latter (Figure 10). A mineral paragenesis for the deposit is presented in Figure 12.

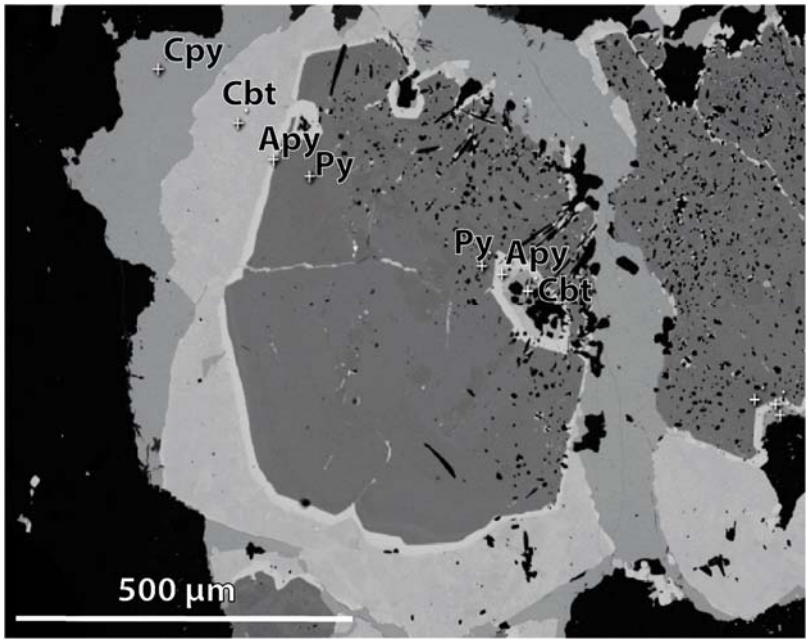

Figure 11: A backscattered electron image of pyrite with arsenopyrite and cobaltite overgrowths and later, fracture-filling chalcopyrite that surrounds and cut through the overgrown pyrite-arsenopyrite-cobaltite grain.

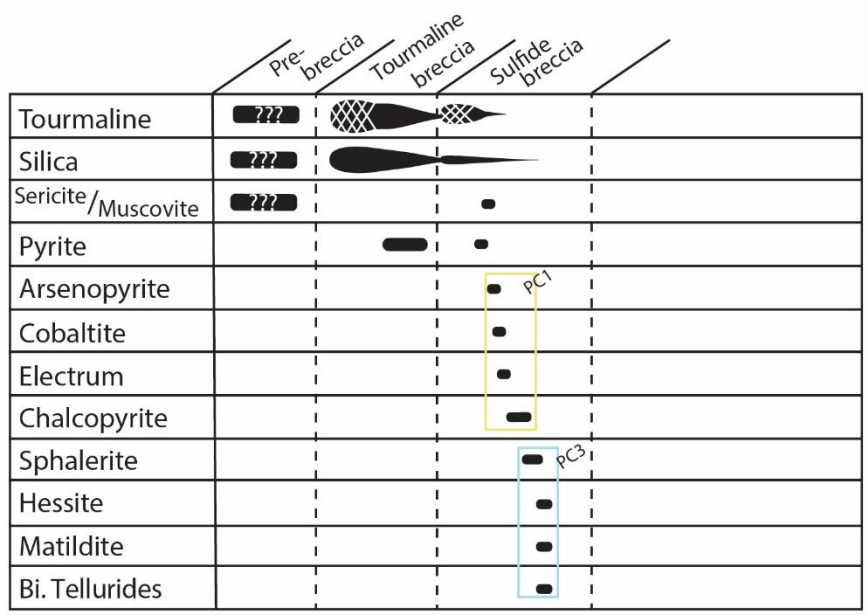

Figure 12: Paragenesis. Note that A-type tourmaline is related to the pre-breccia alteration and is mostly contained in the tourmaline veinlet altered basalt and tourmalinite units, whereas B- and C-type tourmaline are more common in the tourmaline breccia and sulfide breccia units, respectively.

2.5 Tourmaline chemistry

The tourmaline shows evidence of multiple stages of crystallization and some crystals record up to seven stages of tourmaline growth (Figure 13). Three main tourmaline types have been distinguished based on the mode of occurrence of the tourmaline crystals. They are: Type A), which occurs as rare fans in the tourmalinite and tourmaline stockwork; Type B) very fine-grained tourmaline comprising most of the tourmaline breccia and the tourmalinite units; and Type C) cryptocrystalline tourmaline, which is mainly restricted to the sulfide breccia unit. These textural varieties of tourmaline differ in their chemical compositions as described below.

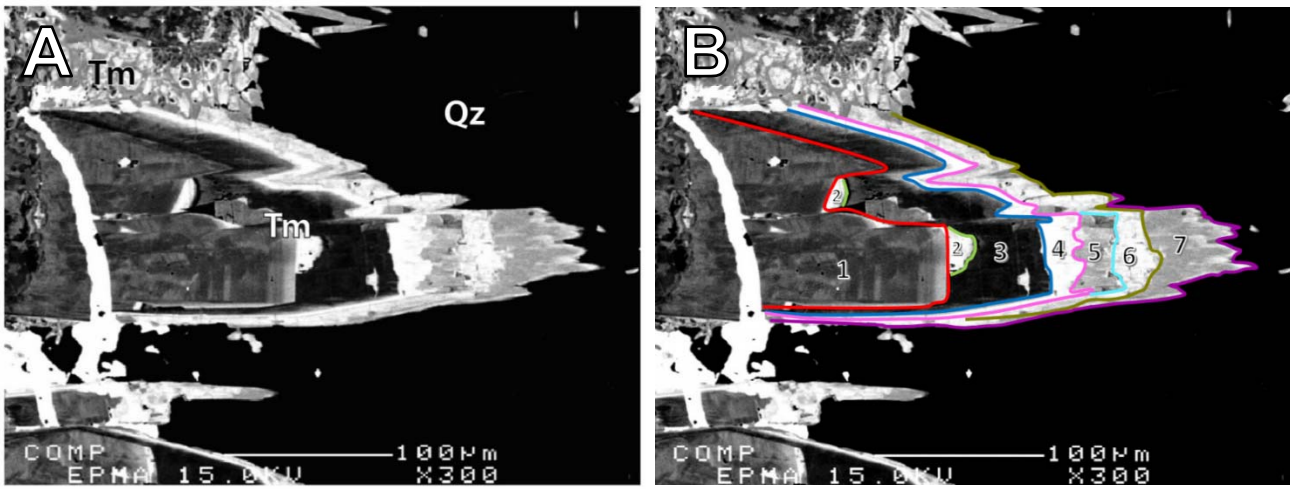

Figure 13: SEM backscattered electron images showing growth zones in a tourmaline crystal from the tourmalinite unit. Zones 1 to 3 correspond to the A-type tourmaline event, whereas zones 4 to 7 and the medium-grained tourmaline matrix (above the zoned grain) are related to the B-type tourmaline event.

Major elements

The variations in the major element compositions of the different tourmaline types provide valuable information regarding the nature and evolution of the fluids responsible for alteration and mineralization. Figure 14 shows compositional data for the A-, B- and C-type tourmaline determined from electron microprobe analyses. Concentrations of Ca and F decrease sharply from Type A to Type C, whereas Ti and Si concentrations decrease more subtly, and that of Fe increases. Sodium is more abundant in Type B tourmaline, whereas Al appears to increase from Type A to Type C tourmaline. Potassium concentrations are relatively similar and constant for the three tourmaline types. Based on Henry et al. (2011), the three types of tourmaline all belong to the alkali, oxy, Al-dominant, and dravite to schorl subgroups. Figure 15a) and b) illustrate the distribution of the three tourmaline types in terms of alkali - calcic - X-site vacancy and composition (schorl to dravite), respectively. As is evident from Figure 15a), Type B tourmaline

plots closer to the potassic and sodic apex and is less calcic than A-type tourmaline. Type C tourmaline has a slightly greater proportion of X-site vacancies than Types A and B. It is also evident that only A-type tourmaline is dominantly dravitic; Type B and Type C tourmalines are schorlitic and there is a progressive increase in the iron content from Type B to Type C (Figure 15b).

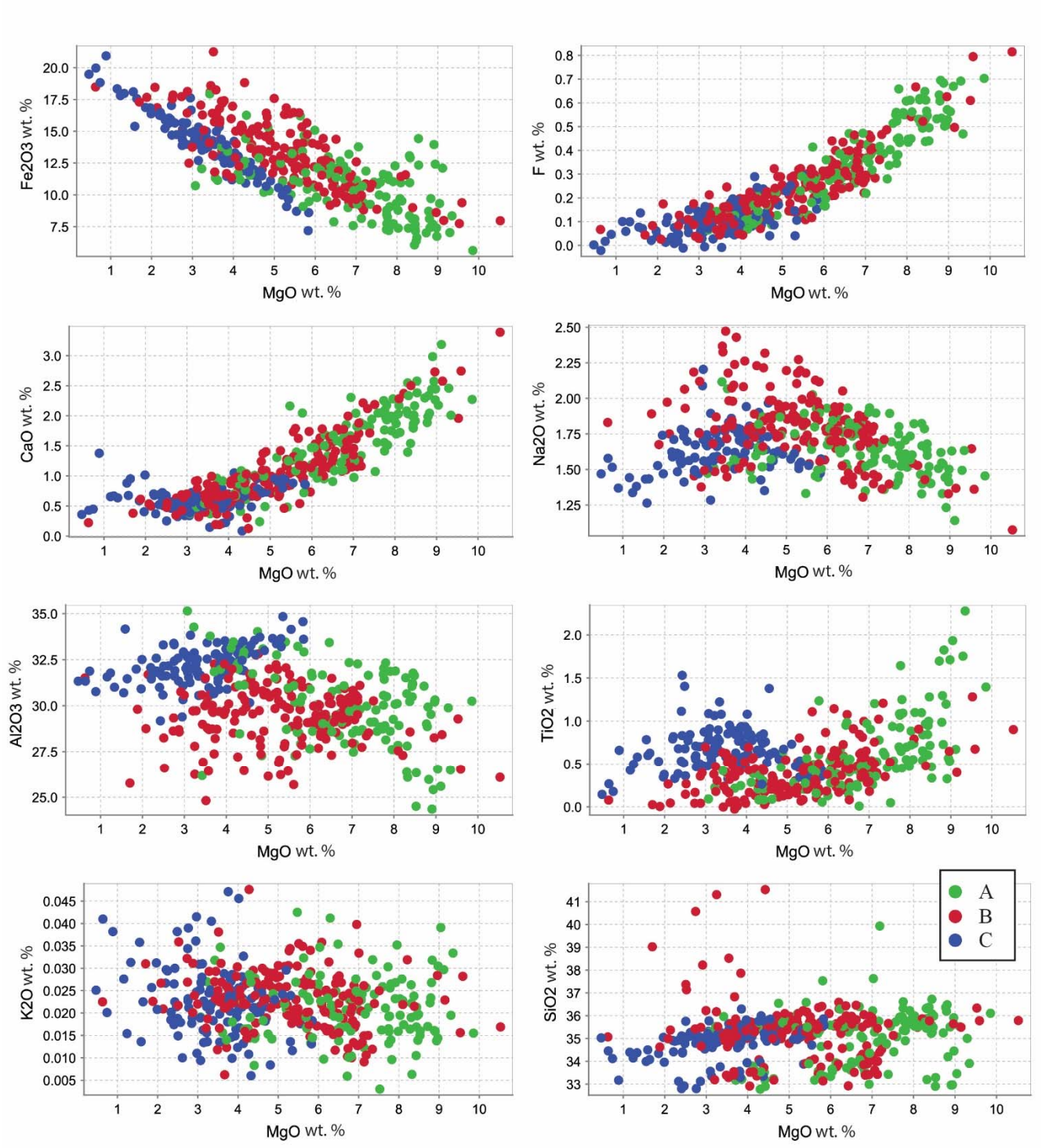

Figure 14: Compositions of individual tourmaline crystals as a function of MgO content. The green symbols correspond to A-type tourmaline, and the red and blue symbols represent the B- and C-type tourmaline, respectively.

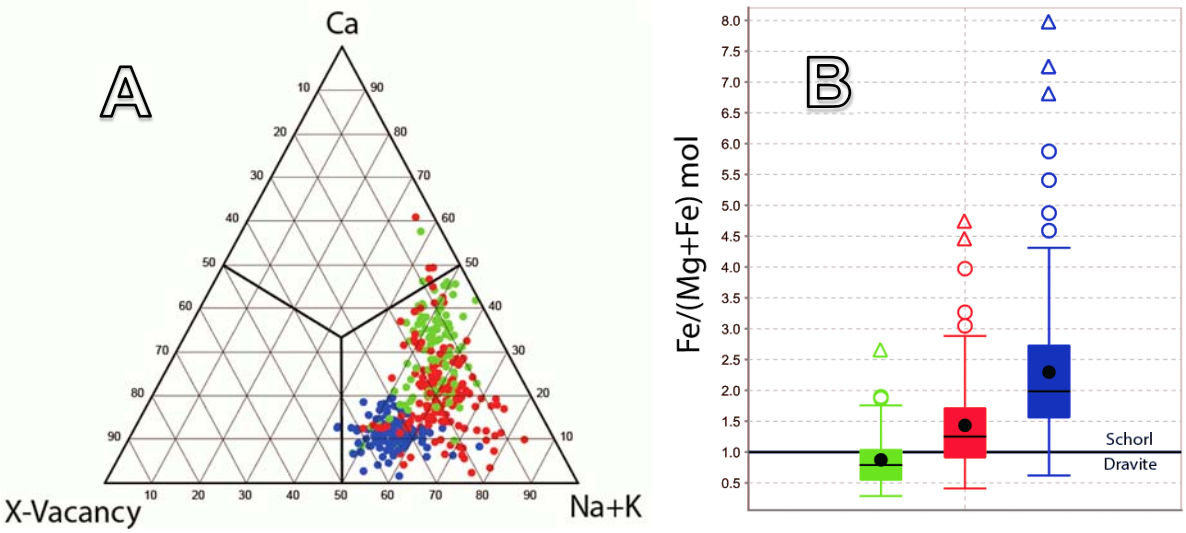

Figure 15: Tourmaline classification diagrams. a) Ternary diagram showing the X site allocation, and b) box-whisker plots of the Fe/(Fe+Mg) molar ratio. Green, red and blue represent A-, B- and C-type tourmaline events, respectively. Almost all tourmaline crystals have compositions that plot in the alkali field in a); b) shows illustrates the evolution of the tourmaline from dravitic to schorlitic compositions.

Trace elements

Figure 16 illustrates trace element concentrations as a function of the Mg content of the tourmaline. The As concentration increased systematically with the evolution of the hydrothermal system from Type A to Type C tourmaline (from an average of ~50 ppm to ~145 ppm). By contrast, Co and Zn concentrations are very similar in Type A and Type B tourmaline (~100 ppm Co and ~250 ppm Zn), whereas their concentrations are significantly higher in Type C tourmaline (200 ppm Co and 800 ppm Zn). Furthermore, whereas the Cu, Ag and Bi contents of Type A and Type B tourmaline are consistently low (means of ~5 ppm Cu, BDL Ag, BDL Bi), they are sporadically elevated in Type C tourmaline (up to 2050 ppm Cu, 25 ppm Ag, 37 ppm Bi). Thus, it appears that the composition of Type C tourmaline reflects a relatively sudden increase in the concentration of Co, Zn, Cu, Ag and Bi in the hydrothermal fluid immediately prior to the formation of the sulfide breccia unit.

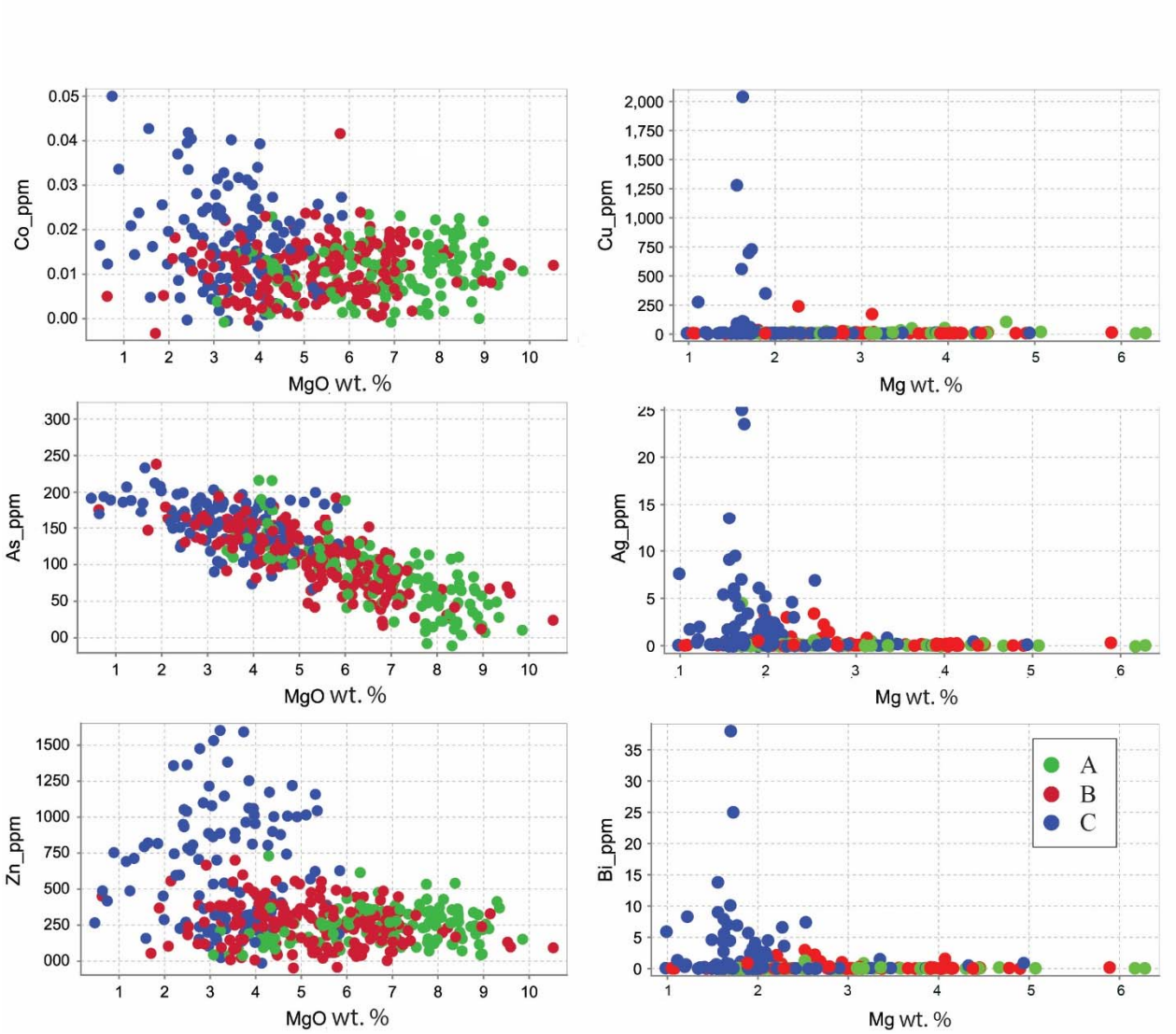

Figure 16: Trace element compositions of tourmaline as a function of MgO content. The green, red and blue symbols represent type A, B and C tourmaline, respectively. C-type tourmaline contains significantly more Co, As and Zn than the other tourmaline types and is closely the sulfide mineralization. This tourmaline type also contains more Cu, Ag and Bi than the other tourmaline types.

2.6 Sulfur Isotopes

Sulfur isotope analyses were conducted on homogenous (at the microscopic scale) pyrite, chalcopyrite and sphalerite crystals that appeared to be in textural equilibrium (Figure 9b) and d).

The $\delta^{34}S$ values for the three sulfide minerals fall in a narrow range from +1.7 and +3.6‰, averaging 2.7 ± 0.1 ‰ and are presented in Figure 17.

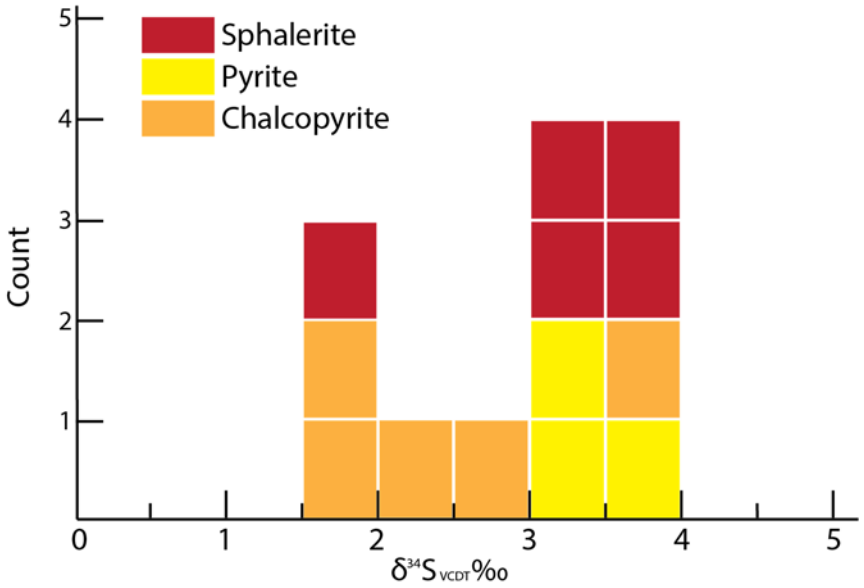

Figure 17: A histogram of sulfur isotope sample values for pyrite, chalcopyrite and sphalerite. VCDT: Vienna-Canyon del Diablo Troilite.

Pyrite, chalcopyrite and sphalerite have average $\delta^{34}S$ values of +3.4, +2.5, and +3.1 ± 0.1 ‰, respectively. These correspond to H_2S equivalent values of +2.0, +2.3 and +2.5 ‰ and fall within the range of granitic rocks (Hoefs, 2018) and magmatic sulfides (Giuliani et al., 2016). The data for the different mineral pairs were used to determine temperatures of deposition based on the sulfur isotope geothermometers proposed by Kajiwra and Krouse (1976) for pyrite-chalcopyrite and pyrite-sphalerite, and that of Li and Liu (2006) for chalcopyrite-sphalerite. Six of the eight pairs analyzed returned results that are geologically reasonable (Table 1). The calculated temperatures range between 414 and 606°C and average 496 ± 20°C. The pyrite-chalcopyrite, pyrite-sphalerite and chalcopyrite-sphalerite pairs yielded average temperatures of 414, 501 and 548 °C, respectively. One sphalerite-pyrite pair returned a higher $\delta^{34}S$ for pyrite than the coexisting sphalerite, precluding a temperature estimate, and a chalcopyrite-sphalerite

pair yielded an unreasonable temperature of 1609 °C. Despite apparent textural equilibrium, some of the sulfides in these pairs were clearly not in isotopic equilibrium.

2.7 Discussion

Although the Black Dog prospect occurs in an area where there are numerous VMS and orogenic gold deposits, it differs from these deposit types in a number of important respects. The most obvious of these differences is in the abundance of tourmaline, which is the dominant mineral at Black Dog, but is a minor phase in some of the orogenic gold deposits and is largely absent from the VMS deposits.

Geometry, textures and mineralogy

There is a striking resemblance of the Black Dog deposit to tourmaline breccias that are associated with porphyry-copper deposits in the Chilean Cordillera. Black Dog and these younger tourmaline breccias are characterized by silicified, jigsaw-textured clasts of varying sizes in a microcrystalline tourmaline matrix, with fracture-filling sulfides localized at or near the breccia margins and/or cross-cutting the breccia (Sillitoe, 1985; Corbett et al., 1997). Both the Chilean breccias and Black Dog deposit contain chalcopyrite and electrum as the main copper- and gold-bearing minerals, respectively, and the tourmaline compositions of both range from alkali, oxy, Al-dominant dravite to schorl (Frikken et al., 2005; Dill et al., 2012). Like the Chilean tourmaline breccia pipes, the Black Dog breccia is sub-vertical and cross-cuts lithologies. The vertical extent of the Black Dog breccia is at least 700 m, which is comparable to the vertical extent of the tourmaline breccia pipes in the Andes and elsewhere (Frikken et al., 2005; Garrido et al., 2010).

Principal component analysis on bulk-rock chemistry

Many processes including initial volcanic environment, sedimentary processes, alteration and mineralization contribute to the final major and trace element composition observed in bulk-rock chemistry. These phenomena will respectively impact certain groups of elements and affect their concentrations simultaneously and generate correlations. Even though how the different processes affect the concentration of affected elements is generally well understood, the suite of elements they affect overlaps frequently and simple correlation matrixes might not be powerful enough to sort through them or quantify their impact.

More information can be extracted from these correlations using principal component analysis to determine the different processes affecting the resulting whole rock chemistry and reduce the number of variables (Grunsky, 2010; Grunsky, 2013; Perrouty, 2019). Samples with missing data were omitted and the data was not log-transformed as there was no important skewness. The high values in Cu, Ag and Bi are rather the effect of a different population than a skew in the data .Principal component analysis was applied to the bulk-rock geochemical data from all the drill hole samples using a Varimax rotation (Figure 18) (Kaiser, 1958). Principal components 1, 2 and 3 explain close to 73% of the total variance. Principal components 1 (PC1) and 3 (PC3) correspond to the base and precious metals, whereas Principal component 2 (PC2) mainly represents the chemical signature of the protolith on the positive side and the alteration on the negative side. The anti-correlation between rock forming elements and alteration is explained by the fact that the rocks that were affected by tourmaline alteration were depleted in primary rock-forming elements and enriched in the alteration minerals, creating an anti-correlation between those two groups. Although B and S appear to have been the only elements that were added to the rock during the tourmaline alteration/brecciation event, i.e., they plot on the negative side of

PC2. It is noteworthy that Ti, K and Fe plot closer to the origin than the other rock-forming elements, particularly Ca, Al, Mg and Na. This difference in correlation likely reflects the addition of K, Fe and small amounts of Ti by the hydrothermal fluids and/or preferential displacement of the other rock-forming elements. Titanium is concentrated in tourmaline, which contains ~0.6 wt.% Ti that was derived from the precursor basalt, whereas the widespread occurrence of sericite in the host rock and pyrite in the tourmaline breccia derived K and Fe from the fluid. Despite this, the hydrothermal alteration resulted in an overall decrease in these elements, but not as much as for Ca, Al, Mg and Na. Although the base and precious metal concentrations are generally correlated, the fact that these groups of elements are attributable to different principal components indicates that the two groups differed in either their timing or mode of deposition. Principal component 1 mostly comprises Au, Co and As ± Cu, whereas PC3 reports Ag, Zn, Bi and Pb ± Cu. As deposition of Au was clearly later than that of Co and As (Figs. 9 and 10), it seems most likely that the association of Au with Co and As in PC1, reflects the well-known affinity of Au for As because of the p-type character of arsenian pyrite and arsenopyrite which promotes deposition of negatively charged gold complexes (Williams-Jones et al., 2009). Support for this interpretation is provided by the fact that electrum is commonly concentrated on the surfaces of pyrite and arsenopyrite crystals (Figs. 9b and c).

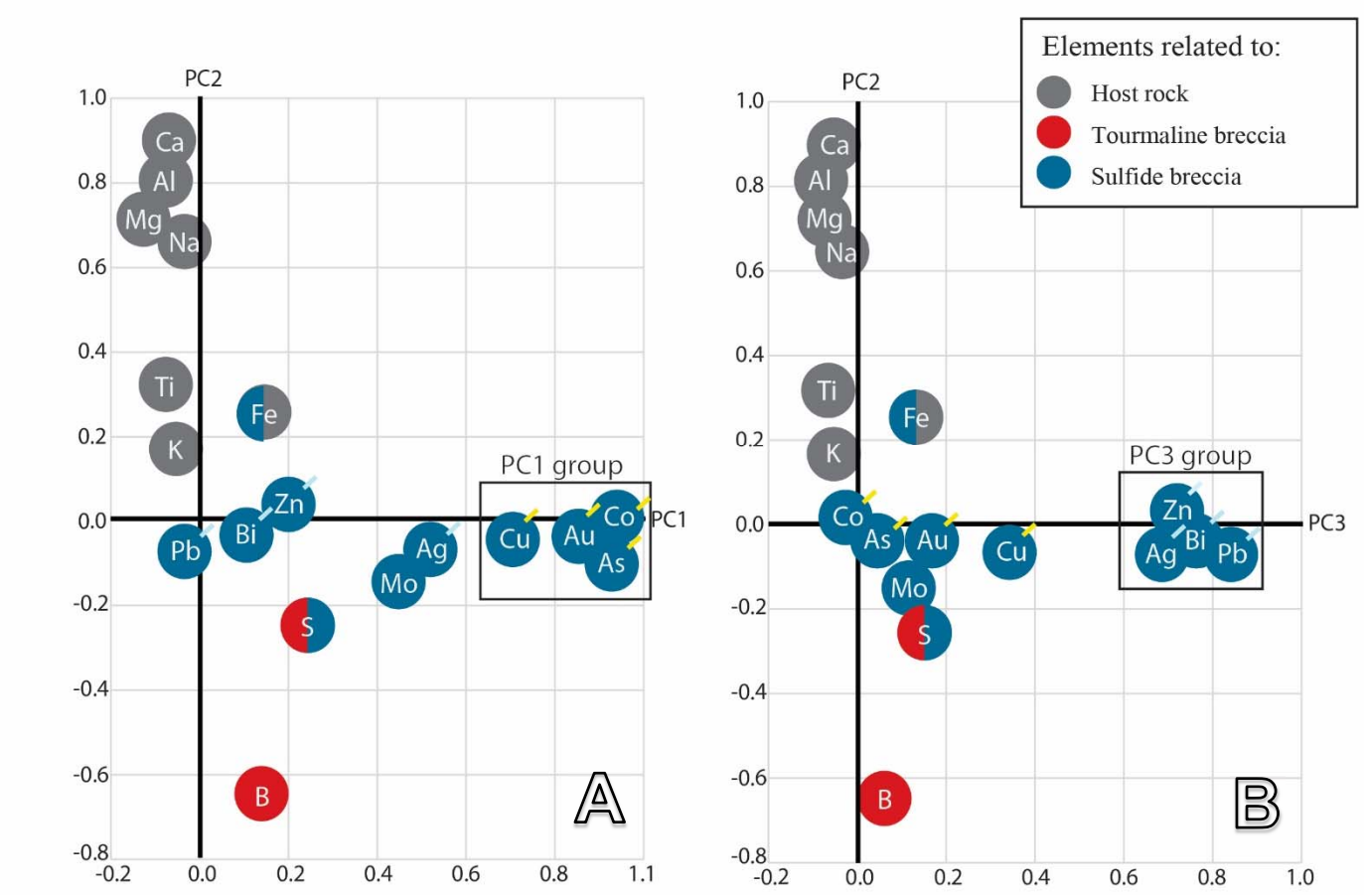

Figure 18: Principal component diagrams illustrating whole rock compositions. PC2 is associated with rock-forming mineral elements on the positive side and tourmaline alteration/on the negative side. PC1 and PC3 are both associated with mineralization, with PC1 being related to Cu, Co, As and Au mineralization, possibly deposited earlier than the PC3 component (Zn, Ag, Pb, Bi).

Tourmaline chemistry

The trace element content of tourmaline can reveal important information concerning the fluids that generated the associated mineralizing system. The ability of tourmaline to incorporate trace elements of various sizes and charges and its resistance to subsequent alteration make tourmaline a potentially powerful exploration tool (Griffin et al., 1996; Koval et al., 1991; Slack et al., 2011). The distribution of the trace metals in tourmaline is homogenous within single crystals in the Black Dog deposit, suggesting that these elements do not occur as inclusions in the

tourmaline but are incorporated in its mineral structure. As is the case with tourmaline in the Chilean breccias, where there is an enrichment in the metals constituting the ore minerals present in the deposit in which they occur (Griffin et al., 1996), the Black Dog tourmaline is also enriched in ore metals. Indeed, the last stage of tourmaline crystallization, which is associated with the gold mineralizing event is enriched in Cu, Zn, Co, As, Ag and Bi, metals that are all present in significant quantities in the ore minerals.

Pressure and temperature conditions of ore deposition

Based on an abundance of chlorite and a general lack of metamorphic amphiboles, basalts in the vicinity of Tourmaline Hill are interpreted to have undergone upper greenschist to lower amphibolite facies metamorphism (Rhéaume et al., 2004), corresponding to temperatures up to 550˚C. In basalts, the brittle-ductile transition takes place between 600 and 850°C depending on the deformation rate (Violay et al., 2015). Assuming an Archean geothermal gradient of 60° C per km (Burke et al., 1978; Lambert, 1980; Jarvis et al., 1983; Martin, 1986), this transition would have occurred at a depth between 9 and 15 km. As the Black Dog deposit is a breccia characterized by angular clasts, it follows that it must have formed at a depth significantly above the brittle/ductile transition. By comparison, tourmaline breccias associated with porphyry systems in Chile are generally interpreted to have formed at depths of 1 to 4 km (Corbett et al., 1993, Profett, 2009, Richards, 2018). This implies a much shallower emplacement of the Black Dog deposit than orogenic gold deposits, which are generally considered to form at depths close to the brittle/ductile transition (Groves et al., 1998; Goldfarb et al., 2005). Considering that the Black Dog tourmaline breccia is undeformed, cuts through regional foliation and contains clasts displaying clear remnants of a pre-existing foliation, we conclude that the alteration and mineralization occurred after regional deformation. However, as this breccia and mineralization

appears to have been produced by fluids released by an intrusion that was cogenetic with the Windfall (2697 ± 0.9 Ma) and Barry (2697 ± 0.6 Ma) intrusions, it is possible that the alteration and mineralization pre-dated peak metamorphism (2643 to 2677 Ma).

Based on the results of the sulfur isotope analyses reported above, the Black Dog deposit is interpreted to have formed at a temperature between 414 and 616 °C; the average temperature is 496 ± 20 °C. These temperatures are very similar to temperatures estimated for the Chilean tourmaline breccias, based on the homogenization of fluid inclusions in quartz, which range from 400 °C to 690 °C (Frikken et al., 2005; Skewes and al., 2002). In summary, the Black Dog tourmaline breccia-hosted Black Dog deposit is interpreted to have formed at a temperature of ~ 500°C and a depth less than 9 km and possibly as little as 1 km.

Competing hypotheses for the genesis of the Black Dog prospect

The origin of the Black Dog Au-Cu prospect has been debated since the late 1980's. Gaboury (1991) proposed that the mineralization had a sedimentary exhalative (SEDEX) origin, mainly because the host rocks had been interpreted to be sedimentary. Although tourmaline can be an important mineral in SEDEX deposits (e.g., Sullivan, BC; Jiang et al., 1999), most of the common features of SEDEX environments are not evident at Black Dog. Typically, SEDEX deposits contain Zn and Pb or Cu but not Au as the principal ore metals, form at low temperature, and are emplaced in extensional basins and hosted by sedimentary rocks (generally shales and carbonates). In contrast, the main ore metals at Black Dog are Cu and Au, which were deposited at relatively high temperature, dominantly in intermediate to mafic volcanic rocks.

Considering that orogenic gold deposits are common in the Abitibi region and in greenstone belts generally, and that in some cases they are associated with quartz-tourmaline veins (e.g., Sigma, (Robert, 1986)), it is reasonable to consider the possibility that Black Dog is a variant of an

orogenic-type deposit. Like Black Dog, the latter deposits commonly occur in the sheared rocks of second order deformation zones (Groves et al., 1998 and Goldfarb et al., 2005). However, to our knowledge, there have been no reports of Archean orogenic-type gold deposits associated with tourmaline breccias. Moreover, orogenic deposits are commonly depleted in chalcopyrite because copper is, in general, highly soluble at typical orogenic conditions (Grondin and Williams-Jones, 2004), whereas the gold at Black Dog is associated with strong copper enrichment. Because the sulfur in orogenic gold deposits commonly comes from a variety of sources, including both metamorphic and magmatic sources (Chang et al., 2008; Hodkiewicz et al. 2008), such deposits commonly display a wide range of sulfur isotope ratios. Indeed, the $\delta^{34}S$ values for pyrite in Archean orogenic gold deposits range between -18 and +12‰ and, even within individual deposits, the range is as high as ~10‰ $\delta^{34}S$ (Molnár et al., 2016; Goldfarb et al., 2005). In contrast, the $\delta^{34}S$ values for the sulfide minerals at Black Dog occupy a narrow range (+1.7 to +3.6‰) corresponding to values for H_2S in the fluid of +1.5 to + 2.9‰. These values are very close to those for sulfide minerals of magmatic origin -0.3 ±2.3‰ (Seal, 2006) and consistent with those reported for sulfides from tourmaline breccias associated with porphyry copper deposits in the Andes and elsewhere (+2‰ average for the mineralizing system, El Salvador copper porphyry, Field et al., 1976; -4.1 to +2.7‰ on pyrite, Sur-Sur tourmaline breccia, Frikken et al., 2005; -0.8 to 1.3 ‰ on chalcopyrite, Tuwu porphyry copper, Wang et al, 2017). Finally, whereas the gold to silver mass ratio in the Black Dog electrum is 1.2:1 on average, in most orogenic gold deposits the ratio varies from 5:1 to 10:1 to (Groves et al., 1998).

As mentioned previously, tourmaline breccias are rare in the Abitibi and other Archean greenstone belts. However, such breccias are observed commonly in Phanerozoic continental volcanic arcs, particularly in association with porphyry deposits. Many of these deposits are

characterized by late stage fracture-filling sulfides with high gold and copper grades (Sillitoe and Sawkins, 1971; Sillitoe, 1985). Indeed, the ore contained in these tourmaline breccias can represent a significant proportion of the total resource of some porphyry copper deposits (Frikken et al., 2005).

Porphyry- and intrusion-related tourmaline breccias tend to be matrix-supported, and the matrix is typically dominated by microcrystalline tourmaline that ranges in composition from dravite to schorl. These features are very similar to those, described above, for the Black Dog breccia. Because of their hydrothermal cement, the shape of their fragments, the mineralogy and the style of mineralization and alteration, these breccias are generally interpreted to be the products of magmatic-hydrothermal processes (Sillitoe and Sawkins, 1971; Sillitoe, 1985). The breccia clasts tend to be strongly silicified, angular, range from millimeters up to a meter in diameter, and locally display jigsaw textures. Tourmaline breccias related to porphyry copper deposits commonly occur within or on the margins of felsic (porphyritic) intrusions, although this is not universally the case. Despite the fact that intrusions are not observed at Black Dog, the Urban-Barry greenstone belt, as noted above, contains many felsic intrusions of calc-alkaline affinity, including the nearby mineralized Barry Lake intrusions (their strong calc-alkaline signature is indicated by a Zr/Y ratio > 20; Kitney et al., 2011), which are located along the same regional deformation trend as Black Dog. Moreover, the gold mineralization at Windfall Lake, which also occurs along the same deformation trend, is located along the margins of intrusions that are of calc-alkaline affinity (Hardie, et al., 2018). Although no intrusions are exposed in the immediate vicinity of the Black Dog prospect, it is important to note that breccias can develop significant distances above magmatic bodies. For example, no drill hole has penetrated below the roots of the Donoso and Sur-Sur breccia pipes in Chile, despite reaching depths of 800 m and 1 km,

respectively (Skewes et al., 2003; Frikken et al., 2005). The observation that tourmaline breccias can extend well beyond their magmatic sources could explain why no intrusions have been discovered at Black Dog. Finally, porphyry copper and other intrusion-related deposits generally display a narrow range of sulfur isotope signatures centered around 0‰, which is consistent with magmatic sources (Hoefs, 2008). Tourmaline crystals in such deposits also display oscillatory growth zoning in which FeO and MgO + CaO are anti-correlated, which is also the case at Black Dog. The contents of the other major elements are relatively constant, except for Ti, which reaches its highest concentration in late tourmaline as is the case at Black Dog (Hohf et al., 2014).

The Genesis of the Black Dog Deposit

In light of the evidence presented above, it appears likely that the alteration and gold and copper mineralization at Black Dog were the products of intrusion-related fluid overpressure-induced brecciation and cooling. This is illustrated in a schematic cross-section (Figure 19). In our model, the mineralizing fluids originated from an underlying intrusion with a composition similar to that of the neighboring Barry Lake and Windfall Lake intrusions. As the magma rose, pressure decreased and the ability of the magma to dissolve an aqueous phase was greatly reduced, leading to aqueous phase saturation. Consequently, there was rapid exsolution of fluid that produced large overpressures, which brecciated the rocks. These processes resulted in a sharp decrease in temperature, which caused tourmaline to precipitate and later the ore minerals associated with gold mineralization. Fluids focused by the breccia pathways infiltrated into the adjacent rocks, leading to pervasive silicification and tourmaline alteration of basalts adjacent to the breccia pipe, and formation of ptygmatic tourmaline veins. The ptygmatic texture of the tourmaline veins was likely controlled by compositional layering in the host rock, which led to

preferential replacement of some layers by tourmaline (Dietrich, 1959). The angular silicified clasts underwent relatively little post-emplacement movement, as indicated by the well-preserved jigsaw breccia texture. Towards the end of the emplacement of the breccia pipe, the fluids became progressively more focused in the remaining permeable parts of the breccia, i.e., its contacts with the adjacent tourmalinite units. Mineralization was therefore concentrated at the margins of the breccia. When the fluids had cooled sufficiently, they became saturated in sulfide minerals and deposited pyrite, arsenopyrite, and cobaltite. With further cooling, the fluids became saturated in chalcopyrite and sphalerite, which then precipitated together with electrum and tellurides. These phases were concentrated at the surfaces of pyrite and arsenopyrite, due perhaps to the positive charge on these surfaces, which would have promoted adsorption of the aqueous gold and silver species

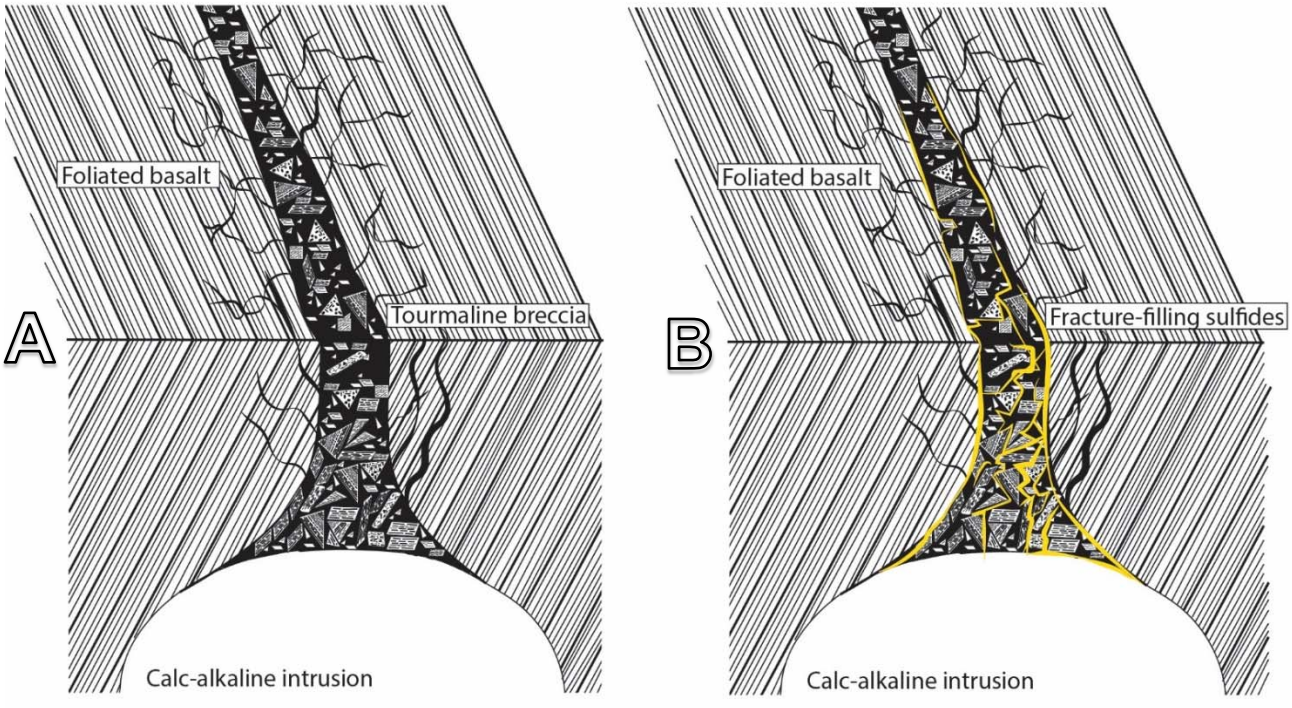

Figure 19: Hypothetical cross-sections of the Black Dog prospect. a) Alteration fluids brecciate through foliated basalt, generating angular silica and tourmaline altered clasts of various shapes and sizes. Some clasts display planar features that appear to be preferential replacement

of certain layers of the foliation. Ptygmatic veinlets sourcing from the main breccia run into the surrounding foliated basalt and are not confined to foliation plans. b) Fracture filling sulfides are injected in the tourmaline matrix and are preferentially located at the contact of the matrix with the host rock.

On the basis of sulfur isotope geothermometry, the breccia pipes are interpreted to have formed at temperatures of ~500 °C, which suggests, in turn, that the gold was transported in solution as chloride complexes (Williams-Jones et al., 2009). At this temperature, the mineralizing fluids were above the critical point and did not boil. In the absence of boiling and evidence of wall-rock interaction, cooling induced by adiabatic expansion of the fluid during brecciation or perhaps mixing with meteoric water was the likely cause for the precipitation of Au and Cu at Black Dog. Indeed, a drop of 100 °C from an initial temperature of 500 °C would have decreased the solubility of gold by roughly an order of magnitude.

2.8 Conclusions

The Black Dog prospect is a unique example of an Archean gold deposit hosted by a tourmaline breccia that is very similar in many respects to breccia pipes associated with porphyry copper deposits in more recent continental arc settings. The alteration, metal signature, mineralization textures, sulfur isotope ratios, and emplacement conditions suggest that Black Dog is the product of dominantly magmatic fluids originating from an underlying intrusion. The evolution of tourmaline trace metal compositions through the different alteration and mineralization stages suggests that Au-Cu deposition was the end stage of a long-lived episode of tourmaline alteration and brecciation. A microcrystalline tourmaline matrix with silicified clasts displaying a jigsaw texture is a common feature of tourmaline breccias associated with Andean porphyry copper deposits. The late stage, fracture-filling texture of the Au-Cu mineralization as well as its concentration at the margins of the breccia and in veins that cross-cut the main breccia body are

also characteristics of these deposits. The limited range of the sulfur isotope values and the temperatures calculated from sulfide pairs suggest that the source of the fluids and the conditions of formation of the Black Dog tourmaline breccia were similar to those of many of the breccias associated with Andean porphyries. Together, these arguments contradict previously proposed models for Black Dog, namely those for SEDEX, VMS or orogenic deposit types. Finally, we note that there is a possibility that Black Dog is related to the nearby Barry Lake deposit and the intrusion-related Windfall Lake deposit, and that all could be expressions of calc-alkaline magmatic hydrothermal systems of the type that formed the porphyry and epithermal deposits of Chilean Andes.

In closing, we note that there is a strong correlation between the trace metal composition of tourmaline and its proximity and timing with respect to gold and copper mineral deposition. In particular, concentrations of Co, As, Zn, Cu, Ag and Bi are elevated in tourmaline associated with Au-Cu mineralization. Given the resistance of tourmaline to chemical weathering, this could be developed as a heavy mineral exploration tool for till and other surface samples in which tourmaline may concentrate.

2.9 Acknowledgements

Funding for this research was provided Osisko Mining, who also provided access to GIS data, to the prospect, to drill core and a large number of whole-rock geochemical analyses, and by the "Fond de Recherche du Québec – Nature et Technologies" in the form of a scholarship to the first author.

Rebecca Paisley and Anna Katharina Jung were of great help with data treatment and instrument operation for LA-ICP-MS analyses, Land Shi has has been essential in performing the EMP analyses and Jean-Philippe Desrochers, Pierre-Hughes Lamirande, Roman Hanes and Antoine

Ouellet were of great help on understanding the mineralizing system, regional geology and metamorphic condition. I would also like to thank Vincent van Hinsberg, Duncan McLeish, Emily Laycock and Édouard C. Lavoie for their invaluable inputs.

2.10 References

Baksheeva I. A., Chitalinb, A. F. , Yapaskurta V. O., Vigasinaa, M. F. ,Bryzgalova, I. A., and Ustinovc, V. I. (2010) Tourmaline in the Vetka Porphyry Copper–Molybdenum Deposit of the Chukchi Peninsula of Russia, Moscow University Geology Bulletin, vol. 65, pp.27–38.

Bandyayera, D., Rhéaume, P., Doyon, J., Sharma, N. M. (2004) Géologie de la région du lac Hébert (32G/03) - RG 2003-07, Ministère des Ressources Naturelles et de la Faune, Québec.

Bandyayera, D., Théberge, L., Fallara, F. (2002) Géologie de la région des lacs Piquet et Mesplet (32G/04 et 32G/13) - RG 2001-14, Ministère des Ressources naturelles et de la Faune, Québec.

Burke, K., Kidd, W. S. F. (1978) Were Archean Continental Geothermal Gradients Much Steeper than those Today?. Nature, vol. 272, pp. 240-241.

Corbett, G.J., Leach, T.M. (1997) South West Pacific Rim Gold-Copper Systems: Structure, Alteration and Mineralization, Short Course Manual, 282 pp.

Card, K.D., Poulsen, K.H. (1998). Archean and Paleoproterozoic Geology and Metallogeny of the Southern Canadian Shield. Exploration and Mining

Chang, Z., Large, R. R., Maslennikov, V. (2008) Sulfur Isotopes in Sediment-hosted Orogenic Gold Deposits: Evidence for an Early Timing and a Seawater Sulfur Source, Geology, vol. 36, pp. 971-974

Clark, A. H. (1965) The Mineralogy and Geochemistry of the Ylöjärvi Cu-W Deposit, Southwest Finland: Mackinawite-Pyrrhotite-Troilite Assemblages, Comptes Rendus de la Société Géologique de la Finlande, vol. 38, pp. 331-342.

Demiral, S., Goncuoglu, M.C., Topuz, G. (2009) Geology and Chemical Variations in Tourmaline from the Quartz-Tourmaline Breccias within the Kerkenez Granite-Monzonite Massif, Central Anatolian Crystalline Complex, Turkey. Canadian Mineralogist, vol. 47, pp. 787-799.

Dietrich, R. V. (1959) Geology and mineral resources of Floyd County of the Blue Ridge Upland, Southwestern Virginia: Virginia Polytech. Inst. Bull., vol. 52, no. 12, 160 p.

Dill, H. G., Garrido, M. M., Melcher, F., Gomez, M. C. (2012) Depth-related Variation of Tourmaline in the Breccia Pipe of the San Jorge Porphyry Copper Deposit, Mendoza, Argentina, Ore Geology Reviews, vol. 48, pp. 271-277.

Field, C. W., Gustafson, L. B. (1976) Sulfur isotopes in the porphyry copper deposit at El Salvador, Chile. Economic Geology, vol. 71, pp. 1533-1548.

Fletcher, C. J. N. (1977) The Geology, Mineralization and Alteration of Ilkwang Mine, Republic of Korea. A Cu-W Bearing Tourmaline Breccia Pipe. Economic Geology, vol. 72, pp. 753-768.

Frikken, P. H., Cooke, D. R., Walshe, J. L. (2005) Mineralogical and Isotopic Zonation in the Sur-Sur Tourmaline Breccia, Rio Blanco - Los Bronces Cu-Mo Deposit, Chile: Implications for Ore Genesis. Economic Geology, vol. 100, pp. 935-961.

Gaboury, D. (1991) Étude Pétrographique et Géochimique des Roches Hôtes de l'Horizon Aurifère Tourmalinisé Barry-Or, Canton Barry, Québec. Thèse de mémoire de projet de fin d'études, Université du Québec à Chicoutimi.

Garrido, M. M., Gómez, M. C., Fernández, M. L., (2010) Brecha de Turmalina del Pórfido de Cobre-Oro San Jorge, Mendoza: Alteración, Mineralización y Origen de los Fluidos. Revista de la Asociación Geológica Argentina, vol. 67, pp. 47-57.

Goldfarb, R., Baker, T., Dubé, B., Groves, D.I., Hart, C.J.R., Gosselin, P. (2005) Distribution, Character, and Genesis of Gold Deposits in Metamorphic Terranes. Economic Geology 100th Anniversary Volume, pp. 407-450.

Griffin, W. L., Slack, J. F., Ramsden, A. R., Win, T. T., Ryan, C. G. (1996) Trace Elements in Tourmalines from Massive Sulphide Deposits and Tourmalinites: Geochemical Controls and Exploration Application. Economic Geology, vol. 91, pp. 657-675.

Grondin, O., Williams-Jones, A. E. (2004) The Onaman Prospect, Ontario: An Unusual Occurrence of Cu-bearing Au Mineralization in a Shear Zone.

Groves, D. I., Goldfarb, R. J., Gebre-Mariam, M., Hagemann, S. G., Robert, F. (1998) Orogenic Gold Deposits: A Proposed Classification in the Context of their Crustal Distribution and Relationship to other Deposit Types, Ore Geology Reviews, vol. 13, pp. 7-27.

Grunsky, E. C. (2013) Predicting Archaean Volcanogenic Massive Sulphide Deposit Potential from Lithogeochemistry: Application to the Abitibi Greenstone Belt. Geochemistry: Exploration, Environment, Analysis, vol. 13, pp. 317–336.

Hardie C., et al. (2018) Preliminary Economic Assessment of the Windfall Lake Project, Lebel-sur-Quévillon, Québec, Canada. NI43-101 Technical Report, Osisko Mining Inc., August 2018, 826 p.

Henry, D. J., Milan, N., Hawthorne, F. C., Ertl, A., Dutrow, L. B., Uher, P., Pezzotta, F. (2011) Nomenclature of the Tourmaline-supergroup Minerals, American Mineralogist, vol. 96, pp. 895-913.

Himmi, R., Huhma, M., Hakli, T. A. (1979) Mineralogy and Metal Distribution in the Copper-Tungsten Deposit at Ylojarvi, Southwest Finland, Economic Geology, vol. 74, pp. 1183-1197.

Hodkiewicz, P. F., Grove, D. I., Davidson, G. J., Weinberg, R. F., Hagemann, S. G. (2008) Influence of Structural Setting on Sulphur Isotopes in Archean Orogenic Gold Deposits, Eastern Goldfields Province, Yilgarn, Western Australia, Mineralium Deposita, vol.44 pp, 129-150.

Hoefs, J. (2018) Isotope Fractionation Processes of Selected Elements, Stable Isotope Geochemistry, Springer Textbooks in Earth Sciences, Geography and Environment, pp. 53-227.

Hohf, M., Siefert, T., Ratschbacher, L., Rabbia, O., Krause, J., Haser, S., Cuadra, P. (2014) Mineralized and Barren Tourmaline Breccia at Rio Blanco-Los Bronces Copper Deposit, Central Chile. Geophysical Research Abstracts, vol. 16

Jarvis, G. T., Campbell, I. H. (1983) Archean Komatiites and Geotherms: Solutions to an Apparent Contradiction, Geophysical Research Letters, vol. 10, pp. 1133-1136.

Kaiser, H. F. (1958) The Varimax Criterion for Analytic Rotation in Factor Analysis, Psychometrika, vol. 3, pp. 187-200.

Kajiwra, Y., Krouse, H. R. (1971) Sulfur Isotope Partitioning in Metallic Sulfide Systems, Canadian Journal of Earth Sciences, vol. 8, pp. 1397-1408

Kitney, E. K., Olivo, G., R., David, D. D., Desrochers, J. P., Tessier, A. (2011) The Barry Gold Deposit, Abitibi Subprovince, Canada: A Greenstone Belt-Hosted Gold Deposit Coeval with Late Archean Deformation and Magmatism. Economic Geology, vol. 106, pp. 1129-1154.

Koval, P. V., Zorina, L. D., Kitajev, A. M., Spiridonov, A. M., Ariunbileg, S. (1991) The Use of Tourmaline in Geochemical Prospecting for Gold and Copper Mineralization, Journal of Geochemical Exploration, vol. 40, pp. 349-360.

Lambert, R. St. J. (1980) The Thermal History of the Earth in the Archean. Precambrian Research, vol. 11, pp. 199-213.

Li, Y., Liu, J. (2006) Calculation of Sulfur Isotope Fractionation in Sulfides, Geochimica et Cosmochimica Acta, vol. 70, pp. 1789-1795.

Martin, H. (1986) Effect of Steeper archean Geothermal Gradient on Geochemistry of Subduction Zone Magmas, Geology, vol. 14, pp. 753-756.

Mlynarczyk, M. S. J. (2005) Constraints on the Genesis of Lode-style Tin Mineralization: Evidence from the San Rafael tin-copper deposit, Peru. PhD Thesis, McGill University.

Molnàr, F., Mänttäri, I., O'Brien, H., Lahaye, Y., Pakkanen, L., Johanson, B., Käpyaho, A., Sorjonen-Ward, P., Whitehouse, M., Sakellaris, G. (2016) Boron, Sulphur and Copper Isotope Systematics in the Orogenic Gold Deposits of the Archaean Hattu schist belt, Eastern Finland, Ore Geology Reviews, vol. 77, pp. 133-162.

Ochoa-Landin, L. H., Valencia-Morena, M., Valmus, T. (2016) Geology and Geochemistry of the Suaqui Verde Deposit: A Contribution to the Knowledge of the Laramide Porphyry Copper Mineralization in South Central Sonora, Mexico. Ore Geology Reviews, vol. 81, *in progress*.

Perrouty, S., Linnen, R. L., Lesher, C. M., Olivo, G. R., Piercey, S. J., Gaillard, N., Clark, J. R., Enkin, R. J. (2019) Expanding the Size of Multi-parameter Metasomatic Footprints in Gold Exploration: Utilization of Mafic Dykes in the Canadian Malartic District, Québec, Canada, Mineralum Deposita, vol. 54, pp. 761-786.

Powell, W. G., Carmichael, D. M., Hodgson, C J. (1995) Conditions and Timing of Metamorphism in the Southern Abitibi Greenstone Belt, Québec. Canadian Journal of Earth Sciences, vol. 32, pp. 787-805.

Profett, J. M. (2009) High Cu Grades in Porphyry Cu Deposits and their Relationship to Emplacement Depth of Magmatic Sources, Geology, vol. 37, pp. 675-678

Rhéaume, P., Bandyayera, D., Fallara, F., Boudrias, G., Cheng, L., Z. (2004) Géologie et Métallogénie de Secteur du Lac aux Loutres, Synthèse métallogénique d'Urban Barry. Ressources Naturelles et de la Faune, RP-2004-05

Rhéaume, P., Bandyayera, D. (2006) Révision Stratigraphique de la Ceinture d'Urban-Barry. Ressources Naturelles et Faune, RP 2006-08.

Richards, J. P. (2018) A Shake-Up in the Porphyry World?, Economic Geology, vol. 113, pp. 1225-1233.

Robert, F., Brown, A. C. (1986) Archean Gold-Bearing Quartz Veins at the Sigma Mine, Abitibi Greenstone Belt, Quebec: Part II. Vein Paragenesis and Hydrothermal Alteration, Economic Geology, vol. 81, pp. 593-616.

Seal, II, R. R., (2006) Sulfur Isotope Geochemistry of Sulfide Minerals, Reviews in Mineralogy and Geochemistry, vol. 61, pp. 633-677.

Sillitoe, R. H. (1985) Ore-Related Breccias in Volcanoplutonic Arcs. Economic Geology, vol. 80, pp. 1467-1514.

Sillitoe, R. H., (2010) Porphyry Copper Systems. Economic Geology, v.105, pp. 3-41.

Sillitoe, R. H., Sawkins, F. J. (1971) Geologic, Mineralogic and Fluid Inclusion Studies Relating to the Origin of Copper-bearing Breccia Pipes, Chile. Economic Geology, vol. 66, pp. 1028-1041.

Skewes, M. A., Holmgren, C., Stern, C.R. (2003) The Donoso Copper-Rich, Tourmaline-Bearing Breccia Pipe in Central Chile: Petrologic, Fluid Inclusion and Stable Isotope Evidence for an Origin from Magmatic Fluids. Mineralium Deposita, vol. 38, pp. 2-21.

Slack, J. F., Trumbull, R, B. (2011) Tourmaline as a Recorder of Ore-Forming Processes. Elements, vol. 7, pp. 321-326

Spooner, E. T. C., Tucker Barrie, C. (1993) Preface in a Special Issue Devoted to Abitibi Ore Deposits in a Modern Context. Economic Geology, vol. 88, pp. 1307-1322.

Thurston, P.C., Ayer, J.A., Goutier, J., Hamilton, M.A. (2008) Depositional Gaps in Abitibi Greenstone Belt Stratigraphy: A Key to Exploration for Syngenetic Mineralization. Economic Geology, vol. 103, pp. 1097–1134.

Violay, M., Gilbert, B., Mainprice, D., Burg, J.P. (2015) Brittle Versus Ductile Deformation as the Main Control of the Deep Fluid Circulation in Oceanic Crust. Geophysical Research Letters, vol. 42, pp. 2767-2773

Wang, Y., Chen, H., Baker, M. J., Han, J., Xiao, B., Yang, J., Jourdan, F. (2017) Multiple Mineralization Events of the Paleozoic Tuwu Porphyry Copper Deposit, Eastern Tianshan: Evidence from Geology, Fluid Inclusions, Sulfur Isotopes, and Geochronology, Mineralum Deposita, vol. 54, pp. 1053-1076.

Warnaars, F. W., Holmgren, D., C., Barassi, F. S. (1985) Porphyry Copper and Tourmaline Breccia at Los Bronces, Chile. Economic Geology, vol. 80, pp. 1544-1565.

Williams, W. C., Meissl, E., Madrid, J., De Machuca, B. C. (1999) The San Jorge, Porphyry Copper Deposit, Mendoza, Argentina: a Combination of Orthomagmatic and Hydrothermal Mineralization. Ore Geology Reviews, vol. 14, pp. 185-201.

Williams-Jones, A., E., Bowell, R., J., Migdisov, A., A. (2009) Gold in solution, Elements, vol. 5, pp. 281-287.

Chapter III: General Conclusions

The Black Dog prospect is a unique example of a mineralized tourmaline breccia in an Archean Greenstone belt. The alteration, metal signature, mineralization textures (microcrystalline matrix, the angular silicified clasts, the jigsaw texture and the late-stage fracture-filling Au-Cu mineralization concentrated at the margins of the breccia), sulfur isotope ratios, and emplacement temperature provide convincing evidence that the alteration and mineralization at Black Dog resulted from the input of dominantly magmatic fluids that likely came from an underlying calc-alkaline intrusion. In nature and origin, Black Dog breccia is remarkably similar to tourmaline breccias that are commonly observed in close association with porphyry-copper deposits in the Andes. It is therefore interpreted to represent an Archean analogue of an Andean subduction-related tourmaline breccia that formed above a subduction zone. The reason why it is unique is unclear. A possible explanation may be that there are relatively few Archean examples of porphyry deposits, which is potentially due to the lack of strong subduction in this eon or the more important erosion that older rocks generally undergo. An alternative explanation is that boron is a highly incompatible element and therefore will have been progressively enriched in the continental crust with time. As porphyry deposits, to a significant extent, are the products of the recycling of crust, it follows that the importance of boron in porphyry-related hydrothermal systems will have increased with time, ensuring the presence of tourmaline breccias in the phanerozoic but not in the Archean.

The progressive changes in the trace element composition of tourmaline through the alteration and mineralization stages at Black Dog record the evolution of a hydrothermal system that culminated with deposition of base metal sulfides and economic concentrations of gold.

In particular, the concentrations of Co, As, Zn, Cu, Ag and Bi are significantly higher in tourmaline associated with the sulfide breccia than the earlier-forming tourmaline. Tourmaline

composition can therefore provide a vector to gold mineralization. Moreover, because tourmaline is resistant to weathering, the trace metal content of tourmaline in till could potentially provide a tool for exploring for gold at the regional scale and perhaps for deposits in addition to those hosted by tourmaline breccias, e.g., the orogenic tourmaline-bearing deposits that constitute much of the gold resource of Archean greenstone belts.

Table 1: Sulfur isotope values of sulfide mineral pairs

Sample	Pyrite δ34S	Chalcopyrite δ34S	Sphalerite δ34S	Temperature (°C)
A1	3.6	2.7		415
A2	3.6		3.1	501
A3		2.7	3.1	606
B	3.2	2.3		414
C		1.8	3.3	598
F		1.7	3.6	440

Appendixes

Appendix 1: Electron Microprobe Analyses of selected major elements in tourmaline. Values are in weight %.

ID	Source	F	Na2O	MgO	K2O	CaO	TiO2	MnO	Fe2O3	CoO	CuO	ZnO	As2O3	SiO2	Al2O3
1	BD-10	0.11	1.76	2.86	0.02	0.52	0.50	0.03	15.6	0.00	0.00	0.04	0.00	33.1	31.3
2	BD-10	0.01	1.56	2.40	0.02	0.72	0.53	0.03	15.9	3.00	0.01	0.02	0.00	32.8	31.8
3	BD-10	0.00	1.70	3.13	0.02	0.56	0.58	0.04	15.0	0.00	0.00	0.02	0.00	33.3	31.3
4	BD-10	0.03	1.48	2.34	0.02	0.69	0.68	0.03	15.9	0.01	0.00	0.02	0.00	33.1	31.9
5	BD-10	0.04	1.56	2.47	0.02	0.68	0.51	0.03	15.9	0.00	0.01	0.03	0.00	32.9	31.6
6	BD-10	0.11	1.58	3.33	0.16	0.64	0.77	0.05	14.3	0.00	0.00	0.01	0.00	33.7	31.6
7	BD-10	0.03	1.70	3.34	0.04	0.51	0.77	0.04	14.5	0.00	0.01	0.03	3.00	33.8	31.6
8	BD-10	0.12	1.68	3.10	0.03	0.58	0.91	0.04	14.7	0.00	0.00	0.03	0.00	33.6	31.5
9	BD-10	0.09	1.71	3.99	0.02	0.63	0.59	0.04	13.1	0.00	0.02	0.01	0.00	33.9	31.7
10	BD-10	0.05	1.59	3.81	0.03	0.60	0.77	0.03	13.5	0.00	0.02	0.02	0.00	33.5	31.5
11	BD-10	0.17	1.76	3.80	0.02	0.59	0.87	0.04	13.3	0.00	0.01	0.02	0.00	33.6	31.3
12	BD-10	0.12	1.57	3.71	0.01	0.96	0.22	0.04	13.8	0.00	0.00	0.00	0.00	33.2	31.8
13	BD-10	0.13	1.55	3.86	0.02	0.92	0.25	0.05	13.4	0.01	0.01	0.02	0.00	33.2	32.0
14	BD-10	0.10	1.52	4.40	0.01	0.77	0.30	0.02	11.5	0.00	0.01	0.02	0.02	33.5	32.7
15	BD-10	0.11	1.60	4.25	0.02	0.87	0.39	0.02	12.4	0.00	0.00	0.02	74.0	33.5	32.2
16	BD-10	0.11	1.52	4.42	0.01	0.92	0.21	0.01	11.6	0.00	0.01	0.02	0.00	33.2	32.9
17	BD-10	0.12	1.43	4.37	0.02	0.94	0.26	0.02	11.8	0.00	0.00	0.02	44.0	33.3	32.5
18	BD-10	0.12	1.65	3.48	0.13	0.53	0.57	0.04	13.9	0.00	0.00	0.01	0.00	33.5	31.7
19	BD-10	0.12	1.71	3.04	0.27	0.44	0.53	0.05	14.8	0.00	0.01	0.04	46.0	33.3	31.3
20	BD-10	0.14	1.57	2.53	0.39	0.50	0.59	0.04	14.8	0.00	0.01	0.02	0.00	33.7	31.9
21	BD-10	0.08	1.49	2.61	0.23	0.59	0.60	0.06	14.5	0.01	0.02	0.03	46.0	33.4	32.1
22	BD-10	0.09	1.58	2.76	0.04	0.54	0.60	0.06	15.7	0.00	0.01	0.02	0.00	32.8	31.6
23	BD-10	0.09	1.66	4.30	0.02	1.09	0.08	0.02	14.4	0.00	0.00	0.01	0.00	32.8	31.1
24	BD-10	0.14	1.63	4.42	0.02	1.04	0.08	0.03	13.8	0.00	0.02	0.01	0.00	32.9	31.1
25	BD-10	0.17	1.57	4.63	0.02	1.01	0.09	0.01	12.9	0.00	0.01	0.02	0.00	33.2	31.7
26	BD-10	0.14	1.50	5.71	0.01	1.07	0.07	0.01	9.37	0.00	0.01	0.01	0.06	33.7	33.0
27	BD-10	0.22	1.51	5.85	0.01	1.14	0.05	0.02	9.48	0.00	0.01	0.01	0.05	33.3	32.9
28	BD-10	0.18	1.45	5.70	0.02	1.10	0.16	0.01	9.09	0.01	0.00	0.02	0.11	33.6	33.2
29	BD-10	0.07	1.79	3.70	0.03	0.60	0.89	0.03	14.4	0.01	0.01	0.01	0.00	33.4	30.6
30	BD-10	0.11	1.79	3.83	0.03	0.59	0.80	0.03	13.9	0.00	0.00	0.03	0.00	33.3	30.9
31	BD-10	0.13	1.76	4.09	0.02	0.58	0.74	0.04	13.2	0.00	0.01	0.03	0.00	33.7	31.2
32	BD-18	0.35	1.80	6.82	0.01	1.10	0.40	0.07	9.46	0.00	0.01	0.03	0.00	34.3	30.9
33	BD-18	0.37	1.68	7.02	0.01	1.17	0.35	0.06	9.32	0.00	0.01	0.03	0.00	34.2	30.8
34	BD-18	0.41	1.69	7.19	0.01	1.16	0.39	0.06	8.82	0.00	0.01	0.01	0.00	34.4	31.1
35	BD-18	0.22	1.81	6.97	0.01	1.15	0.44	0.05	9.43	0.00	0.00	0.02	0.00	34.2	30.5
36	BD-18	0.46	1.77	7.09	0.01	1.16	0.43	0.09	9.76	0.01	0.00	0.02	0.00	34.0	30.6
37	BD-18	0.34	1.94	6.32	0.02	1.15	0.36	0.05	11.8	0.00	32.0	0.00	0.00	35.6	28.6
38	BD-18	0.36	1.89	6.15	0.02	1.01	0.66	0.03	12.7	0.00	0.00	0.02	0.00	33.8	29.0
39	BD-18	0.40	1.91	6.28	0.02	1.00	0.59	0.06	12.1	0.00	0.00	0.04	0.00	34.6	29.5
40	BD-18	0.34	1.88	6.77	0.02	1.18	0.62	0.04	11.5	0.00	0.00	0.03	0.00	34.3	29.0
41	BD-18	0.22	1.87	4.84	0.01	1.00	0.46	0.04	15.3	0.00	0.00	0.03	0.00	35.7	27.3
42	BD-18	0.28	1.89	7.53	0.00	1.07	0.05	0.08	10.8	0.00	0.01	0.01	0.00	34.4	29.1
43	BD-18	0.39	1.76	6.39	0.02	1.33	0.58	0.08	12.3	0.00	0.00	0.03	0.00	33.7	29.4
44	BD-18	0.40	1.66	6.81	0.02	1.29	0.63	0.07	10.9	0.00	0.01	0.02	0.00	34.1	29.8
45	BD-18	0.13	1.72	3.54	0.02	0.80	0.52	0.08	15.7	0.00	0.00	0.03	0.00	33.3	30.2
46	BD-18	0.16	1.84	3.67	0.02	0.82	0.55	0.06	15.7	0.00	0.00	0.02	0.00	33.5	30.0
47	BD-18	0.15	1.74	5.51	0.02	1.07	0.50	0.09	13.0	0.00	18.0	0.04	0.00	34.0	29.8
48	BD-18	0.19	1.94	4.82	0.02	1.10	0.26	0.07	15.5	0.00	0.01	0.03	0.00	35.3	27.8
49	BD-18	0.19	1.80	4.17	0.02	0.97	0.57	0.06	15.2	0.00	0.00	0.02	0.00	35.3	28.5

50	BD-18	0.03	1.97	2.08	0.03	0.54	0.26	0.06	18.5	0.00	0.00	0.01	0.00	35.0	28.8
51	BD-18	0.08	1.75	2.72	0.03	0.51	0.25	0.03	14.7	0.00	0.01	0.02	0.00	46.4	24.3
52	BD-18	0.08	2.06	2.51	0.02	0.48	0.15	0.04	17.5	0.01	0.00	0.02	0.00	37.4	28.2
53	BD-18	0.32	1.87	5.70	0.03	1.04	0.44	0.06	14.1	0.01	0.01	0.04	0.00	33.5	29.2
54	BD-18	0.30	1.84	5.77	0.02	1.07	0.50	0.05	12.7	0.00	0.00	0.05	0.00	33.7	29.8
55	BD-18	0.14	1.79	3.49	0.01	0.87	0.40	0.09	16.4	0.00	0.02	0.04	0.00	33.4	30.0
56	BD-18	0.23	1.76	4.11	0.02	0.93	0.40	0.08	15.5	0.01	0.02	0.04	0.00	33.4	29.7
57	BD-18	0.11	2.18	2.73	0.03	0.35	0.04	0.04	17.7	0.01	0.01	0.01	0.00	35.4	28.6
58	BD-18	0.12	2.07	3.66	0.02	0.47	0.37	0.03	16.8	0.00	0.00	0.03	0.00	35.2	28.7
59	BD-18	0.18	1.75	2.87	0.02	0.69	0.36	0.04	16.4	0.00	0.00	0.03	0.00	35.5	28.7
60	BD-18	0.32	1.85	5.40	0.02	1.27	0.41	0.07	14.8	0.00	0.00	0.03	0.00	35.3	27.9
61	BD-18	0.36	1.83	6.82	0.01	1.18	0.34	0.08	11.2	0.00	0.00	0.02	0.00	34.1	29.7
62	BD-18	0.27	1.84	6.13	0.01	0.96	0.34	0.10	11.9	0.00	0.00	0.03	0.00	33.9	30.0
63	BD-18	0.36	1.93	6.50	0.01	0.91	0.14	0.15	12.1	0.00	0.01	0.03	0.00	34.0	29.2
64	BD-18	0.24	1.55	3.74	0.03	0.79	0.41	0.07	14.4	0.01	0.01	0.03	0.00	45.0	22.6
65	BD-18	0.14	2.12	3.42	0.03	0.54	0.42	0.04	17.9	0.00	0.00	0.00	0.00	36.0	26.2
66	BD-18	0.30	1.81	5.41	0.02	1.18	0.46	0.08	13.4	0.00	0.00	0.04	0.00	33.9	29.3
67	BD-18	0.18	1.78	4.06	0.02	0.92	0.43	0.09	15.0	0.00	0.00	0.03	0.00	33.5	30.1
68	BD-18	0.20	1.78	4.39	0.02	0.88	0.45	0.09	14.8	0.00	0.00	0.03	0.00	33.7	29.7
69	BD-18	0.25	1.81	3.67	0.01	0.84	0.47	0.10	15.9	0.00	0.00	0.04	0.00	33.4	29.7
70	BD-18	0.23	1.85	4.63	0.02	0.99	0.36	0.10	14.7	0.00	0.01	0.04	0.00	33.2	29.6
71	BD-18	0.22	1.73	4.22	0.01	0.98	0.45	0.10	15.3	0.00	0.00	0.04	0.00	33.4	29.6
72	BD-18	0.16	1.81	3.59	0.03	0.99	0.32	0.06	16.4	0.01	0.01	0.03	0.00	34.8	28.7
73	BD-18	0.11	2.33	3.45	0.03	0.62	0.24	0.04	18.6	0.00	0.00	0.00	0.00	34.9	26.9
75	BD-18	0.28	1.83	6.72	0.01	1.08	0.48	0.08	9.89	0.00	0.01	0.02	0.00	34.2	30.4
76	BD-18	0.30	1.80	7.13	0.01	1.25	0.36	0.08	9.93	0.01	0.00	0.03	0.00	34.0	30.3
77	BD-18	0.46	1.82	6.74	0.01	1.09	0.48	0.08	10.6	0.00	0.00	0.04	0.00	33.9	30.2
78	BD-18	0.10	1.68	3.20	0.02	0.91	0.38	0.10	17.1	0.00	0.01	0.04	0.00	33.2	29.7
79	BD-18	0.21	1.78	3.25	0.02	0.79	0.47	0.08	16.3	0.00	0.01	0.01	0.00	36.2	27.8
80	BD-18	0.20	1.79	4.20	0.02	0.98	0.44	0.09	15.5	0.00	0.00	0.03	0.00	33.5	29.2
81	BD-18	0.13	1.93	2.52	0.04	0.55	0.27	0.03	17.9	0.00	0.00	0.02	0.00	37.1	26.6
82	BD-18	0.05	2.47	3.51	0.04	0.53	0.19	0.03	21.3	0.00	13.0	0.01	0.00	34.6	24.8
83	BD-18	0.13	1.87	3.28	0.03	0.32	0.30	0.07	15.1	0.00	0.04	0.04	0.00	35.5	29.7
84	BD-18	0.37	1.87	6.90	0.02	1.20	0.57	0.06	10.5	0.01	0.00	0.02	0.00	34.0	29.5
85	BD-18	0.24	1.85	6.42	0.01	1.14	0.51	0.06	11.2	0.00	0.00	0.03	0.00	35.7	28.6
86	BD-18	0.38	1.80	6.82	0.02	1.19	0.53	0.06	11.2	0.00	0.00	0.02	0.00	34.2	29.4
87	BD-18	0.32	1.94	6.18	0.02	1.07	0.55	0.06	12.7	0.00	0.00	0.01	0.00	33.9	29.0
88	BD-18	0.56	1.63	9.04	0.04	2.18	1.93	0.04	9.32	0.00	0.02	0.03	0.00	33.5	26.5
89	BD-18	0.54	1.54	8.83	0.03	2.04	1.82	0.01	9.71	0.00	0.00	0.02	0.00	34.2	26.0
90	BD-18	0.47	1.63	9.35	0.03	2.01	2.28	0.06	8.35	0.00	0.00	0.04	0.00	33.9	26.5
91	BD-18	0.26	1.78	6.76	0.01	1.10	0.01	0.09	11.9	0.00	0.00	0.02	0.00	33.8	29.1
92	BD-18	0.30	1.75	6.72	0.01	1.23	0.23	0.11	11.2	0.00	0.00	0.02	0.00	34.0	29.6
93	BD-18	0.31	1.83	6.54	0.02	1.09	0.23	0.08	12.1	0.00	0.00	0.02	0.00	33.9	29.2
94	BD-18	0.22	1.90	7.01	0.02	0.98	0.35	0.06	11.1	0.00	0.00	0.03	0.00	36.2	28.5
95	BD-18	0.17	1.82	4.32	0.03	0.96	0.37	0.08	16.3	0.00	0.01	0.04	0.00	33.5	28.5
96	BD-18	0.34	1.80	6.70	0.02	1.09	0.26	0.11	12.3	0.00	0.00	0.02	0.00	34.1	28.4
97	BD-18	0.12	1.65	3.16	0.02	0.70	0.61	0.05	14.8	0.00	0.00	0.03	0.00	43.1	24.2
98	S45240	0.20	1.71	6.05	0.03	1.10	0.54	0.04	9.78	0.00	0.01	0.01	0.00	33.6	31.6
99	S45240	0.17	1.67	6.03	0.03	1.04	0.41	0.02	9.83	0.01	0.00	0.03	0.00	33.7	31.8
100	S45240	0.30	1.60	6.81	0.02	1.36	0.47	0.01	9.00	0.00	0.00	0.01	0.00	33.7	31.1
101	S45240	0.27	1.35	6.93	0.03	1.67	0.47	0.02	7.58	8.00	0.00	0.02	0.00	33.0	32.3
102	S45240	0.38	1.36	7.39	0.02	1.81	0.60	0.01	7.71	0.00	0.01	0.01	0.00	33.4	31.6
103	S45240	0.50	1.46	8.94	0.01	2.57	0.57	0.01	12.4	0.00	0.00	0.00	0.00	33.0	25.4
104	S45240	0.51	1.40	8.32	0.01	2.34	0.64	0.00	12.9	0.01	0.01	0.01	0.00	33.2	26.1

105	S45240	0.35	1.49	6.83	0.02	1.85	0.36	0.03	13.2	0.00	0.00	0.03	0.00	33.5	27.9
106	S45240	0.50	1.40	8.53	0.02	2.38	0.33	0.02	12.3	0.00	0.01	0.02	0.00	33.3	26.3
107	S45240	0.17	1.67	6.00	0.03	1.19	0.38	0.02	10.6	0.00	57.0	0.04	12.0	33.3	30.9
108	S45240	0.26	1.64	5.61	0.02	1.09	0.43	0.05	11.0	0.00	0.00	0.03	0.00	33.2	31.1
109	S45240	0.27	1.53	6.84	0.02	1.57	0.81	0.03	9.79	0.00	0.00	0.02	0.00	33.4	30.3
110	S45240	0.28	1.45	6.92	0.02	1.61	0.65	0.04	9.32	0.01	0.00	0.02	0.00	33.4	30.4
111	S45240	0.40	1.40	7.13	0.01	1.71	0.76	0.02	9.10	0.01	0.00	0.03	0.00	33.4	30.5
112	S45240	0.24	1.51	6.49	0.04	1.67	0.53	0.02	12.0	0.00	0.00	0.03	0.00	33.6	29.0
113	S45240	0.27	1.50	5.77	0.03	1.37	0.61	0.04	11.7	0.01	0.00	0.03	0.00	33.4	30.2
114	S45240	0.50	1.23	8.91	0.02	2.99	0.32	0.01	14.0	0.00	24.0	0.01	0.00	33.0	24.4
115	S45240	0.44	1.40	8.53	0.02	2.58	0.47	0.01	14.4	0.00	0.00	0.01	0.00	32.9	24.5
116	S45240	0.04	1.50	3.50	0.03	0.72	0.63	0.09	13.1	0.00	0.00	0.05	0.00	35.2	31.5
117	S45240	0.04	1.34	2.62	0.02	0.46	0.54	0.04	12.2	0.00	0.01	0.04	0.00	45.4	25.0
118	S45240	0.14	1.41	3.04	0.01	0.51	0.51	0.06	12.7	0.00	0.00	0.04	0.00	40.5	27.7
119	S45240	0.24	1.42	6.43	0.03	1.65	0.44	0.03	10.7	0.01	0.01	0.02	0.00	32.9	30.5
120	S45240	0.15	1.52	4.14	0.02	0.68	0.56	0.07	12.3	0.01	0.01	0.03	0.00	33.5	32.0
121	S45240	0.04	1.68	4.05	0.03	0.87	0.69	0.09	12.9	0.00	0.00	0.05	0.00	32.9	31.5
122	S45240	0.24	1.56	5.82	0.03	1.17	0.67	0.04	11.0	0.00	0.00	0.01	0.00	33.1	31.0
123	S45240	0.01	1.16	2.42	0.03	0.63	0.44	0.10	11.5	0.01	0.00	0.05	0.00	45.9	26.0
124	S45240	0.12	1.45	3.55	0.02	0.63	0.58	0.08	11.8	0.00	0.02	0.07	0.00	38.5	28.8
125	S45240	0.05	1.55	3.96	0.03	0.69	0.52	0.10	11.4	0.01	0.00	0.05	0.00	35.3	32.3
126	S45240	0.00	0.83	1.67	0.02	0.50	0.39	0.09	9.47	0.00	0.00	0.06	0.00	59.6	20.3
127	S45240	0.07	1.57	3.42	0.03	0.69	0.63	0.06	14.1	0.00	0.00	0.04	0.00	35.1	30.6
128	S45240	0.30	1.70	6.08	0.02	1.23	0.59	0.02	10.7	0.00	0.00	0.03	0.00	35.6	30.0
129	S45240	0.33	1.69	6.22	0.02	1.22	0.65	0.03	10.2	0.00	0.01	0.01	0.00	35.4	30.0
130	S45240	0.29	1.66	4.96	0.03	0.84	0.55	0.06	11.7	0.00	0.00	0.05	0.00	35.4	30.7
131	S45240	0.00	1.04	1.81	0.00	0.18	0.15	0.05	9.12	0.00	0.02	0.00	0.00	57.9	18.1
132	S45240	0.04	1.38	2.91	0.02	0.64	0.39	0.09	12.5	0.00	0.01	0.07	0.00	38.2	30.8
133	S45240	0.09	1.51	3.83	0.02	0.67	0.42	0.05	11.7	0.00	0.00	0.05	0.00	37.9	29.7
134	S45240	0.10	1.34	2.29	0.03	0.69	0.66	0.11	13.2	0.00	0.00	0.06	0.00	44.0	26.2
135	S45240	0.03	1.49	3.00	0.02	0.70	0.70	0.09	13.7	0.00	0.01	0.04	0.00	36.2	30.6
136	S45240	0.31	1.33	5.88	0.01	1.24	0.43	0.01	7.15	0.00	0.00	0.01	0.00	44.9	25.5
137	S45240	0.28	1.45	7.23	0.02	2.21	1.02	0.01	10.9	0.01	0.00	0.01	0.00	34.5	27.7
138	S45240	0.20	1.56	5.16	0.02	1.03	0.50	0.05	9.92	0.01	0.00	0.02	0.00	43.2	25.5
139	S45240	0.32	1.53	6.37	0.02	1.49	0.73	0.02	9.18	0.01	0.01	0.03	0.00	36.4	29.4
140	S45240	0.36	1.36	7.34	0.01	2.12	1.21	0.02	10.6	0.00	0.00	0.02	0.00	34.7	28.4
141	S45240	0.30	1.31	6.87	0.01	2.00	1.00	0.03	9.67	0.00	0.00	0.02	0.00	34.7	29.6
142	S45240	0.33	1.50	6.77	0.02	1.78	0.85	0.03	9.86	0.00	0.00	0.01	0.00	35.5	29.3
143	S45240	0.25	1.39	6.62	0.02	1.79	0.91	0.03	10.1	0.00	0.00	0.03	0.00	36.5	28.6
144	S45240	0.40	1.45	6.62	0.02	1.76	0.91	0.03	10.3	0.01	0.00	0.02	0.00	35.8	29.5
145	S45240	0.31	1.77	5.98	0.02	1.14	0.38	0.05	12.2	0.00	0.01	0.05	0.00	34.2	29.1
146	S45240	0.35	1.67	6.80	0.02	1.44	0.35	0.09	10.6	0.00	0.01	0.05	0.00	33.9	29.7
147	S45240	0.36	1.65	7.06	0.02	1.62	0.53	0.07	10.6	0.00	0.00	0.03	0.00	33.6	29.2
148	S45240	0.32	1.76	6.85	0.02	1.48	0.39	0.07	11.4	0.00	14.0	0.03	0.00	33.4	29.3
149	S45240	0.29	1.75	6.57	0.03	1.41	0.45	0.03	11.9	0.00	0.01	0.02	0.00	33.5	29.1
150	S45240	0.30	1.74	6.90	0.02	1.46	0.36	0.07	10.6	0.01	0.00	0.03	0.00	33.9	29.6
151	S45240	0.18	2.08	4.60	0.03	0.68	0.20	0.03	15.4	0.00	0.01	0.03	0.00	35.0	28.4
152	S45240	0.08	2.18	3.57	0.03	0.66	0.16	0.04	18.3	0.00	0.00	0.01	0.00	35.2	26.4
153	S45240	0.08	1.68	1.88	0.02	0.61	0.00	0.05	17.7	0.00	0.01	0.04	0.04	34.6	29.8
154	S45240	0.04	1.48	2.34	0.01	0.44	0.08	0.03	12.4	0.00	0.01	0.01	0.00	47.9	22.1
155	S45240	0.13	1.75	2.73	0.03	0.41	0.08	0.03	13.8	0.00	0.00	0.01	0.00	45.1	23.9
156	S45240	0.07	1.30	2.44	0.02	0.24	0.00	0.01	11.4	0.01	0.00	0.02	0.00	58.5	20.2
157	S45240	0.18	1.66	4.42	0.02	1.03	0.42	0.03	13.7	0.00	0.01	0.02	0.00	41.5	26.4
158	S45240	0.35	1.65	7.09	0.02	1.82	0.26	0.07	10.5	0.00	0.01	0.03	0.00	35.6	28.7

159	S45240	0.30	1.77	6.30	0.02	1.50	0.24	0.09	11.6	0.01	0.00	0.04	0.00	35.5	29.0
160	S45240	0.23	1.89	5.44	0.03	1.25	0.27	0.10	13.3	0.01	0.00	0.03	0.00	35.5	28.7
161	S45240	0.32	1.59	7.16	0.02	1.89	0.35	0.05	10.7	0.00	0.00	0.04	0.00	35.8	28.6
162	S45240	0.36	1.79	6.06	0.02	1.47	0.28	0.11	12.1	0.00	0.00	0.03	0.00	35.6	28.6
163	S45240	0.29	1.80	5.69	0.02	1.29	0.40	0.08	13.4	0.00	0.00	0.03	0.00	35.2	28.6
164	S45240	0.33	1.75	6.52	0.02	1.68	0.40	0.06	11.4	0.00	0.00	0.04	0.00	35.5	28.6
165	S45240	0.36	1.93	7.03	0.02	1.25	0.90	0.09	9.27	0.00	0.02	0.02	0.00	37.6	27.5
166	S45240	0.42	1.68	7.35	0.03	1.83	0.64	0.07	9.25	0.00	0.01	0.03	0.00	34.8	30.0
167	S45240	0.47	1.52	6.94	0.02	2.31	0.97	0.03	10.3	0.00	0.00	0.03	0.00	34.4	29.7
168	S45240	0.29	1.33	5.47	0.04	2.16	0.57	0.03	11.2	0.00	0.00	0.02	0.00	33.9	31.0
169	S45240	0.18	1.42	2.69	0.06	1.85	0.97	0.04	14.2	0.01	0.00	0.01	0.00	32.9	32.8
170	S45240	0.31	1.77	6.17	0.02	1.33	0.29	0.08	11.6	0.00	0.00	0.01	0.00	35.6	29.5
171	S45240	0.47	1.71	7.39	0.02	1.71	0.35	0.09	10.8	0.00	0.00	0.01	0.00	35.7	28.5
172	S45240	0.63	1.33	8.96	0.03	2.73	0.65	0.02	8.61	0.00	0.00	0.02	0.00	35.6	28.3
173	S45240	0.82	1.08	10.5	0.02	3.39	0.90	0.01	7.97	0.00	0.00	0.01	0.00	35.8	26.1
174	S45240	0.49	1.40	7.51	0.03	2.19	0.52	0.03	8.86	0.01	0.01	0.03	0.00	35.1	30.3
175	S45240	0.79	1.36	9.59	0.03	2.75	0.67	0.02	9.38	0.00	0.00	0.01	0.00	35.8	26.5
176	S45240	0.52	1.43	8.38	0.02	2.50	0.48	0.03	9.00	0.00	0.00	0.02	0.00	35.8	28.6
177	S45240	0.50	1.37	9.14	0.02	2.58	0.40	0.04	7.99	0.00	0.00	0.03	0.00	35.5	28.4
178	S45240	0.45	1.46	7.13	0.03	1.88	0.50	0.04	9.97	0.01	0.01	0.04	0.00	35.4	29.5
179	S45240	0.28	1.69	7.00	0.02	1.35	0.29	0.01	9.64	0.00	0.01	0.01	0.00	35.9	30.3
180	S45240	0.30	1.88	5.70	0.02	1.18	0.29	0.07	12.9	0.00	0.03	0.03	0.00	35.5	28.9
181	S45240	0.31	1.75	6.51	0.02	1.27	0.44	0.05	10.1	0.00	0.00	0.03	0.00	36.0	30.1
182	S45240	0.21	1.77	6.26	0.03	1.27	0.17	0.01	12.7	0.01	0.00	0.03	0.00	35.8	28.5
183	S45240	0.30	1.71	7.01	0.03	1.46	0.18	0.03	12.6	0.00	0.00	0.01	0.00	35.7	28.0
184	S45240	0.31	1.47	6.52	0.03	1.33	0.08	0.02	9.40	0.00	0.01	0.02	0.00	35.6	31.5
185	S45240	0.26	1.78	6.95	0.04	1.15	0.28	0.02	9.71	0.01	0.00	0.01	0.00	36.0	30.2
186	S45240	0.25	1.69	5.68	0.03	1.63	0.32	0.02	15.4	0.00	0.00	0.01	0.00	35.4	27.3
187	S45240	0.12	2.24	3.73	0.03	0.65	0.07	0.04	17.2	0.00	0.00	0.02	0.00	35.1	28.2
188	S45240	0.16	2.09	3.71	0.02	0.73	0.00	0.05	17.4	0.00	0.00	0.02	0.00	35.9	27.4
189	S45240	0.04	1.89	1.70	0.03	0.38	0.02	0.04	17.3	33.0	0.01	0.01	0.00	39.0	25.8
190	S45240	0.24	1.74	4.83	0.03	1.37	0.26	0.04	16.1	0.01	0.00	0.00	0.00	35.2	27.4
191	S45240	0.09	2.12	2.88	0.03	0.43	0.04	0.04	18.1	0.00	0.00	0.01	0.00	34.7	28.6

Appendix 2: LA-ICP-MS values of selected trace elements in tourmaline. Values are in PPM.

ID	Source	Mg	B	Ti	Au	Ag	Zn	Cu	Co	Bi	As
1	NIST	427	337	448.0	23.9	246.0	468.0	450.0	413.0	382.0	324.0
2	NIST	431	355	494.0	23.1	253.1	462.0	438.0	396.0	387.0	324.0
3	NIST	427	346	451.0	23.6	249.3	466.0	445.0	409.0	384.0	324.0
7	BD-05	25610	32800	1840.0	0.0	0.0	397.0	10.0	34.2	0.0	394.0
8	BD-05	26300	33200	1920.0	0.0	0.1	450.0	10.5	36.9	0.0	350.0
9	BD-05	17300	31500	2990.0	0.1	0.3	796.0	9.6	80.5	0.0	161.0
10	BD-05	18890	32200	2942.0	0.0	1.6	829.0	350.0	79.5	0.1	160.0
11	BD-05	17100	31000	3400.0	0.4	0.9	805.0	60.0	89.5	0.0	152.0
12	BD-05	15600	29920	3140.0	0.1	0.2	739.0	14.4	69.7	0.0	101.0
17	BD-05	22900	35100	1716.0	0.5	3.0	450.0	12.4	38.1	3.6	228.0
18	BD-05	13650	38600	1879.0	0.1	0.1	714.0	12.0	112.0	0.2	235.0
19	BD-05	11910	37400	1669.0	0.1	0.3	703.0	15.5	91.8	0.3	173.0
20	BD-05	11100	38400	1594.0	0.0	1.7	688.0	277.0	78.4	1.3	179.0
21	BD-05	15400	36400	1601.0	0.0	1.7	800.0	36.9	89.3	0.7	148.0
24	BD-05	18100	34800	2260.0	0.0	0.7	815.0	8.7	154.0	1.1	122.9
28	BD-05	16950	35180	2485.0	0.0	7.0	807.0	700.0	86.6	10.1	102.0
29	BD-05	13460	38520	2170.0	0.2	0.3	4500.0	45.0	138.0	0.3	320.0
30	BD-05	12100	37200	1813.0	0.1	0.5	6810.0	58.0	144.0	0.3	274.0
32	NIST	432	350	452.0	23.0	251.0	400.0	440.0	410.0	380.0	310.0
33	NIST	432	350	452.0	23.6	251.0	460.0	441.0	410.0	384.0	325.0
37	BD-16	32800	31200	1130.0	0.0	0.0	393.0	4.8	13.2	0.0	-9.6
38	BD-16	30900	30100	1052.0	0.0	0.0	364.0	3.1	18.2	0.0	-17.5
39	BD-16	31440	30900	1084.0	0.0	0.0	399.0	4.0	17.2	0.0	-19.1
40	BD-16	28370	29680	939.0	0.0	0.0	289.0	3.2	18.2	0.0	-14.1
41	BD-16	31700	28700	1460.0	1.6	0.5	289.0	6.7	20.4	0.8	-28.2
42	BD-16	29300	25450	1979.0	0.7	0.3	249.0	17.9	21.1	1.0	-5.7
43	BD-16	35600	30800	2310.0	3.9	0.1	279.0	9.0	23.5	0.1	-18.6
44	BD-16	41400	34300	1497.0	0.5	0.1	307.0	8.1	14.7	0.0	-41.0
45	BD-16	50700	37400	1911.0	0.0	0.0	317.0	19.6	20.5	0.0	-19.7
46	BD-16	46700	34900	1736.0	0.0	0.0	314.0	106.0	20.7	0.2	-21.6
47	BD-16	39600	34200	1360.0	0.0	0.0	288.0	52.8	18.8	0.1	386.0
48	BD-16	35800	31700	1242.0	0.0	0.0	220.0	51.0	17.7	0.0	182.0
49	BD-16	25900	30200	706.0	0.0	0.0	161.2	24.7	16.5	0.1	28.6
50	BD-16	28200	30790	706.0	0.0	0.1	158.6	24.2	16.2	0.1	14.5
52	NIST	432	350	450.0	24.0	251.0	460.0	440.0	410.0	380.0	320.0
53	NIST	432	346	452.0	23.6	251.0	460.0	441.0	410.0	383.7	324.9
55	BD-19	9810	11920	1247.0	0.0	0.1	214.0	9.2	55.1	0.1	104.0
56	BD-19	9890	11790	1255.0	0.0	7.6	137.0	8.2	82.0	5.9	59.5
57	BD-19	22600	13110	1312.0	0.0	0.9	78.9	8.6	20.1	0.8	216.0
58	BD-19	21000	13580	1500.0	0.0	0.1	76.0	8.8	25.0	0.1	227.0
59	BD-19	28200	12990	1389.0	0.1	0.1	74.4	5.1	9.1	0.0	362.0

60	BD-19	26300	12960	1190.0	0.1	2.2	123.6	6.9	9.1	2.2	308.0
61	BD-19	22100	12790	1527.0	0.0	3.0	183.0	6.8	17.9	2.1	182.0
62	BD-19	19600	12240	1766.0	0.1	3.3	176.0	5.8	25.1	2.3	108.0
64	BD-19	25300	13930	989.0	0.1	6.9	123.2	5.8	17.9	7.4	586.0
65	BD-19	22400	14210	1303.0	0.1	0.2	138.9	7.4	13.0	0.1	115.0
67	BD-19	18940	13000	2213.0	0.1	6.1	195.8	5.4	25.0	5.7	65.0
68	BD-19	19420	13190	2149.0	0.2	3.8	208.9	6.3	18.8	3.2	72.1
69	BD-19	19700	13320	2108.0	0.1	5.2	201.4	7.0	19.7	4.1	67.1
70	BD-19	19740	14220	2185.0	0.0	2.7	213.8	6.7	18.9	2.1	72.0
71	BD-19	15580	13470	1744.0	0.0	13.5	186.8	1280.0	30.8	13.8	87.5
73	BD-19	17280	12980	1680.0	0.1	23.5	183.7	729.0	36.8	25.0	40.4
74	BD-19	16120	13110	1595.0	0.1	6.0	193.5	560.0	39.7	4.4	46.0
75	BD-19	16250	12820	1713.0	0.5	9.5	187.7	2040.0	32.4	5.6	44.0
76	BD-19	15590	12320	1540.0	0.1	9.1	167.6	92.0	34.4	9.0	49.0
77	BD-19	14900	14890	1449.0	0.1	5.4	193.9	9.0	30.8	4.6	127.3
78	BD-19	20600	15150	1740.0	0.0	0.3	154.0	5.8	11.1	0.2	135.0
79	BD-19	18260	14660	1680.0	0.1	0.1	170.7	4.3	25.5	0.1	167.0
80	BD-19	19860	14580	2168.0	0.0	2.6	194.9	5.0	18.4	2.3	76.0
81	BD-19	20140	14690	2162.0	0.1	2.1	209.9	7.0	19.3	2.1	77.2
82	BD-19	20680	14840	2055.0	0.0	2.4	205.5	5.0	17.8	2.5	75.6
83	BD-19	25900	16790	1097.0	0.0	0.8	111.8	10.2	10.1	0.6	149.8
84	BD-19	20310	15690	1435.0	0.1	0.2	179.0	7.2	16.3	0.0	118.0
85	BD-19	20800	16140	1480.0	0.0	1.2	166.0	5.7	14.8	1.5	139.7
86	BD-19	19690	15920	2200.0	0.0	0.0	201.0	6.2	18.4	0.0	70.5
87	BD-19	19800	15580	2131.0	0.0	0.0	197.0	5.5	17.3	0.0	71.8
88	BD-19	19850	15980	2070.0	0.0	0.1	195.0	6.0	16.2	0.0	80.9
90	BD-19	25200	17870	983.0	4.8	3.4	94.2	8.3	7.6	3.0	151.0
92	BD-19	26660	18040	1187.0	0.6	1.4	94.7	7.7	11.7	0.9	277.0
93	BD-19	20960	16220	2314.0	0.5	1.8	205.2	8.6	21.5	1.9	85.1
94	BD-19	19150	16780	2454.0	0.3	2.3	193.7	9.4	25.8	2.4	66.7
95	BD-19	20900	16580	2241.0	0.2	0.4	205.3	8.8	23.4	0.1	76.2
96	BD-19	26900	22180	1109.0	1.3	1.4	104.9	6.4	7.0	1.2	780.0
97	BD-19	29400	23480	977.0	0.0	0.2	92.7	7.5	8.0	0.1	960.0
98	BD-19	29100	22700	1027.0	0.0	0.0	83.7	7.9	7.2	0.0	684.0
99	BD-19	31200	21510	1170.0	0.0	0.8	87.6	173.0	11.7	0.3	887.0
100	BD-19	27800	21590	1424.0	0.0	0.4	98.9	27.9	10.7	0.0	568.0
101	BD-19	22700	18910	1738.0	0.0	0.4	156.3	240.0	21.8	0.2	177.0
103	BD-19	17840	18450	1890.0	0.0	0.2	203.4	6.3	30.9	0.1	52.6
104	BD-19	16560	19950	1857.0	0.1	0.3	194.4	7.0	33.2	0.2	39.4
105	BD-19	16800	21070	1837.0	0.0	0.5	186.0	7.4	30.0	0.7	44.1
106	BD-19	16330	21190	1795.0	0.1	0.1	196.0	6.9	34.1	0.0	39.1
107	BD-19	16940	21350	1845.0	0.0	0.3	194.0	7.3	29.6	0.2	36.1
108	BD-19	16720	22700	1840.0	0.1	0.4	186.6	14.5	31.9	0.6	88.8
109	BD-19	16400	22780	1836.0	0.1	0.1	182.1	8.6	29.8	0.1	97.2
110	BD-19	15160	21300	1644.0	0.0	0.5	162.0	6.4	30.5	0.4	61.6
111	BD-19	16000	23640	1570.0	0.5	0.2	176.0	7.6	33.4	0.1	46.0

112	BD-19	16880	22100	1892.0	0.1	0.1	178.0	5.6	33.1	0.0	44.0
113	BD-19	18300	23600	1940.0	0.0	0.0	162.0	7.6	32.9	0.0	117.0
114	BD-19	13400	23700	1702.0	0.1	0.1	183.1	7.3	36.5	0.0	65.0
116	BD-19	14280	24270	1880.0	0.4	0.1	207.0	7.2	40.2	0.0	52.1
117	BD-19	14300	23700	1770.0	0.1	0.1	185.0	8.2	40.9	0.0	56.0
118	BD-19	21000	23400	2386.0	18.0	1.2	215.0	9.0	24.5	1.9	88.3
119	BD-19	20350	23480	2532.0	0.8	0.5	198.9	7.1	24.5	0.4	91.7
120	BD-19	20090	22810	2431.0	2.4	2.6	179.5	7.7	20.4	2.8	86.0
121	BD-19	20530	24010	2420.0	0.5	0.4	191.2	8.2	22.4	0.7	85.3
123	BD-19	23100	23200	1327.0	0.2	0.3	178.0	6.2	26.5	0.1	207.0
124	BD-19	27700	27300	1390.0	0.8	0.2	109.9	7.0	17.1	0.3	475.0
125	BD-19	20840	25500	2260.0	0.4	1.7	176.0	8.3	22.5	2.6	123.0
126	BD-19	19300	26500	2406.0	0.9	0.2	187.0	8.1	25.3	0.2	95.0
128	BD-19	20580	27600	1877.0	0.7	0.2	174.0	5.7	25.0	0.2	84.2
130	NIST	432	350	452.0	23.6	251.0	460.0	441.0	410.0	384.0	325.0
131	NIST	432	350	452.0	23.6	251.0	460.0	441.0	410.0	384.0	325.0
133	BD-18	28500	29300	1739.0	0.2	0.1	176.8	6.7	11.1	0.0	44.0
134	BD-18	29300	29780	1706.0	0.1	0.1	167.0	5.9	10.7	0.0	48.3
135	BD-18	28800	29800	1878.0	0.0	0.1	155.4	6.5	11.8	0.0	43.0
136	BD-18	33800	31800	1715.0	1.4	0.0	184.7	6.8	9.7	0.0	74.8
137	BD-18	32100	29000	971.0	0.0	0.1	162.1	6.9	7.3	0.0	126.6
138	BD-18	33100	32100	948.0	0.0	0.1	161.4	12.5	6.8	0.1	143.0
139	BD-18	33900	31500	925.0	0.1	0.1	157.2	8.0	6.0	0.0	130.0
140	BD-18	30100	28900	430.0	2.1	0.1	157.0	5.9	3.2	0.0	71.8
141	BD-18	18000	31600	546.0	1.2	0.3	256.7	37.0	29.6	0.2	73.0
142	BD-18	22700	29300	1676.0	0.7	0.1	204.0	3.8	16.9	0.0	50.0
143	BD-18	17290	28000	1472.0	0.2	0.1	179.0	5.2	19.8	0.0	16.5
144	BD-18	19400	28590	1598.0	0.2	0.0	164.3	7.4	17.6	0.0	27.8
145	BD-18	28700	32600	1678.0	0.1	0.0	196.2	5.0	13.1	0.0	93.0
146	BD-18	20840	29300	1565.0	0.0	0.0	167.4	5.5	16.4	0.0	45.4
147	BD-18	16800	27900	1460.0	0.1	0.0	160.0	4.7	15.1	0.0	15.3
148	BD-18	15610	27200	1270.0	0.1	0.1	177.0	3.5	11.2	0.0	11.9
149	BD-18	16900	29000	1011.0	0.4	0.1	243.0	6.0	11.4	0.0	9.7
150	BD-18	14900	27300	1005.0	0.2	0.1	169.0	4.1	8.6	0.0	14.0
151	BD-18	17700	28830	1523.0	0.1	0.0	168.3	6.3	20.5	0.0	17.5
152	BD-18	23340	31400	1567.0	0.2	0.0	227.3	5.3	24.5	0.0	32.2
153	BD-18	27700	33500	616.0	0.2	0.1	156.0	6.2	8.3	0.0	271.0
154	BD-18	40100	32100	3190.0	0.3	0.1	163.0	6.5	14.4	0.0	44.0
155	BD-18	19400	28890	1750.0	0.2	0.0	175.9	5.3	19.0	0.0	31.3
156	BD-18	15980	25530	1624.0	0.0	0.1	158.5	5.1	12.2	0.0	12.7
157	BD-18	17200	27230	1686.0	0.0	0.0	173.0	5.7	13.5	0.0	11.4
158	BD-18	16140	27340	1595.0	0.1	0.1	148.6	5.8	12.9	0.0	16.0
159	BD-18	17240	26610	1636.0	0.2	0.0	173.0	4.8	13.2	0.0	19.0
161	BD-18	29200	29520	2370.0	0.6	0.2	271.0	6.0	25.0	0.2	42.0
162	BD-18	31500	32300	1170.0	0.2	0.1	213.0	7.4	9.7	0.0	72.3
163	BD-18	20600	30420	927.0	0.3	0.0	223.0	6.7	23.3	0.0	48.8

164	BD-18	18100	28300	1192.0	0.3	0.2	196.0	24.0	19.4	0.1	40.7
165	BD-18	10780	23900	456.0	0.3	0.1	64.3	7.7	7.5	0.0	34.2
166	BD-18	10500	34100	680.0	0.1	0.0	218.0	9.9	18.5	0.1	360.0
168	BD-18	29700	29900	209.0	0.0	0.1	144.7	8.6	2.1	0.0	133.0
169	BD-18	30300	28460	152.4	0.1	0.1	123.8	13.5	1.5	0.1	34.2
170	BD-18	31800	29300	133.0	0.7	0.0	2090.0	10.0	384.0	0.0	79.0
171	BD-18	44600	34700	1970.0	0.1	0.1	221.0	18.8	20.0	0.1	62.0
172	BD-18	34500	32300	2400.0	0.3	0.2	298.0	33.0	26.1	0.1	45.1
173	BD-18	17900	28030	1579.0	0.9	0.0	245.0	11.7	27.6	0.0	22.7
174	BD-18	17640	29000	1489.0	0.1	0.0	187.0	9.9	16.8	0.0	29.1
175	BD-18	14260	24800	1347.0	0.0	0.1	92.0	2.7	8.0	0.1	10.7
176	BD-18	14900	28200	1220.0	0.0	0.1	177.0	5.4	18.4	0.0	44.7
177	BD-18	29900	29700	512.0	0.0	0.0	177.2	8.4	7.5	0.0	73.0
178	BD-18	29700	29700	196.0	0.0	0.0	120.0	8.4	4.6	0.0	90.0
179	BD-18	45000	33000	780.0	0.0	0.2	1630.0	23.0	312.0	0.1	161.0
180	BD-18	37900	32300	3300.0	0.1	0.1	291.9	8.9	21.1	0.0	33.5
181	BD-18	17000	27100	1650.0	0.1	4.5	176.8	9.6	16.0	0.0	34.9
182	BD-18	17050	28600	1639.0	0.1	0.3	165.8	17.2	12.4	0.0	13.6
183	BD-18	33700	28400	350.0	0.1	0.1	146.0	9.2	5.2	0.0	157.0
184	BD-18	30800	29010	326.0	0.0	0.1	182.0	15.1	4.8	0.0	113.0
185	BD-18	30500	29000	357.0	0.0	0.1	148.0	6.9	5.0	0.0	76.3
186	BD-18	28200	29200	1910.0	0.0	0.2	1840.0	13.9	354.0	0.0	42.2
187	BD-18	24900	29700	1527.0	0.0	0.1	256.0	10.0	22.5	0.0	36.5
188	BD-18	25900	27660	1652.0	0.1	0.0	153.0	6.5	12.2	0.0	27.7
189	BD-18	28560	27620	1813.0	0.1	0.1	167.0	6.2	11.2	0.0	32.5
190	BD-18	28300	27900	1440.0	0.5	0.1	158.6	6.0	11.4	0.0	42.3
191	BD-18	25200	26690	1607.0	0.2	0.0	166.5	7.3	13.7	0.1	24.0
192	BD-18	30900	29000	1724.0	0.3	0.1	187.9	7.7	11.0	0.0	43.9
193	BD-18	26200	28100	1611.0	0.0	0.1	160.0	6.2	13.0	0.0	73.3
194	BD-18	31400	29960	401.0	6.9	0.2	224.0	19.0	37.0	0.2	247.0
195	BD-18	41400	28700	5200.0	13.6	0.3	267.0	10.0	21.2	0.1	65.0
196	BD-18	58900	33600	11290.0	11.6	0.3	151.0	15.1	17.7	0.2	23.2
197	BD-18	44500	28900	5400.0	7.8	0.2	245.0	10.1	14.4	0.2	37.6
198	BD-18	40700	27740	6570.0	16.7	0.2	289.0	12.4	12.4	0.1	41.6
199	BD-18	40800	28700	3860.0	7.5	0.1	276.0	9.8	15.5	0.1	33.1
200	BD-18	33600	29610	504.0	2.5	0.2	215.3	9.0	20.4	0.1	222.0
201	BD-18	29800	28300	920.0	11.0	0.1	207.0	7.0	16.7	0.0	63.3
202	BD-18	18660	27100	1502.0	3.8	0.0	186.0	9.6	30.5	0.0	27.6
203	BD-18	19180	28270	1586.0	3.4	0.0	202.0	8.3	26.9	0.0	36.3
204	BD-18	18600	26620	1671.0	1.5	0.1	148.2	7.6	20.1	0.0	23.9
205	BD-18	17770	26580	1668.0	0.8	0.0	142.2	8.3	17.8	0.0	17.1
209	NIST	432	350	452.0	23.6	251.0	460.0	441.0	410.0	384.0	325.0
210	NIST	432	350	452.0	23.6	251.0	460.0	441.0	410.0	384.0	325.0
212	S4502	39100	36200	2980.0	0.4	0.1	208.0	8.1	27.3	0.0	49.3
213	S4502	37400	34600	2520.0	0.0	0.2	177.0	7.6	24.5	0.0	69.0
214	S4502	30200	32500	1154.0	0.1	0.0	140.7	5.9	9.2	0.0	227.8

215	S4502	44400	36500	1451.0	0.0	0.1	115.4	14.3	15.4	0.0	157.0
216	S4502	44200	37000	1348.0	0.2	0.1	161.0	9.8	20.3	0.0	98.0
217	S4502	40200	37200	2647.0	0.1	0.0	180.0	9.2	13.1	0.0	214.0
218	S4502	47800	39730	3140.0	0.0	0.0	116.7	9.1	18.6	0.1	91.0
219	S4502	49000	39100	1771.0	0.0	0.0	156.6	8.9	24.5	0.0	38.0
221	S4502	23500	30460	2040.0	1.1	0.0	307.0	7.6	27.4	0.0	65.6
223	S4502	18100	31600	2382.0	0.2	0.1	433.0	9.7	34.5	0.0	38.9
224	S4502	40500	36600	3140.0	0.2	0.1	158.0	9.2	14.1	0.0	257.5
225	S4502	38000	35440	3120.0	0.1	0.0	194.0	9.7	15.1	0.0	229.7
226	S4502	22500	31400	2490.0	0.0	0.0	338.0	11.0	22.4	0.0	70.0
227	S4502	20100	31900	2054.0	0.1	0.0	391.0	7.8	21.5	0.0	126.8
228	S4502	18840	33100	2085.0	0.2	0.0	378.0	5.4	19.5	0.0	117.6
229	S4502	17920	31200	2015.0	0.1	0.1	419.0	8.9	26.5	0.0	134.0
230	S4502	21500	28900	2600.0	0.1	0.7	362.0	4.1	29.6	0.3	138.0
231	S4502	21600	30590	2480.0	0.1	1.2	300.0	4.7	26.8	0.5	167.0
232	S4502	38600	33900	3870.0	0.1	0.0	185.0	15.4	21.1	0.1	70.5
233	S4502	33500	34000	3670.0	0.0	0.8	258.0	7.1	27.3	1.5	99.0
234	S4502	29000	30800	3190.0	0.2	0.1	246.0	9.5	29.7	0.1	75.0
235	S4502	32500	31900	2810.0	0.1	0.0	239.0	5.2	27.7	0.1	80.4
236	S4502	34700	31370	2970.0	0.2	0.2	256.0	11.0	22.8	0.1	181.8
238	NIST	432	350	452.0	23.6	251.0	460.0	441.0	410.0	384.0	325.0
239	NIST	432	350	452.0	23.6	251.0	460.0	441.0	410.0	384.0	325.0
241	BSU220	23300	29400	614.0	0.0	0.1	272.0	10.2	25.0	0.0	32.0
242	BSU220	24200	28800	628.3	0.1	0.0	262.0	9.4	26.1	0.0	30.3
243	BSU220	23100	29300	658.0	0.2	0.0	220.4	9.0	23.6	0.0	39.7
244	BSU220	22450	27500	568.0	0.1	0.2	230.3	13.4	24.1	0.0	31.6
245	BSU220	23200	28030	691.0	0.1	0.0	223.8	8.8	24.9	0.0	37.4
246	BSU220	24600	28700	739.0	0.1	0.1	246.0	8.4	27.9	0.0	35.9
247	BSU220	25180	30200	696.0	0.1	0.1	268.0	8.6	27.6	0.0	32.1
248	BSU220	22400	30800	664.0	0.7	0.1	186.4	11.2	11.0	0.0	51.4
249	BSU220	22000	30200	569.0	0.2	0.0	149.0	12.0	10.4	0.0	48.6
250	BSU220	22800	27900	615.0	0.2	0.1	158.0	9.6	10.8	0.0	46.2
251	BSU220	23890	26550	613.0	0.2	0.1	220.0	8.4	16.3	0.0	31.5
252	BSU220	23290	26670	595.0	0.4	0.2	191.9	10.5	18.4	0.0	35.0
253	BSU220	22600	26500	525.0	0.5	0.1	200.0	9.3	18.3	0.1	27.6
254	BSU220	21600	26560	522.0	0.4	0.2	210.0	9.2	19.1	0.0	28.6
255	BSU220	22300	28700	575.0	0.5	0.0	190.1	9.4	25.2	0.0	30.9
257	BSU220	23900	30300	1106.0	10.3	0.0	152.0	8.6	11.5	0.0	47.6
258	BSU220	22400	29030	689.0	56.0	0.2	131.0	11.3	11.9	0.0	54.6
259	BSU220	22000	29000	630.0	10.0	0.0	150.0	21.0	22.0	0.0	44.0
260	BSU220	22100	28900	610.0	9.0	0.1	177.0	8.9	16.6	0.0	40.0
261	BSU220	23000	28000	640.0	3.4	0.2	170.0	9.3	19.0	0.0	54.0
262	BSU220	22410	27010	654.0	31.0	0.1	176.8	7.1	17.6	0.0	38.6
263	BSU220	22000	26100	771.0	60.0	0.1	191.0	10.1	18.8	0.0	35.2
264	BSU220	21900	27700	561.0	110.0	0.1	202.5	12.5	19.1	0.0	27.9
266	BSU220	19480	27000	468.0	0.1	0.2	243.0	3.5	28.0	0.0	36.3

267	BSU220	20000	27100	640.0	0.2	0.2	239.2	5.5	28.9	0.0	31.5
268	BSU220	23000	28000	590.0	0.6	0.0	240.0	3.1	37.0	0.0	21.0
270	BSU220	16210	23600	340.0	0.1	0.0	186.0	5.7	21.9	0.0	50.6
271	BSU220	14900	22600	324.0	0.0	0.1	186.0	5.9	18.6	0.0	40.9
272	BSU220	16000	24000	430.0	0.3	0.2	210.0	9.3	23.0	0.0	56.0
273	BSU220	15500	21900	468.0	0.7	0.0	194.0	6.7	17.5	0.0	65.0
274	BSU220	17470	26500	476.0	0.0	0.2	192.0	7.6	18.1	0.0	34.1
275	BSU220	18000	29000	660.0	0.0	0.0	240.0	12.0	24.0	0.0	27.0
276	BSU220	18280	28300	611.0	0.1	0.0	228.0	8.7	22.5	0.0	35.2
277	BSU220	20000	30000	560.0	0.5	0.4	230.0	7.2	26.0	0.0	40.0
278	BSU220	19030	31290	570.0	0.1	0.0	235.0	8.7	27.5	0.0	26.3
279	BSU220	19000	28000	540.0	0.6	0.1	240.0	4.4	29.0	0.0	25.0
280	BSU220	21260	28900	539.0	0.2	0.0	233.0	8.4	26.8	0.0	26.8
281	BSU220	20400	27400	469.0	0.1	0.0	259.0	8.5	28.9	0.1	36.1
282	BSU220	21790	27000	808.0	0.0	0.0	178.0	8.9	36.3	0.0	37.5
284	BSU220	15400	19700	537.0	0.0	0.0	161.0	5.8	18.5	0.0	68.0
285	BSU220	17160	24900	622.0	0.0	0.0	205.0	4.4	23.3	0.0	44.1
286	BSU220	16000	26000	560.0	0.0	0.1	210.0	9.8	24.0	0.0	28.0
287	BSU220	18000	28600	539.0	0.0	0.0	238.0	7.6	22.6	0.0	23.3
288	BSU220	17000	30000	470.0	0.0	0.0	240.0	8.4	25.0	0.0	25.0
289	BSU220	17800	29800	548.0	0.0	0.1	247.7	8.4	26.8	0.0	20.1
291	NIST	432	350	452.0	23.6	251.0	460.0	441.0	410.0	384.0	325.0
292	NIST	432	350	452.0	23.6	251.0	460.0	441.0	410.0	384.0	325.0
294	VEINLET	12200	9400	390.0	0.2	2.0	98.0	1.8	7.6	8.3	57.0
295	VEINLET	44400	31440	2763.0	2.7	0.3	139.0	7.5	16.5	0.1	12.9
296	VEINLET	43000	32900	2791.0	1.3	0.1	155.0	5.6	17.7	0.0	15.7
298	VEINLET	50400	35800	3500.0	5.9	0.1	206.0	8.0	13.3	0.2	49.1
299	VEINLET	48200	33500	3248.0	2.8	0.0	278.0	5.7	15.1	0.2	34.3
301	VEINLET	48000	32600	3550.0	13.0	0.0	206.0	8.9	14.5	0.2	38.2
302	VEINLET	48400	34700	3606.0	80.0	0.1	197.5	7.1	15.0	0.0	30.4
303	VEINLET	51900	36290	3450.0	20.0	0.1	219.0	7.6	14.5	0.0	49.7
304	VEINLET	48300	34300	3650.0	1.7	0.0	212.4	6.9	14.7	0.0	33.9
305	VEINLET	33590	29860	1483.0	0.8	0.0	231.0	15.7	22.3	0.2	19.3
306	VEINLET	31000	29500	1440.0	0.3	0.0	160.0	11.2	19.5	0.1	12.3
308	VEINLET	28000	28290	1273.0	0.1	0.0	134.0	6.1	15.8	0.0	18.0
309	VEINLET	20000	18000	960.0	0.0	0.0	92.0	3.6	10.0	0.0	39.0
310	VEINLET	24200	21500	1060.0	0.6	0.0	108.0	8.9	13.0	0.0	39.4
311	VEINLET	31700	28700	1669.0	0.1	0.0	173.0	8.8	17.5	0.0	9.7
312	VEINLET	38700	32700	2059.0	0.3	0.0	208.0	9.2	21.6	0.0	10.0
313	VEINLET	36600	31800	1869.0	0.0	0.0	190.0	7.0	27.3	0.0	26.1
314	VEINLET	40400	32900	3160.0	0.1	0.0	168.0	8.8	17.1	0.0	16.3
315	VEINLET	40200	33100	2110.0	0.2	0.2	224.0	8.4	16.1	0.0	19.6
316	VEINLET	41600	34200	3830.0	0.0	0.0	183.6	8.3	19.1	0.0	17.1
317	VEINLET	41400	34400	2069.0	0.0	0.0	217.3	8.7	18.8	0.0	17.4
318	VEINLET	43300	31400	1768.0	0.0	0.5	189.8	16.1	22.1	0.5	35.0
319	VEINLET	49400	26140	1720.0	0.0	0.1	179.1	11.2	21.0	0.9	44.8

321	VEINLET	25200	19600	2240.0	0.2	0.6	114.0	3.9	10.9	1.3	72.0
324	VEINLET	40700	32500	2273.0	0.1	0.2	218.0	6.9	18.1	1.6	28.5
325	VEINLET	39100	33600	1956.0	0.1	0.2	218.0	7.2	18.2	0.2	19.8
326	VEINLET	39500	33000	1948.0	0.0	0.2	214.0	7.5	20.3	0.1	19.1
327	VEINLET	61700	41300	8180.0	0.1	0.0	157.6	7.8	20.7	0.0	6.9
328	VEINLET	62800	41300	9070.0	0.0	0.0	139.0	10.1	20.3	0.0	9.5
329	VEINLET	39100	32400	2657.0	0.0	0.0	215.8	6.1	20.2	0.0	18.5
330	VEINLET	43800	34800	3556.0	0.0	0.0	205.4	8.2	19.9	0.0	17.3
332	NIST	432	350	452.0	23.6	251.0	460.0	441.0	410.0	384.0	325.0
333	NIST	432	350	452.0	23.6	251.0	460.0	441.0	410.0	384.0	325.0
335	BD-10	15530	32970	2521.0	0.1	0.0	197.7	10.5	28.9	0.0	120.0
336	BD-10	16660	32500	2430.0	0.1	4.2	194.9	10.9	29.6	7.0	171.0
337	BD-10	16000	33000	2200.0	0.2	0.0	190.0	8.6	31.0	0.0	140.0
338	BD-10	16510	32060	2149.0	0.1	0.9	195.4	9.6	30.4	0.8	154.3
339	BD-10	22100	30000	2400.0	1.3	0.0	178.0	11.2	18.6	0.0	160.0
340	BD-10	27900	34100	1300.0	0.5	0.1	85.0	9.9	6.4	0.3	363.0
341	BD-10	21120	31180	2415.0	0.1	1.8	195.6	8.8	25.3	4.5	187.0
342	BD-10	19940	31600	2610.0	0.1	1.3	182.0	11.8	31.5	1.9	113.0
344	BD-10	15770	30800	2085.0	0.1	0.1	202.0	13.1	41.0	0.1	41.0
345	BD-10	15530	31700	2076.0	0.1	0.0	182.0	10.6	36.3	0.1	50.0
346	BD-10	16000	31000	1800.0	0.1	0.0	160.0	6.0	40.0	0.0	38.0
347	BD-10	16100	30600	2070.0	0.0	0.1	170.0	9.6	34.4	0.0	48.9
349	BD-10	15510	28500	1819.0	0.2	0.0	167.0	8.4	36.1	0.0	30.9
350	BD-10	22700	32700	1112.0	8.0	4.6	180.3	8.7	15.4	6.6	315.0
355	BD-10	15950	30800	2067.0	0.0	0.3	193.0	8.3	31.6	0.4	54.1
356	BD-10	16230	32600	2056.0	0.1	5.2	193.3	111.0	33.0	7.9	60.2
357	BD-10	16890	30700	2218.0	0.0	0.4	188.0	8.6	29.2	0.5	42.1
359	BD-10	16870	29330	2085.0	0.0	0.4	196.6	6.8	35.0	0.2	32.8
360	BD-10	17200	31600	2400.0	0.1	0.1	185.7	6.9	31.0	0.1	51.2
361	BD-10	19840	31300	2633.0	0.2	1.3	190.8	7.5	25.5	1.9	93.7
363	BD-10	22890	35680	475.0	0.1	0.1	68.8	11.1	4.7	0.0	211.0
365	BD-10	20630	29500	2695.0	0.1	0.2	193.6	10.7	23.6	0.2	127.1
366	BD-10	19000	28000	2800.0	0.0	0.4	190.0	11.0	16.0	0.0	110.0
367	BD-10	19650	28800	2825.0	0.2	0.1	192.2	10.9	24.8	0.0	98.4

Appendix 3: Selected elements from whole rock analyses of Black Dog drill core samples. Values are in weight % for SiO2, Al2O3, Feo, MgO, K, Na and Ca and in PPM for Au, Ag, Cu, Zn, Nb, Zr and Y.

HOLE	ID	LITHO	SIO2	Al2O3	FeO	MgO	K	Na	Ca	Au	Ag	Cu	Zn	Nb	Zr	Y
16-001	XX001	V1	59.1	4.3	6.4	2.0	1.0	0.1	2.2	0.0	0.2	51	94	7	250	33
16-001	XX002	V2	56.2	4.4	5.9	1.9	1.0	0.1	2.3	0.0	0.2	31	88	7	244	34
16-001	XX003	V1	62.9	3.4	5.9	1.7	0.8	0.1	1.7	0.0	0.2	42	93	9	323	38
16-001	XX004	V2	53.9	5.0	5.0	2.8	1.0	0.1	2.3	0.0	0.2	102	113	6	187	28
16-001	XX005	V1	60.7	5.4	5.3	2.4	1.0	0.2	2.3	0.0	0.2	92	107	7	224	23
16-001	XX006	V2	56.4	5.1	7.4	3.5	0.9	0.1	3.3	0.0	0.2	112	99	8	242	28
16-001	XX007	V1	55.0	4.4	6.9	2.7	0.8	0.1	3.0	0.0	0.2	105	95	8	238	28
16-001	XX008	V2	56.0	4.9	6.2	2.3	0.7	0.2	3.0	0.0	0.6	124	116	8	234	26
16-001	XX009	V1	59.7	4.5	5.2	2.2	0.7	0.2	2.6	0.0	0.2	82	80	6	217	22
16-001	XX010	V1	69.6	1.5	1.5	0.4	0.4	0.0	2.6	0.0	0.2	16	119	8	71	13
16-001	XX011	V2	55.4	4.3	6.9	1.9	1.2	0.1	3.0	0.0	0.2	117	161	9	260	39
16-001	XX012	V1	60.7	3.2	6.4	1.4	0.8	0.1	1.9	0.0	0.2	69	104	12	315	44
16-001	XX013	V1	57.5	4.9	8.2	1.7	0.9	0.0	2.9	0.0	0.2	78	141	10	295	43
16-001	XX014	V1	58.4	3.3	7.1	1.6	1.0	0.1	2.3	0.0	0.2	37	149	11	304	43
16-001	XX015	V2	57.2	4.1	7.3	2.0	1.3	0.1	2.4	0.0	0.3	157	112	10	275	41
16-001	XX016	V2GN	55.5	3.9	8.3	1.9	1.1	0.0	2.6	0.0	0.5	167	99	12	330	49
16-001	XX017	V1	53.3	3.3	8.0	1.8	0.8	0.0	2.6	0.0	0.2	71	50	12	321	48
16-001	XX018	V2	55.3	5.2	8.8	2.8	1.6	0.1	2.0	0.0	0.2	66	49	10	275	39
16-001	XX019	V2GN	50.5	7.0	11.2	3.5	2.4	0.1	1.6	0.0	0.2	20	94	3	128	20
16-001	XX020	V2GN	51.6	4.7	9.0	2.2	1.0	0.0	3.4	0.2	1.0	186	125	8	220	34
16-001	XX021	V2	55.3	5.7	8.8	3.0	1.1	0.1	1.6	0.0	0.2	62	61	6	148	24
16-001	XX022	I2	52.5	3.0	4.1	2.2	0.3	0.1	2.0	0.0	0.5	200	44	7	167	28
16-001	XX023	V2GN	52.9	7.5	9.9	3.5	1.4	0.2	1.2	0.1	0.4	102	182	7	168	28
16-002	XX024	V2GN	48.6	9.0	13.9	3.3	2.8	0.1	0.4	0.3	0.5	236	51	8	159	27
16-002	XX025	TMBX	68.9	0.1	1.2	0.0	0.0	0.0	0.4	0.0	0.2	20	2	8	175	18
16-002	XX026	V2GN	52.9	5.1	11.1	2.1	0.9	0.0	0.5	0.0	0.3	46	187	10	244	29
16-002	XX027	V2GN	61.1	4.2	8.1	1.7	1.5	0.0	0.6	0.0	0.3	17	17	11	283	32
16-002	XX028	V2GN	62.8	4.8	7.3	1.4	1.3	0.0	1.2	0.0	0.2	14	31	10	275	36
16-002	XX029	V2GN	50.6	6.7	12.5	2.6	1.8	0.0	0.4	0.1	0.2	58	53	8	162	26
16-002	XX030	V2	49.1	4.4	8.4	3.4	1.1	0.1	3.3	0.0	0.3	99	70	7	155	26
16-002	XX031	I1	72.4	1.7	1.7	0.5	0.2	0.1	1.3	0.0	0.2	21	104	8	77	14
16-002	XX032	I1	67.3	2.7	3.0	1.2	0.6	0.1	1.0	0.0	0.2	42	75	3	114	8
16-002	XX033	V2	50.8	9.8	8.7	3.5	0.7	0.4	4.4	0.0	0.2	110	151	7	157	26
16-002	XX034	V2	50.7	5.1	8.6	3.6	0.6	0.1	4.0	0.0	0.2	124	95	7	166	27
16-003	XX035	V2	52.5	3.0	3.7	2.4	0.1	0.1	0.8	0.0	0.2	63	49	3	109	20
16-003	XX036	I2	52.8	4.8	5.8	3.1	0.0	0.0	2.8	0.0	0.2	102	78	6	178	24
16-003	XX037	V2	50.7	3.4	4.2	2.3	0.5	0.1	1.8	0.0	0.2	101	48	7	167	25
16-003	XX038	V2	54.0	5.0	8.8	1.9	0.9	0.0	3.6	0.0	0.3	119	226	11	263	40
16-003	XX039	V2GN	54.1	5.9	11.1	2.2	0.8	0.0	2.6	0.0	0.9	151	257	9	244	36
16-003	XX040	V2	56.1	4.5	7.8	2.0	1.0	0.0	2.8	0.0	0.2	70	135	12	298	42
16-003	XX041	V1	44.5	4.6	5.7	2.0	0.1	0.0	4.2	0.0	0.2	18	110	12	326	34
16-003	XX042	V2	50.4	6.1	8.2	3.3	0.2	0.2	3.2	0.0	0.9	112	462	7	182	29

16-003	XX043	V1	65.8	3.1	4.4	0.8	0.6	0.1	1.4	0.0	0.3	9	32	9	213	24
16-003	XX044	V2	52.0	4.3	7.5	2.3	0.4	0.1	3.8	0.0	0.6	205	109	9	210	32
16-003	XX045	V1	49.7	1.5	4.7	1.9	0.3	0.0	2.6	0.0	1.2	38	53	19	262	25
16-003	XX046	V1	66.7	2.3	5.3	1.2	0.3	0.0	0.7	0.0	0.2	19	106	9	210	22
16-003	XX047	V2	60.0	3.6	11.2	1.5	0.2	0.0	0.4	0.0	0.7	12	134	9	211	28
16-003	XX048	V1	59.6	2.9	9.9	1.1	0.2	0.0	0.4	0.0	0.4	32	98	11	289	31
16-003	XX049	V2	56.6	2.2	7.2	0.8	0.2	0.0	0.4	0.0	0.7	63	40	10	221	22
16-003	XX050	V1	65.6	1.7	4.3	0.9	0.2	0.0	1.0	0.0	0.2	27	238	9	207	23
16-003	XX051	V2	52.4	4.0	7.5	2.8	0.6	0.2	4.0	0.0	0.2	96	102	9	218	29
16-003	XX052	V2MT	57.7	2.2	12.4	1.0	0.1	0.0	0.3	3.0	129.0	288	230	2	132	21
16-003	XX053	V2	56.6	5.8	6.7	2.5	0.6	0.2	3.9	0.0	0.3	57	175	10	225	28
16-003	XX054	V2	56.9	4.1	8.2	2.9	0.1	0.1	3.6	0.0	0.3	112	288	10	245	32
16-003	XX055	V2	53.1	4.2	7.1	2.5	0.6	0.2	2.9	0.0	0.3	93	103	9	220	29
16-003	XX056	V2	50.6	4.4	8.7	3.7	0.4	0.1	3.6	0.0	0.2	84	87	6	151	25
16-003	XX057	V1	73.7	1.2	1.3	0.6	0.1	0.1	0.3	0.0	0.2	7	45	9	73	15
16-003	XX058	V2	60.1	4.6	9.4	1.7	0.4	0.0	1.6	0.2	0.2	85	139	17	403	58
16-005	XX059	V2	53.6	3.7	3.8	2.7	0.0	0.1	2.4	0.0	0.2	69	670	4	104	17
16-005	XX060	V2	63.8	2.4	3.5	0.9	0.2	0.0	2.7	0.0	0.2	21	29	8	201	24
16-005	XX061	V2	64.3	2.6	6.4	1.0	0.4	0.0	0.8	0.0	0.5	28	155	9	198	23
16-005	XX062	V2	63.8	2.1	5.1	1.8	0.4	0.0	2.2	0.0	0.4	63	78	9	242	31
16-005	XX063	V2TM	73.9	0.9	3.9	0.2	0.1	0.0	0.5	0.1	0.5	233	27	7	190	20
16-005	XX064	V2	54.4	3.2	7.2	2.9	0.6	0.1	2.5	0.0	0.2	79	120	10	220	29
16-005	XX065	V2MT	63.0	1.1	7.5	0.3	0.1	0.0	0.2	0.2	1.6	60	68	5	106	14
16-005	XX066	V2	55.5	2.9	7.4	3.0	0.3	0.1	2.5	0.0	0.2	91	168	10	237	31
16-005	XX067	V2	55.2	2.5	7.0	1.8	0.1	0.1	2.8	0.0	0.3	88	73	9	212	29
16-005	XX068	V2	53.5	2.4	7.0	2.8	0.3	0.1	2.6	0.0	0.2	70	69	8	180	22
16-006	XX069	V2	54.2	4.5	4.6	3.6	0.6	0.1	1.8	0.0	0.2	77	54	3	104	16
16-006	XX070	V2	58.0	2.2	2.8	1.1	0.0	0.1	1.4	0.0	0.2	92	343	5	155	26
16-006	XX071	V2	52.7	3.9	3.7	3.0	0.3	0.1	1.7	0.0	0.2	65	207	3	94	17
16-006	XX072	V2TM	37.4	4.7	6.5	2.2	0.5	0.0	6.1	0.0	0.2	180	267	3	85	17
16-006	XX073	V2	62.9	3.3	4.6	1.4	0.7	0.1	1.4	0.0	0.2	7	78	6	166	19
16-006	XX074	V2	52.4	4.0	5.3	2.7	0.2	0.1	2.7	0.0	0.2	79	53	3	78	18
16-006	XX075	V2	64.0	3.0	4.7	1.3	0.9	0.1	1.1	0.0	0.2	4	77	6	182	20
16-006	XX076	V2	53.5	5.2	5.7	2.9	1.2	0.1	2.9	0.0	0.2	71	117	4	112	21
16-006	XX077	V2	55.7	9.3	6.5	3.8	1.4	0.3	2.7	0.0	0.2	78	219	4	131	20
16-006	XX078	V2	52.8	3.7	5.4	2.6	0.2	0.1	1.8	0.0	0.2	53	68	4	144	19
16-006	XX079	V2	48.4	3.1	3.3	2.5	0.0	0.1	1.6	0.0	0.2	114	45	8	198	30
16-006	XX080	V2	50.1	6.9	9.4	2.7	1.2	0.1	4.1	0.0	0.2	101	174	7	168	30
16-006	XX081	V2	59.3	3.6	5.8	1.4	1.2	0.1	1.3	0.0	0.2	62	93	12	322	47
16-006	XX082	V2	49.0	4.9	7.3	2.6	0.4	0.1	2.8	0.0	0.7	78	154	6	168	27
16-006	XX083	V2	52.4	3.2	4.0	2.3	0.1	0.1	1.7	0.0	0.2	88	54	6	168	29
16-006	XX084	V1	65.9	0.6	2.5	0.9	0.1	0.0	1.6	0.0	0.2	13	37	3	123	8
16-006	XX085	V2GN	54.8	4.1	12.6	2.1	0.4	0.0	0.4	0.2	0.9	152	623	8	201	23
16-006	XX086	V2	53.0	5.1	6.6	2.3	0.3	0.3	3.5	0.0	0.2	91	145	8	206	27
16-006	XX087	V2	51.1	5.4	8.5	3.0	0.6	0.3	3.5	0.0	0.2	84	94	6	153	26
16-006	XX088	V1	71.3	1.1	2.3	1.0	0.1	0.1	1.6	0.0	0.2	19	54	10	85	15

16-006	XX089	V1	73.2	1.2	1.7	0.5	0.1	0.1	0.6	0.0	0.2	6	54	9	70	15
16-006	XX090	V2	51.9	7.9	8.7	2.4	0.6	0.4	3.8	0.0	0.2	114	117	8	206	33
16-006	XX091	V2	49.9	6.3	8.0	4.5	0.3	0.1	4.3	0.0	0.2	72	82	3	115	19
16-006	XX092	V2GN	51.7	5.9	8.7	2.8	0.3	0.1	3.2	0.0	0.2	66	101	7	164	29
16-006	XX093	V2	47.4	6.3	7.8	4.2	0.8	0.1	4.3	0.0	0.2	95	92	6	161	24
16-006	XX094	V2	48.4	5.1	7.0	2.4	0.7	0.1	4.9	0.0	0.2	78	84	7	168	26
16-006	XX095	V2	59.8	8.0	7.7	3.3	0.6	0.2	5.7	0.0	0.2	59	76	6	158	17
16-008	XX096	FLT	49.1	4.4	4.5	3.2	0.4	0.0	2.7	0.0	0.2	66	61	2	73	17
16-008	XX097	V2	68.6	3.4	3.4	1.9	0.1	0.0	1.0	0.0	0.2	9	73	5	178	8
16-008	XX098	V2	47.8	5.7	5.8	4.3	0.2	0.0	3.5	0.0	0.2	69	60	2	74	17
16-008	XX099	V2	49.8	5.2	5.3	3.8	0.5	0.0	2.7	0.0	0.2	72	58	2	76	19
16-008	XX100	V2	50.9	1.8	1.9	1.3	0.0	0.1	0.9	0.0	0.2	70	28	2	75	17
16-008	XX101	V2	54.6	4.5	4.0	3.8	0.1	0.0	0.5	0.0	0.2	65	48	2	84	17
16-008	XX102	V2	52.1	2.0	2.2	1.4	0.0	0.1	2.0	0.0	0.2	78	25	2	75	17
16-008	XX103	V2	52.9	2.4	2.5	1.5	0.1	0.1	1.2	0.0	0.2	74	28	2	96	19
16-008	XX104	V2	30.0	7.0	7.3	7.4	0.2	0.0	9.3	0.0	0.2	48	73	18	249	34
16-008	XX105	V2	53.2	4.7	4.6	3.2	0.0	0.1	2.1	0.0	0.2	82	52	2	86	19
16-008	XX106	V2	52.4	2.3	2.4	1.2	0.2	0.1	1.6	0.0	0.2	68	31	2	94	20
16-008	XX107	V2	55.6	3.3	3.5	2.0	0.2	0.1	1.5	0.0	0.2	39	50	8	180	32
16-008	XX108	V2	51.4	3.3	3.4	2.1	0.2	0.1	1.8	0.0	0.2	58	40	2	92	18
16-008	XX109	V2	54.4	2.7	3.1	1.8	0.2	0.1	1.2	0.0	0.2	77	38	4	152	26
16-008	XX110	V2	49.9	5.0	4.9	3.2	0.2	0.1	2.8	0.0	0.2	59	58	2	118	22
16-008	XX111	V2	51.1	6.1	5.7	3.0	1.1	0.2	4.2	0.0	0.2	77	127	3	107	21
16-008	XX112	V2	53.3	7.4	6.6	3.4	1.2	0.2	4.2	0.0	0.2	74	134	3	100	19
16-008	XX113	V2	51.1	5.5	5.2	3.6	0.2	0.1	4.3	0.2	0.2	80	127	3	93	17
16-008	XX114	V2	52.6	3.9	4.9	2.6	0.3	0.1	3.0	0.0	0.2	66	109	4	104	20
16-008	XX115	V2	54.6	2.4	2.8	1.8	0.5	0.1	0.9	0.0	0.2	64	92	3	108	17
16-008	XX116	V1	71.2	0.8	0.8	0.1	0.3	0.0	1.5	0.0	0.2	5	41	8	68	14
16-008	XX117	V1	70.9	0.9	1.0	0.2	0.4	0.0	1.3	0.0	0.2	4	53	9	73	14
16-008	XX118	V1	70.9	0.9	1.0	0.2	0.3	0.0	1.5	0.0	0.2	6	61	9	71	13
16-008	XX119	V2	56.0	1.9	2.4	1.4	0.2	0.1	1.4	0.0	0.2	75	93	4	130	20
16-008	XX120	V2	53.8	3.5	4.1	2.6	0.6	0.1	1.2	0.0	0.2	69	153	4	112	18
16-008	XX121	V2	50.2	5.8	5.6	4.7	1.1	0.0	2.7	0.0	0.2	64	207	3	113	19
16-008	XX122	V2GN	55.2	4.6	6.2	1.9	1.1	0.1	3.0	0.0	0.2	83	608	6	169	32
16-008	XX123	V2	53.6	9.6	7.0	4.6	1.5	0.1	4.8	0.0	0.2	67	112	3	108	17
16-008	XX124	V2	55.8	7.8	6.9	4.9	1.0	0.1	3.4	0.0	0.2	67	112	3	114	18
16-008	XX125	V2	51.2	4.2	4.5	2.8	0.5	0.1	2.4	0.0	0.2	77	62	4	120	19
16-008	XX126	V2	54.2	3.9	3.6	2.9	0.7	0.1	1.7	0.0	0.2	74	44	4	111	19
16-008	XX127	V2	55.7	4.3	4.1	3.1	0.8	0.1	2.2	0.0	0.2	79	56	3	110	20
16-008	XX128	V2	56.5	2.5	4.0	1.5	0.1	0.1	1.5	0.0	0.2	76	49	3	115	21
16-008	XX129	V2	50.6	6.0	6.4	4.7	0.9	0.1	2.7	0.0	0.2	79	80	3	89	17
16-008	XX130	V2	49.0	4.3	4.4	3.2	0.4	0.1	2.8	0.0	0.2	70	56	2	51	12
16-008	XX131	V2	50.5	2.9	5.5	1.8	0.4	0.0	2.7	0.0	0.2	86	81	4	117	23
16-008	XX132	V2	61.1	3.3	5.7	2.5	0.5	0.1	1.2	0.0	0.2	60	84	6	189	27
16-008	XX133	V2	59.8	3.3	5.6	1.3	0.3	0.1	1.7	0.0	0.2	80	103	8	236	33
16-008	XX134	V2	59.8	4.8	6.5	2.0	0.8	0.2	1.8	0.0	0.2	62	90	8	224	31

16-008	XX135	V2	51.4	3.1	6.1	2.4	0.1	0.1	2.1	0.0	0.2	101	106	7	170	31
16-008	XX136	V2GN	74.7	1.8	1.2	0.5	0.2	0.1	0.7	0.0	0.2	12	50	9	73	13
16-008	XX137	V2	57.3	3.4	5.7	1.8	1.0	0.1	1.7	0.0	0.2	115	119	11	276	41
16-008	XX138	I1	70.8	0.9	1.0	0.2	0.3	0.0	1.9	0.0	0.2	9	30	9	69	14
16-008	XX139	V2GN	59.2	6.7	7.4	1.7	1.5	0.2	2.5	0.0	0.2	66	121	12	301	44
16-008	XX140	V2	55.8	4.4	8.1	2.0	1.5	0.1	2.1	0.0	0.2	144	165	13	315	50
16-008	XX141	V2GN	56.5	7.3	9.1	2.0	2.0	0.1	1.8	0.0	0.3	55	88	16	381	52
16-008	XX142	V2	51.5	2.8	5.2	2.7	0.1	0.1	2.4	0.0	0.4	89	71	7	165	28
16-008	XX143	TMBX	65.0	0.6	5.0	0.5	0.1	0.0	1.2	0.2	13.6	941	104	6	147	20
16-008	XX144	TMBX	55.0	2.8	7.5	1.0	0.7	0.0	0.7	0.0	0.4	87	10	10	252	18
16-008	XX145	V2GN	57.9	2.5	6.2	1.0	0.7	0.0	0.7	0.0	0.3	25	76	11	249	28
16-008	XX146	TMBX	70.0	0.2	1.3	0.1	0.0	0.0	1.1	0.0	0.5	112	9	8	188	28
16-008	XX147	V2GN	56.5	4.9	10.0	2.5	1.5	0.1	1.5	0.0	0.2	32	12	8	224	31
16-008	XX148	V2TM	64.7	1.9	5.3	0.7	0.5	0.0	1.1	0.0	1.2	24	1650	8	215	19
16-008	XX149	V2GN	55.1	5.2	11.1	2.7	1.8	0.1	0.8	0.0	0.5	103	41	8	215	27
16-008	XX150	V2	50.0	6.7	8.3	3.9	1.2	0.2	3.2	0.0	0.3	97	260	6	146	26
16-008	XX151	V2GN	50.8	6.5	16.6	3.5	0.5	0.0	0.5	0.3	1.7	1030	776	6	156	26
16-008	XX152	V2	48.4	10.1	9.1	3.5	1.6	0.4	4.5	0.0	0.2	99	166	8	207	34
16-008	XX153	V1	55.9	4.7	8.1	2.1	0.9	0.1	3.1	0.0	0.2	119	101	9	266	42
16-009	XX154	V2	53.8	4.5	4.8	3.4	0.1	0.1	1.4	0.0	0.2	65	54	2	85	19
16-009	XX155	V2	53.6	2.6	2.7	1.5	0.2	0.1	1.7	0.0	0.2	68	34	2	123	25
16-009	XX156	V2	55.0	3.0	2.9	1.9	0.0	0.1	1.9	0.0	0.2	47	42	2	96	17
16-009	XX157	V2	52.2	3.4	3.2	2.0	0.4	0.1	2.1	0.0	0.2	74	44	2	104	22
16-009	XX158	V2	55.0	3.6	4.3	2.0	0.4	0.1	1.5	0.0	0.2	81	65	3	134	25
16-009	XX159	V2	52.9	2.9	3.3	1.6	0.4	0.1	2.3	0.0	0.2	96	44	2	114	25
16-009	XX160	V2	50.3	3.1	5.0	2.0	0.5	0.1	1.6	0.0	0.2	82	58	2	111	25
16-009	XX161	V2	54.3	4.8	6.6	3.3	0.8	0.1	2.4	0.0	0.2	114	118	7	217	30
16-009	XX162	V2MT	53.3	3.9	6.8	3.0	0.7	0.1	1.4	0.1	0.2	109	85	6	193	28
16-009	XX163	V2GN	53.7	3.4	7.1	2.1	0.7	0.1	2.4	0.0	0.2	150	101	11	278	45
16-009	XX164	V1	68.2	0.9	1.1	0.2	0.2	0.0	3.2	0.0	0.7	14	101	7	62	13
16-009	XX165	V2	53.2	4.1	6.8	2.0	1.4	0.1	1.3	0.0	0.2	126	107	10	289	47
16-009	XX166	V2	55.7	3.5	5.6	1.7	0.9	0.1	2.0	0.0	0.2	118	98	8	254	41
16-009	XX167	V2GN	55.1	4.9	7.8	2.0	1.5	0.1	2.7	0.0	0.3	107	149	9	258	41
16-009	XX168	V1	60.1	5.4	7.6	1.6	1.4	0.1	2.2	0.0	6.4	95	188	11	312	45
16-009	XX169	V1	59.5	3.5	6.2	1.5	1.4	0.0	1.3	0.0	0.2	61	186	10	300	45
16-009	XX170	V1	57.2	4.5	6.3	1.4	0.9	0.0	1.0	0.0	0.2	113	50	10	293	48
16-009	XX171	V2	56.8	5.0	8.1	2.0	1.8	0.1	2.2	0.0	0.2	89	89	10	279	42
16-009	XX172	V1	59.0	4.0	7.4	2.1	1.4	0.1	2.2	0.0	0.2	77	50	9	274	38
16-009	XX173	V2GN	54.2	4.8	8.6	2.1	1.4	0.1	1.7	0.0	0.5	172	82	12	302	47
16-009	XX174	V1	56.8	6.5	8.2	1.6	1.8	0.1	2.8	0.0	0.3	75	91	13	361	52
16-010	XX175	V2	55.2	2.3	2.3	1.6	0.6	0.1	0.7	0.0	0.2	74	30	2	67	14
16-010	XX176	V2	51.8	2.9	2.8	1.7	0.5	0.1	1.9	0.0	0.2	50	33	3	88	19
16-010	XX177	V2	51.1	2.3	2.6	1.6	0.0	0.1	0.8	0.0	0.2	88	34	3	89	19
16-010	XX178	V2	53.2	1.5	1.8	1.0	0.0	0.1	1.1	0.0	0.2	71	20	3	82	17
16-010	XX179	I1	70.3	1.8	2.0	0.6	0.4	0.0	2.5	0.0	0.2	4	50	7	104	8
16-010	XX180	V2	51.0	2.9	2.8	1.9	0.1	0.1	1.8	0.0	0.2	75	36	2	86	16

16-010	XX181	V2	52.4	6.3	6.2	3.2	1.7	0.1	4.9	0.0	0.2	68	78	4	112	14
16-010	XX182	V2	51.7	6.3	4.3	3.7	0.5	0.1	3.8	0.0	0.2	55	48	3	83	15
16-010	XX183	V2	54.2	3.9	1.9	1.5	0.1	0.2	1.6	0.0	0.2	64	21	2	83	15
16-010	XX184	V2	49.0	5.1	3.4	3.1	0.6	0.1	2.9	0.0	0.2	58	38	2	83	15
16-010	XX185	V2	52.4	3.5	2.2	1.9	0.1	0.2	1.2	0.0	0.2	69	26	2	86	15
16-010	XX186	V2	49.6	2.5	2.0	1.6	0.2	0.1	0.9	0.0	0.2	64	24	3	87	17
16-010	XX187	V2	72.4	2.0	2.0	1.5	0.1	0.1	1.0	0.0	0.2	64	20	6	192	7
16-010	XX188	V2	51.6	2.4	1.9	1.3	0.0	0.1	1.5	0.0	0.2	68	20	3	95	17
16-010	XX189	V2	50.4	4.9	4.1	2.9	0.6	0.2	2.3	0.0	0.2	57	41	3	85	16
16-010	XX190	V2	54.0	2.5	2.5	1.8	0.1	0.1	1.2	0.0	0.2	61	30	3	101	16
16-010	XX191	V2	52.6	3.8	3.0	2.7	0.4	0.1	4.6	0.0	0.2	48	31	3	84	14
16-010	XX192	V2	51.3	8.2	5.4	3.4	1.2	0.2	4.1	0.0	0.2	75	63	4	90	16
16-010	XX193	V2	51.9	3.2	3.6	2.2	0.3	0.1	1.6	0.0	0.2	74	49	3	119	22
16-010	XX194	V2	54.4	5.3	7.1	2.7	0.1	0.1	2.2	0.0	0.2	76	97	3	104	20
16-010	XX195	V2	54.3	2.4	4.1	1.4	0.3	0.1	1.3	0.0	0.2	73	54	7	175	29
16-010	XX196	V1	56.2	2.7	9.3	2.0	0.8	0.1	2.2	0.0	0.2	128	99	12	328	48
16-010	XX197	V2	53.5	2.9	4.8	2.4	0.1	0.1	1.7	0.0	0.2	63	65	6	160	25
16-010	XX198	V1	72.0	2.1	1.7	0.8	0.4	0.1	1.0	0.0	0.2	10	38	8	77	13
16-010	XX199	V2GN	55.0	5.5	6.2	1.9	0.9	0.1	2.8	0.0	0.2	132	468	10	269	41
16-010	XX200	V2	54.6	4.5	7.4	2.0	0.7	0.1	3.3	0.0	0.2	133	126	10	272	43
16-010	XX201	V2GN	54.9	4.5	7.9	2.2	1.1	0.1	3.0	0.0	0.2	110	141	11	262	41
16-010	XX202	V2GN	57.5	6.4	7.9	2.2	1.6	0.2	3.2	0.0	0.4	132	78	11	278	41
16-010	XX203	V2	58.3	2.6	6.0	1.3	0.5	0.1	1.5	0.0	0.2	170	64	11	287	42
16-010	XX204	V2GN	57.0	7.1	8.5	2.1	2.1	0.1	1.9	0.6	0.7	115	280	11	273	38
16-010	XX205	V2	57.6	3.5	5.1	1.4	1.1	0.1	1.4	0.0	0.2	117	75	10	275	40
16-010	XX206	V2	54.8	4.0	7.5	2.0	1.1	0.1	2.7	0.0	0.2	115	100	10	261	37
16-011	XX207	V2GN	50.8	7.3	12.0	2.7	1.9	0.0	0.4	0.0	1.6	694	71	7	164	25
16-011	XX208	TMBX	70.8	0.1	1.2	0.0	0.0	0.0	0.3	0.0	0.8	270	4	7	179	22
16-011	XX209	TMBX	60.4	0.1	1.3	0.1	0.0	0.0	0.6	0.1	0.7	448	5	7	188	22
16-011	XX210	V2GN	53.5	6.1	9.0	2.6	2.0	0.1	0.8	0.0	0.5	156	84	6	168	25
16-011	XX211	TMBX	64.9	0.5	3.8	0.1	0.1	0.0	0.2	0.1	0.5	32	3	3	126	11
16-011	XX212	TMBX	11.8	0.2	28.5	0.0	0.0	0.0	0.2	3.1	61.4	30800	120	5	162	22
16-011	XX213	TMBX	68.3	0.1	3.1	0.0	0.0	0.0	0.3	0.4	1.9	579	4	8	188	35
16-011	XX214	SILTM	61.5	0.3	1.9	0.1	0.0	0.0	0.4	0.1	0.9	76	29	6	142	23
16-011	XX215	V2GN	40.9	6.9	17.8	2.9	1.4	0.0	0.5	0.5	0.7	126	68	6	164	30
16-011	XX216	V2GN	49.8	7.6	12.1	3.0	2.5	0.1	0.5	0.1	0.2	39	17	6	144	26
16-011	XX217	V2	47.6	2.1	7.1	3.7	0.2	0.1	4.8	0.0	0.2	32	71	6	158	25
16-011	XX218	I1	69.7	3.0	2.3	1.1	0.2	0.1	1.2	0.0	0.2	17	41	4	118	11
16-011	XX219	V2	0.0	8.6	7.2	2.8	0.7	0.4	4.3	0.0	0.2	82	74	0	0	0
16-012	XX220	V2	50.6	4.2	9.6	3.1	1.1	0.1	2.4	0.0	0.2	45	85	6	141	23
16-012	XX221	V2GN	49.4	9.4	14.6	3.3	2.8	0.1	0.7	0.0	0.5	162	106	8	172	27
16-012	XX222	TMBX	73.9	0.1	0.9	0.0	0.0	0.0	0.3	0.0	0.2	4	2	9	176	21
16-012	XX223	TMBX	71.8	0.1	0.9	0.0	0.0	0.0	0.4	0.0	0.3	3	2	8	169	20
16-012	XX224	TMBX	65.5	0.1	1.5	0.1	0.0	0.0	0.6	0.0	0.3	23	4	7	173	24
16-012	XX225	TMBX	49.9	3.1	7.8	1.0	0.9	0.0	0.5	0.0	2.3	251	164	11	240	20
16-012	XX226	V2GN	57.5	4.5	8.9	1.5	1.3	0.0	0.5	0.0	0.2	15	66	8	190	16

16-012	XX227	V2GN	53.4	5.0	9.7	3.2	1.6	0.1	1.3	0.0	1.0	96	105	6	163	26
16-012	XX228	TMBX	57.8	3.5	7.5	2.0	1.1	0.1	0.7	0.0	0.2	69	9	8	200	30
16-012	XX229	V2GN	52.2	5.1	9.0	2.4	0.8	0.0	2.9	0.0	0.3	83	32	7	177	26
16-012	XX230	TMBX	59.2	1.5	6.4	1.3	0.3	0.0	2.1	0.1	0.2	96	67	8	192	24
16-012	XX231	V2GN	54.2	3.5	10.7	1.7	0.8	0.1	1.2	0.0	0.5	20	62	9	200	28
16-012	XX232	V2TM	50.7	4.1	10.7	2.6	1.2	0.0	1.1	0.0	0.4	47	175	7	164	34
16-012	XX233	V2TM	49.4	5.4	14.7	2.8	1.5	0.1	0.3	0.0	0.5	78	15	6	150	24
16-012	XX234	V2	52.4	5.1	8.8	3.6	1.0	0.1	2.9	0.0	0.3	156	178	7	167	28
16-012	XX235	V2	50.7	9.0	7.9	3.3	1.1	0.4	3.3	0.0	0.2	62	152	7	163	27
16-012	XX236	I1	69.9	2.3	1.7	1.0	0.2	0.1	1.0	0.0	0.3	42	48	7	99	14
17-013	XX237	V2GN	56.4	6.4	8.4	2.1	1.4	0.2	3.2	0.0	0.3	110	173	10	271	40
17-013	XX238	V2GN	56.8	6.6	7.9	2.1	1.3	0.2	2.9	0.0	0.3	116	219	12	311	48
17-013	XX239	V1	58.3	7.1	8.0	1.4	1.4	0.2	2.9	0.0	0.3	53	108	16	411	54
17-013	XX240	V1	61.1	7.4	7.8	1.4	1.4	0.3	2.5	0.0	0.9	70	84	16	409	54
17-013	XX241	V2GN	51.4	6.6	10.4	4.3	1.0	0.1	3.3	0.0	3.1	643	50	6	164	26
17-013	XX242	V2GN	48.6	7.1	10.3	5.2	0.9	0.1	3.3	0.0	0.4	93	143	4	140	23
17-013	XX243	V2TM	48.0	7.7	10.4	4.6	2.1	0.2	3.8	0.0	0.5	68	64	5	140	22
17-013	XX244	V2GN	50.4	7.2	10.7	3.2	1.7	0.1	2.0	0.0	3.5	624	116	6	166	30
17-013	XX245	V2TM	48.5	3.8	8.1	3.9	1.0	0.1	3.2	0.0	0.2	46	80	5	144	25
17-013	XX246	V2	52.6	3.8	4.7	2.6	0.9	0.1	1.8	0.0	0.2	88	42	5	166	28
17-013	XX247	V2TM	49.8	8.8	13.9	3.1	3.0	0.1	0.6	0.0	0.2	19	47	5	146	16
17-013	XX248	TMBX	71.0	0.1	1.5	0.2	0.0	0.0	0.8	0.0	0.2	7	6	6	165	15
17-013	XX249	V2	56.8	1.6	3.5	0.3	0.4	0.0	0.5	0.1	0.2	6	43	13	286	33
17-013	XX250	V2GN	51.5	6.9	8.8	3.0	1.8	0.1	2.7	0.0	0.3	52	144	3	113	16
17-013	XX251	V2GN	66.2	1.6	5.6	0.5	0.3	0.0	0.7	0.1	0.5	56	71	8	200	21
17-013	XX252	V2TM	61.2	2.4	5.9	0.6	0.6	0.0	0.4	0.0	0.2	12	34	9	219	20
17-013	XX253	TMBX	53.9	2.8	5.9	1.2	0.7	0.0	0.9	0.2	1.4	145	91	10	266	54
17-013	XX254	TMBX	59.8	0.9	2.4	0.2	0.2	0.0	0.7	0.0	0.2	27	10	10	241	23
17-013	XX255	TMBX	67.6	0.4	1.1	0.4	0.1	0.0	1.2	0.0	0.4	28	9	7	184	20
17-013	XX256	TMBX	71.9	0.1	0.9	0.0	0.0	0.0	0.3	0.1	8.1	398	3	6	176	19
17-013	XX257	V2TM	57.8	0.1	4.5	0.1	0.0	0.0	0.9	0.1	1.3	177	657	8	190	25
17-013	XX258	TMBX	63.7	0.1	3.2	0.1	0.0	0.0	0.6	0.1	0.8	143	4	9	207	23
17-013	XX259	V2TM	57.1	2.9	12.9	1.4	0.6	0.0	0.5	0.0	0.4	134	15	8	190	26
17-013	XX260	V2	56.4	7.0	7.7	2.0	1.1	0.3	2.7	0.0	0.2	83	110	10	228	29
17-013	XX261	I1	71.6	1.5	1.2	0.3	0.1	0.1	0.7	0.0	0.4	42	137	7	79	13
17-013	XX262	V2	49.6	10.1	9.1	3.6	0.5	0.4	4.0	0.0	0.2	94	122	5	142	23
17-014	XX263	V2	57.0	4.1	7.5	1.6	1.1	0.1	2.9	0.0	0.2	69	134	9	285	43
17-014	XX264	V1	58.0	6.5	8.2	1.5	1.2	0.2	3.2	0.0	2.5	279	84	18	451	60
17-014	XX265	V2	50.6	2.8	5.1	3.0	0.1	0.1	2.5	0.0	0.5	183	80	6	142	24
17-014	XX266	TMBX	75.5	0.4	2.3	0.7	0.0	0.0	1.3	0.0	15.2	1830	484	3	105	16
17-014	XX267	V2	50.7	5.0	10.3	3.5	1.3	0.1	1.4	0.0	0.2	14	81	7	162	26
17-014	XX268	TMBX	70.0	0.4	3.4	0.2	0.0	0.0	0.8	0.0	0.8	349	17	6	156	18
17-014	XX269	V2TM	63.3	2.8	5.1	0.9	0.5	0.0	0.4	0.0	0.2	13	96	8	198	15
17-014	XX270	TMBX	57.5	2.1	5.9	0.8	0.6	0.0	0.9	0.0	0.6	8	66	8	207	60
17-014	XX271	V2	50.5	5.5	8.7	2.4	1.3	0.1	1.7	0.0	0.2	41	107	3	118	18
17-014	XX272	TMBX	63.2	1.0	3.9	0.4	0.3	0.0	0.7	0.1	0.2	4	41	10	222	24

17-014	XX273	TMBX	68.6	1.2	2.6	1.0	0.3	0.0	1.5	0.0	1.2	16	42	7	174	23
17-014	XX274	TMBX	69.6	0.2	1.2	0.2	0.0	0.0	0.8	0.1	1.8	23	7	7	164	19
17-014	XX275	SILTM	65.7	1.0	2.5	0.2	0.3	0.0	0.3	0.0	0.2	9	69	9	215	22
17-014	XX276	TMBX	60.8	0.1	3.9	0.3	0.0	0.0	0.9	0.2	1.0	11	3	6	176	20
17-014	XX277	TMBX	64.0	0.1	0.9	0.1	0.0	0.0	0.6	0.0	0.9	148	5	9	221	31
17-014	XX278	TMBX	70.4	0.1	1.2	0.0	0.0	0.0	0.1	0.1	1.3	261	5	7	67	15
17-014	XX279	TMBX	66.1	0.1	2.9	0.0	0.0	0.0	0.2	0.0	0.8	12	15	9	211	20
17-014	XX280	V2TM	52.4	3.6	12.5	1.7	0.7	0.0	0.3	0.0	0.6	97	8	6	162	23
17-014	XX281	V2	51.4	4.5	7.9	3.6	0.6	0.1	3.1	0.0	0.2	110	141	5	144	23
17-014	XX282	V2TM	69.3	1.5	1.6	0.6	0.1	0.1	1.9	0.0	0.2	12	41	6	73	14
17-014	XX283	V2	50.6	9.7	7.9	3.2	0.8	0.4	4.5	0.0	0.2	103	143	6	158	26
17-017	XX284	V2	60.2	4.8	5.9	2.1	1.6	0.1	1.5	0.0	0.3	59	269	6	227	30
17-017	XX285	V2	59.0	6.3	6.3	2.3	0.9	0.3	3.3	0.0	0.2	91	93	8	253	28
17-017	XX286	I2	72.3	0.7	0.7	0.1	0.2	0.0	1.6	0.0	0.2	8	18	7	66	12
17-017	XX287	V2	49.9	4.0	7.2	2.7	0.1	0.1	2.5	0.0	0.2	101	83	6	174	30
17-017	XX288	V2	55.2	6.0	7.2	1.4	0.8	0.2	2.7	0.0	0.2	120	193	9	256	37
17-017	XX289	V2	69.1	1.0	1.3	0.3	0.2	0.0	2.4	0.0	0.2	26	67	7	66	12
17-017	XX290	V2	54.4	5.7	8.6	2.7	1.2	0.1	3.5	0.0	0.2	92	239	11	288	45
17-017	XX291	V2	50.9	3.1	5.4	3.2	0.1	0.1	3.6	0.0	0.6	151	72	5	164	27
17-017	XX292	V2	49.2	7.1	10.5	3.9	2.1	0.1	2.1	0.0	0.2	40	154	6	157	25
17-017	XX293	V2	49.0	9.8	14.3	4.6	3.3	0.1	1.1	0.0	0.3	98	50	6	159	28
17-017	XX294	V1	65.0	3.3	6.9	1.1	0.9	0.0	0.3	0.1	0.2	4	14	7	190	22
17-017	XX295	V2GN	50.4	9.6	10.3	3.0	2.6	0.2	2.0	0.0	0.8	131	149	3	118	16
17-017	XX296	TMBX	68.5	1.2	2.6	0.5	0.3	0.0	0.9	0.0	1.7	318	146	7	177	21
17-017	XX297	V1	63.4	3.4	7.2	1.1	1.0	0.0	0.4	0.1	0.2	9	22	7	186	23
17-017	XX298	V2TM	66.1	1.7	2.9	0.8	0.4	0.0	1.1	0.0	0.6	103	210	7	184	23
17-017	XX299	TMBX	67.7	0.8	2.5	0.4	0.1	0.0	0.8	0.0	0.2	76	144	8	194	26
17-017	XX300	TMBX	72.8	0.2	2.1	0.1	0.0	0.0	0.4	0.0	0.4	59	5	7	158	20
17-017	XX301	V2GN	53.5	4.7	9.0	1.5	1.6	0.0	0.5	0.1	0.3	4	107	8	218	15
17-017	XX302	V2GN	56.6	6.6	9.7	2.3	2.0	0.1	1.0	0.0	0.5	78	193	9	218	28
17-017	XX303	V2	49.0	10.0	8.7	3.5	1.4	0.4	4.9	0.0	0.5	109	237	5	152	26
17-017	XX304	I1	74.2	0.5	0.4	0.0	0.1	0.0	0.1	0.1	1.6	80	8	4	73	13
17-017	XX305	V2	50.5	4.4	6.9	3.0	0.7	0.1	3.1	0.1	0.2	184	75	6	168	28
17-017	XX306	I1	70.4	0.9	0.7	0.2	0.1	0.0	0.9	0.1	0.2	37	12	9	78	14
17-017	XX307	V2	52.5	8.8	8.0	3.5	0.9	0.3	3.8	0.0	0.2	103	188	6	162	27
17-018	XX308	V2	47.7	5.8	7.4	5.0	0.7	0.1	4.2	0.0	0.2	86	80	5	118	20
17-018	XX309	V1	57.7	3.8	5.8	2.2	0.8	0.1	2.4	0.0	0.2	90	89	10	270	32
17-018	XX310	V2	57.0	2.5	5.8	1.5	0.4	0.0	1.9	0.0	0.4	96	82	8	229	26
17-018	XX311	V2	47.3	3.9	8.7	3.2	0.7	0.0	3.8	0.0	0.2	120	108	6	154	29
17-018	XX312	V2	58.1	4.3	7.7	2.0	1.0	0.1	2.5	0.0	0.2	121	117	11	285	43
17-018	XX313	V2GN	60.3	7.3	7.6	1.7	1.3	0.2	3.9	0.0	0.2	40	138	12	309	43
17-018	XX314	I1	72.1	1.5	1.3	0.4	0.2	0.0	1.6	0.0	0.3	15	171	9	69	13
17-018	XX315	V2	57.4	4.0	8.0	1.9	1.2	0.1	2.6	0.0	0.2	48	148	10	282	41
17-018	XX316	V2	55.5	5.8	8.4	1.7	0.8	0.2	3.7	0.0	0.3	76	178	14	368	53
17-018	XX317	V1	70.3	2.4	2.6	1.0	0.2	0.0	1.1	0.0	0.2	14	51	6	204	12
17-018	XX318	V2	48.2	4.5	7.9	4.7	0.2	0.0	3.9	0.0	0.2	96	132	6	156	27

17-018	XX319	V2TM	48.2	4.2	7.8	4.0	0.9	0.1	4.2	0.0	0.2	49	89	5	142	24
17-018	XX320	V2	52.4	4.1	5.3	3.2	0.9	0.1	3.5	0.0	0.3	118	70	5	156	26
17-018	XX321	V2GN	50.1	7.9	13.4	3.0	2.2	0.1	0.9	0.0	0.2	30	158	6	160	27
17-018	XX322	TMBX	66.0	0.2	1.4	0.1	0.0	0.0	0.6	0.1	0.6	111	338	7	200	22
17-018	XX323	V2GN	52.1	5.7	12.3	3.0	0.7	0.0	0.5	0.0	0.4	62	142	6	170	27
17-018	XX324	V2TM	48.8	6.0	9.3	3.8	1.4	0.1	2.4	0.0	0.2	69	136	5	152	26
17-018	XX325	V2TM	51.5	4.6	7.7	3.3	0.7	0.1	3.4	0.0	0.2	110	141	6	167	26
17-018	XX326	V2	51.4	3.0	7.3	3.5	0.2	0.1	2.6	0.0	0.2	187	165	6	161	26
17-018	XX327	V2TM	49.0	4.1	6.6	3.0	0.6	0.2	4.2	0.0	0.2	66	72	4	146	23
17-018	XX328	V2	48.6	7.6	7.5	3.8	1.0	0.3	4.9	0.0	0.2	82	85	6	151	25
17-018	XX329	V2TM	46.3	6.1	7.8	3.5	0.8	0.2	4.4	0.0	0.2	94	95	5	157	25
17-018	XX330	V2	56.3	3.7	8.0	1.7	0.7	0.1	2.8	0.0	0.2	69	102	10	282	41
17-018	XX331	V2TM	51.0	4.6	8.2	2.8	0.7	0.2	3.2	0.0	0.2	98	94	7	186	28
17-018	XX332	V2	51.0	6.0	7.8	5.2	0.5	0.0	3.1	0.0	0.2	62	84	3	121	19
17-019	XX333	V2	48.9	6.9	6.6	3.4	0.1	0.1	5.2	0.0	0.2	66	69	3	72	15
17-019	XX334	V2	50.7	6.2	6.1	3.8	0.1	0.1	4.6	0.0	0.2	65	64	3	73	17
17-019	XX335	V2	53.6	3.2	3.2	2.0	0.1	0.1	1.9	0.0	0.2	74	37	2	93	18
17-019	XX336	V2	48.5	5.3	5.0	4.5	1.0	0.0	1.6	0.0	0.2	76	49	3	74	17
17-019	XX337	V2	51.0	6.4	6.9	4.1	0.5	0.0	4.3	0.0	0.2	58	75	4	97	19
17-019	XX338	V2	54.3	2.7	3.0	1.6	0.3	0.1	1.2	0.0	0.2	33	49	4	121	24
17-019	XX339	V2	51.3	4.5	4.8	2.9	0.0	0.1	3.6	0.0	0.2	70	60	3	110	21
17-019	XX340	V1	68.0	2.5	2.2	1.1	0.2	0.0	1.9	0.0	0.2	16	53	8	85	16
17-019	XX341	V1	72.5	1.0	1.0	0.2	0.3	0.0	1.5	0.0	0.2	6	53	8	71	13
17-019	XX342	V2	53.3	3.2	2.9	2.4	0.4	0.1	0.8	0.0	0.2	77	37	2	112	21
17-019	XX343	V2	53.3	1.7	2.1	0.9	0.1	0.1	1.4	0.0	0.2	78	21	4	114	22
17-019	XX344	V2	51.7	6.2	6.6	4.0	0.7	0.0	3.9	0.0	0.2	67	68	3	108	21
17-019	XX345	V1	71.3	1.3	1.2	0.4	0.5	0.0	1.3	0.0	0.2	1	85	8	72	14
17-019	XX346	V2	40.7	8.4	6.2	8.2	3.2	0.0	7.6	0.0	0.2	32	80	11	219	21
17-019	XX347	V2	53.0	2.6	3.2	2.0	0.0	0.1	1.5	0.0	0.2	70	164	4	110	18
17-019	XX348	V1	72.5	1.1	1.1	0.3	0.2	0.0	1.2	0.0	0.2	4	56	8	71	13
17-019	XX349	V2	56.4	2.9	3.2	2.2	0.9	0.1	0.8	0.0	0.2	55	37	3	109	17
17-019	XX350	V2	51.2	4.5	4.5	3.6	0.3	0.1	0.5	0.0	0.2	64	101	3	118	24
17-019	XX351	V2	49.3	2.5	2.4	1.1	0.0	0.1	2.7	0.0	0.2	91	157	3	80	18
17-019	XX352	V2	52.8	12.8	7.2	4.8	2.1	0.2	3.8	0.0	0.2	40	518	3	116	18
17-019	XX353	V2	56.7	2.5	2.5	2.0	0.0	0.1	1.2	0.0	0.2	71	151	3	103	16
17-019	XX354	V2	57.0	2.9	2.9	2.1	0.5	0.1	1.1	0.0	0.2	72	64	3	106	16
17-019	XX355	V2	49.6	4.7	4.7	2.8	0.1	0.1	4.1	0.0	0.2	79	78	2	78	17
17-019	XX356	V1	73.4	2.2	1.1	0.2	0.3	0.1	1.8	0.0	0.2	8	56	10	73	12
17-019	XX357	V2	52.3	4.3	3.9	2.5	0.0	0.1	2.4	0.0	0.2	86	65	3	79	15
17-019	XX358	V2	55.0	2.6	3.0	2.0	0.6	0.1	1.0	0.0	0.2	68	36	2	113	18
17-019	XX359	V2	54.8	5.8	5.3	4.2	1.0	0.1	1.9	0.0	0.2	109	70	4	112	17
17-019	XX360	V2	55.9	5.9	6.3	4.4	1.1	0.1	1.8	0.0	0.2	97	75	3	114	19
17-019	XX361	V2	49.8	4.9	4.6	3.7	0.1	0.1	2.2	0.0	0.2	74	57	2	70	14
17-019	XX362	V2	54.3	5.4	6.8	4.1	0.9	0.1	1.2	0.0	0.4	47	230	4	138	23
17-019	XX363	V2	63.0	2.7	6.0	1.6	0.5	0.1	1.8	0.0	0.2	59	91	7	212	29
17-019	XX364	V2	58.2	2.6	6.5	1.4	0.2	0.1	1.5	0.0	0.2	65	82	9	253	35

17-019	XX365	V2	50.5	3.5	6.2	2.9	0.1	0.1	1.6	0.0	0.2	111	77	7	170	31
17-019	XX366	V2	49.1	4.4	7.3	3.1	0.4	0.1	3.3	0.0	0.2	127	96	7	174	32
17-019	XX367	V2TM	53.3	9.9	9.0	2.1	1.7	0.4	4.6	0.0	0.3	124	258	10	256	40
17-019	XX368	V2TM	53.0	4.4	10.0	2.5	1.2	0.0	2.7	0.0	0.4	155	288	12	304	47

Appendix 4: Thin section descriptions. All pictures are subject to a 10x magnification in addition to the magnification mentioned in the description. A 5x picture is therefore magnified by a factor of 50x. Respectively, the 5x, 10x and 40x pictures have a width of 5.5, 2.8 and 0.7mm.

BD-01

Macro description:
Tourmaline breccia is observable on one side of a vein and tourmalinite on the other. The vein (black linear feature at the middle of the thin section) is mostly comprised of sulfides with 1% quartz. This thin section seems to be a small scale representation of the larger fracture filling chalcopyrite seen on the trench. Its position between the strong tourmaline alteration and tourmaline breccia units also supports this fact.

The tourmaline breccia portion has very sharp contacts with the silica clasts, while the strong tourmaline alteration unit has mostly sharp contacts.

Minerals:
30% Microcrystalline tourmaline: is found on both the strong tourmaline alteration and tourmaline breccia. It has a higher proportion over the fine grained tourmaline in the breccia portion.
15% Fine grained tourmaline: This type of tourmaline is twice as abundant in the strong tourmaline alteration portion as in the tourmaline breccia portion. Crystal width can reach 100um but crystals are not euhedral. They almost always are in fan or star like habitus.
50% Quartz: Very equigranular, is a growing medium for the larger tourmaline crystals. Also hosts microcrystalline tourmaline. Generally 10 to 20 micron large.
10% Pyrite: Pyrite is mostly contained in the fracture separating the two different lithologies but it is also commonly found in association with the larger tourmaline crystals. Has a tendency to be euhedral compared to chalcopyrite and pyrrhotite.
5% Pyrrhotite: In the fracture. Has grown in equilibrium with chalcopyrite and sphalerite. 120 degree angles can be observed.
2% Chalcopyrite:
1% Sphalerite: Contains pyrite exsolution in little uniformly dispersed bubbles.
Traces Arsenopyrite: On pyrrhotite border associated with pyrite.
Traces Muscovite: Muscovite is very coarse, grains can reach a mm in length and is very uniform (i.e. does not have a sericitic texture) It is closely associated with sulfides in the fracture.

Paragenetic sequence:
Qz --------- --
Tm --------
Py --
Apy --
Cpy --
Sp --
Ag -
Ep -
Mv -

Pictures:
BD-01_01 (5x): Sharp angles of quartz clasts in a very fine grained tourmaline matrix (polarized).

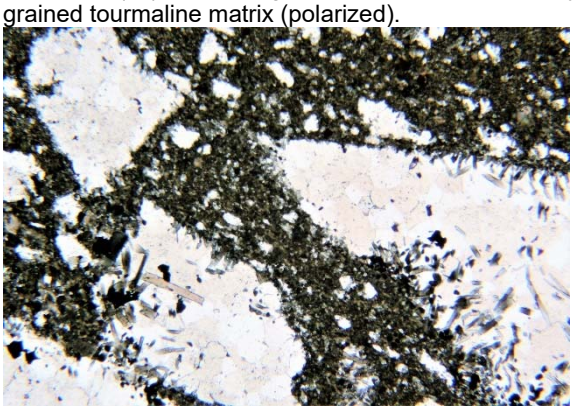

BD-01_02 (5x): Less sharp contacts in the tourmaline altered portion of the thin section (analyzed).

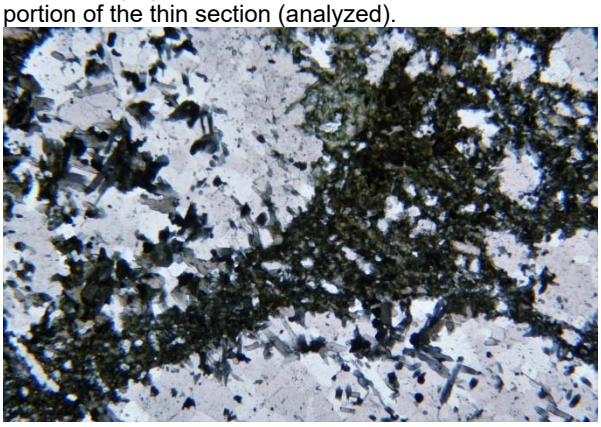

BD-01_04 (5X) : Pyrite and coexisting chalcopyrite and pyrrhotite. Pyrite is at the left hand side (polarized reflected).

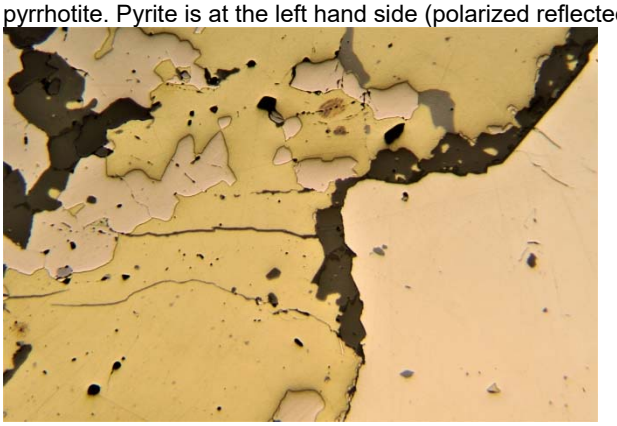

BD-01_05 a), b) and c) (5x): Late fracture filling sulphides with muscovite, epidote and carbonates..

a. Polarized

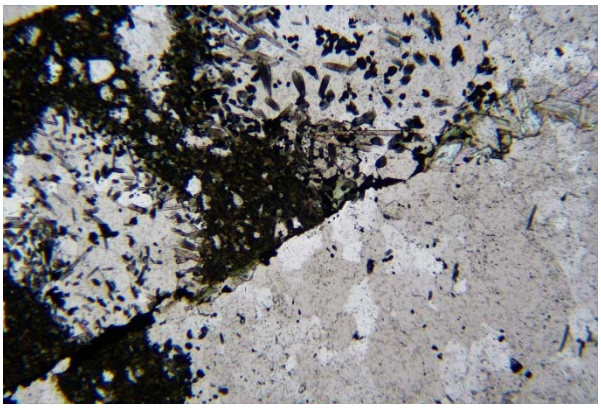

b. Analyzed

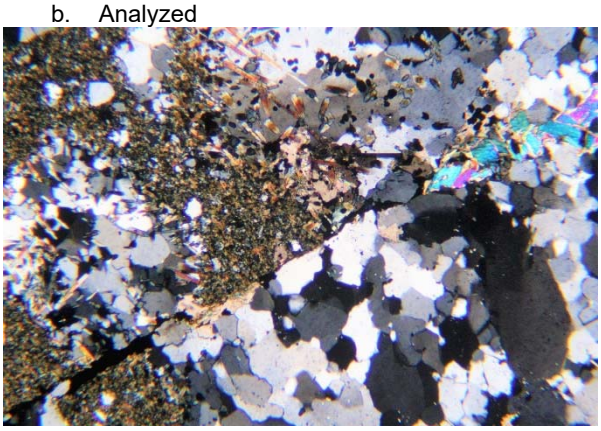

c. Reflected polarized

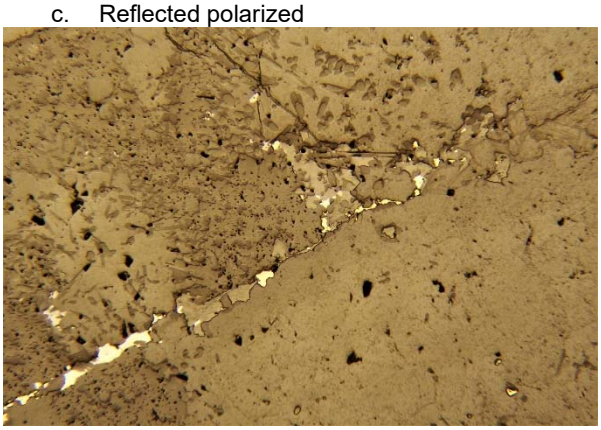

Microprobe circles:

BD-01-C01_1 (50x): Native silver in a fracture in pyrite (polarized analyzed):

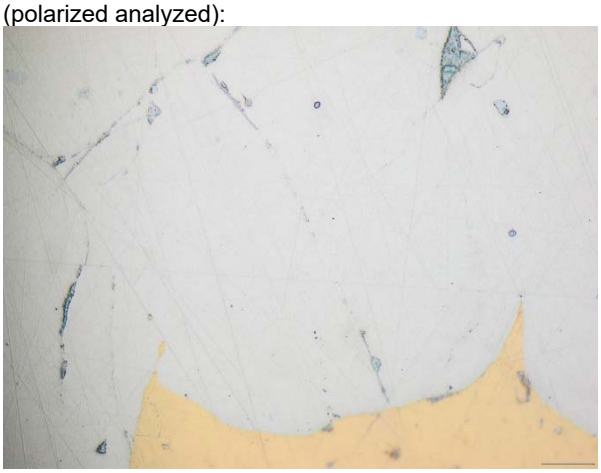

BD-01_C01_EM1: Native silver in a fracture in pyrite (EMP).

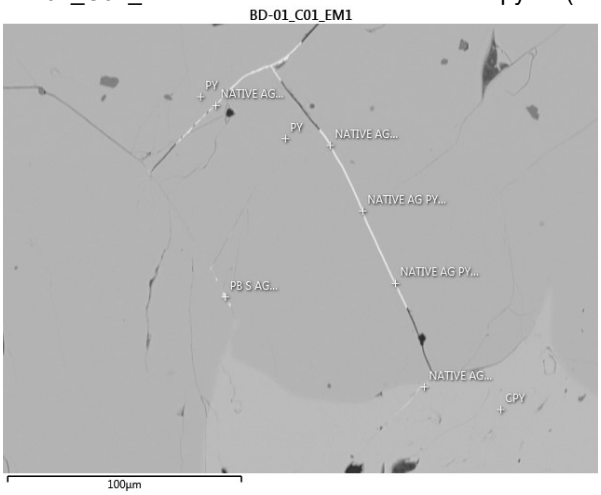

BD-02

Macro description:
Pyrrhotite-rich sulfide breccia material. Pyrrhotite is unusual on the field.

Minerals:
20% Sericite: Mostly preferentially oriented, but can also be messy.
40% Quartz: Generally equigranular, but some late stages can have very coarse grains reaching 5mm in length. The coarser grains are associated with the sulfides.
10% Pyrrhotite: In very homogenous pods in equilibrium with chalcopyrite.
2% Chalcopyrite: Seems to be in close relation with pyrrhotite but will sometimes cut through it.
10% Tourmaline: Similar proportions of microcrystalline and fine grained tourmaline.
1% Pyrite: Euhedral and in association with other sulfides.
5% Muscovite: Can reach a mm in length and appears to be 'floating' in pyrrhotite most of the time.
5% Calcite: (or other carbonate, EDS will tell). Clearly cuts through the pyrrhotite.
3% Magnetite: Dispersed through the quartz.

Paragenetic sequence:
Si --------- --
TM --------
PY --
APY --
CPY --
SP --
MT -
EP -
MV -

Pictures:
BD-02_01 (10x): Chalcopyrite cutting through pyrrhotite (Reflected polarized)

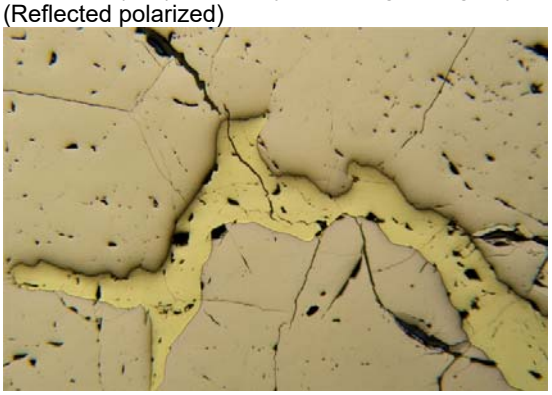

BD-02_02 a) and b) (10x): Tourmaline clast supported breccia(?) cemented by chalcopyrite. This is in favor of a simultaneous deposition.
a. Analyzed

b. Reflected polarized

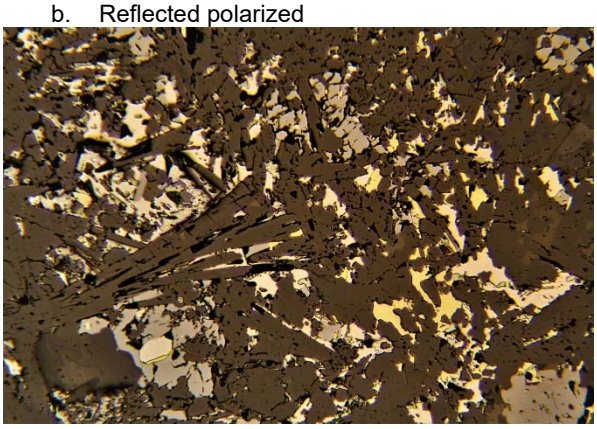

BD-02_03 a) and b) (10x): In equilibrium pyrite, chalcopyrite and pyrrhotite. Reflected polarized.

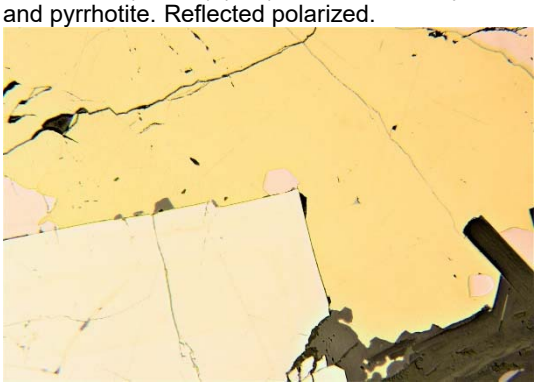

BD-03

Macro description: Sheared andesite with quartz boudins.

Minerals:
30% Quartz: Either fine grained disseminated through sericite or medium grained and contained in boudins up to 5 mm long, with a general aspect ratio of 5:1.
60% Hornblende:
4% Chlorite: Crystals can be distinguished, does not have the usual very fine grained aspect and pervasive disseminated pattern. Chlorite is often in late straight fractures.
2% Magnetite: Exclusively contained in sericite.
Traces Pyrite:
Traces Chalcopyrite:

General comments:
The rock was most likely an andesite at first because of its Ti/Zr ratio like most of host rocks at Black Dog. It is likely that there was a first quartz alteration which later was transformed into boudins. Magnetite seems to be forming out of another mineral that I can't identify. It could also not be the original mineral. Magnetite was most likely already crystallized before deformation. It could also be crystallizing from a carbonate since the rock reacts to acid. Hornblende seems to be well aligned along the foliation so it is likely that it crystallised during this event.

Pictures:
BD-03_01 (10x): General aspect of thin section

.

BD-04

Macro description: Amphibolite with visible amphibole crystals at a macro scale. Moderately magnetic. Represents the typical host rock at Black Dog.

Minerals:
55 % Quartz: Microcrystalline and equigranular. Also as inclusions in amphiboles.
40% Hornblende: Large crystal up to 2mm large and 15mm long.
2% Chlorite: As large nice and uniform crystals
2% Ilmenite: Elongated crystals aligned in the foliation.
1% Magnetite: Disseminated
1% Muscovite: Generally fine grained but not as fine as sericite in general.

General comments:
It is likely that only few on the minerals in this thin section were present at the formation of the rock. Amphiboles were crystallised prior to foliation along with a certain proportion of the quartz according to their deformation textures. Ilmenite, sericite and chlorite seem to have developed during foliation asthey tend to align in its fabric.

Pictures:
BD-04_01 (5x): General pictures: Ilmenite aligned along foliation and preferentially crystallizing in hornblende, big hornblendes and equigranular quartz texture. Polarized.

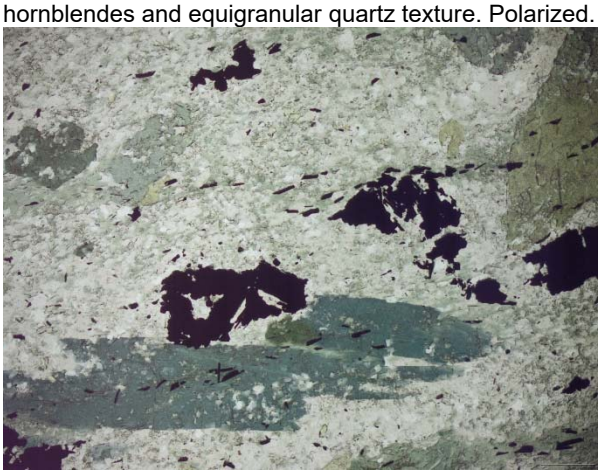

BD-05

Macro description: Sulfide breccia through a very fine grained tourmaline matrix. Cobaltite grew over earlier pyrite and a chalcopyrite + sphalerite vein cuts through the resulting polyphased crystal.

Minerals:
40% Tourmaline: The most microcrystalline tourmaline that I have seen in these thin sections. There is no large tourmaline crystal visible. Can sometimes by intergrowing with sulfides.
10% Quartz: Medium size grain, up to 0.5 mm, in association to the sulfide breccia.
20% Pyrite: In tourmaline or bathing in chalcopyrite.
10% Chalcopyrite:
15% Sphalerite: Along with chalcopyrite, cuts through pyrite and holds some tourmaline clasts, pyrite and arsenopyrite.
2% Cobaltite: Disseminated in tourmaline

General comments:
Strong tourmaline alteration: Protolith cannot be determined due to the strong tourmaline alteration. In this thin section, tourmaline is mostly a tourmaline vein as no silica is visible. There is a link to be made between very small microcrystalline tourmaline without quartz and tourmaline veins.

Sulfide breccia: Sulfides brecciate through the strong tourmaline altered matrix. They are accompanied by coarse (up to 0.5 mm) quartz. Pyrite is the first sulfide to form. It also fill space that is not exactly in the breccia. Then cobaltite and arsenopyrite crystallized, as picture BD-05_C2 shows. Chalcopyrite and sphalerite came later and filled open space around the pyrite. Arsenopyrite seems to have the same timing as pyrite as is it surrounded by chalcopyrite and sphalerite.

Paragenetic sequence:
Si ---------
Tm --------
Py --
Apy --
Co --
Cpy --
Sp --

Pictures:
BD-05_01 (5x): 1) Cpy, 2) Apy, 3) Py. Reflected polarized.

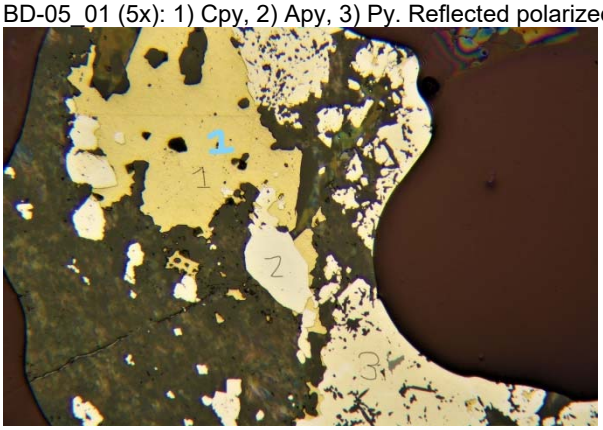

Selected microprobe circles:
BD-05_C02: Cobaltite overgrowing pyrite later cut by a chalcopyrite vein. The chalcopyrite seems to have wedged away the pyrite crystal from the tourmaline matrix as can be seen on the left of the pyrite/cobaltite crystal. Reflected analyzed.

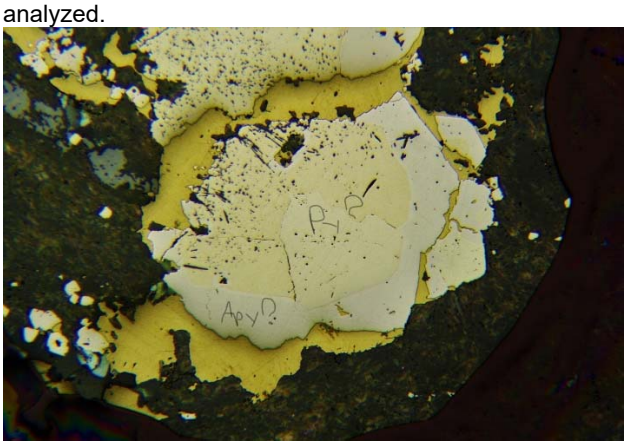

BD-05_C02_EM1: Microprobe picture of BD-05_C02. From core to rim the zonations range from pyrite to a first fine coat of arsenic rich cobaltite, followed by a larger rim of cobaltite and ends with a chalcopyrite outer rim. The chalcopyrite cuts through all previous rims. EMP picture.

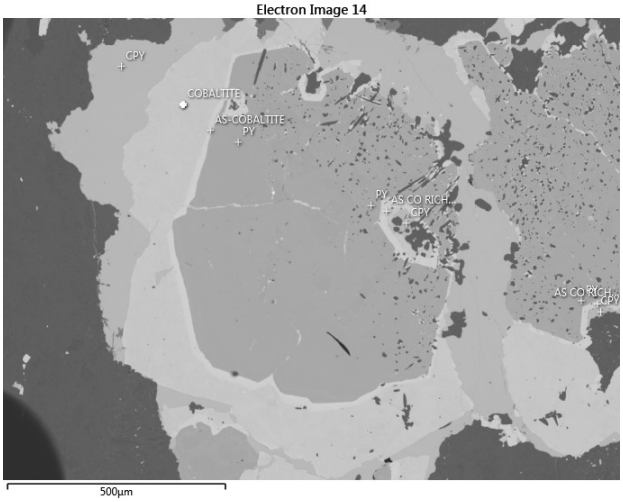

BD-06

Macro description: Fine grained sheared amphibolite. A typical host-rock at Black Dog.

Minerals:
35% Quartz: Equigranular, recrystallized.
60% Hornblende: Mostly lined up along the foliation.
3% Magnetite:

General comments:
Rock was most likely an andesite before going through alteration, deformation and metamorphism. Quartz seems to have been present before the foliation. Hornblende was probably partly present before the main deformation event but most of it seems to have crystallized during deformation.

Pictures:
BD-06_01 (5x): General picture

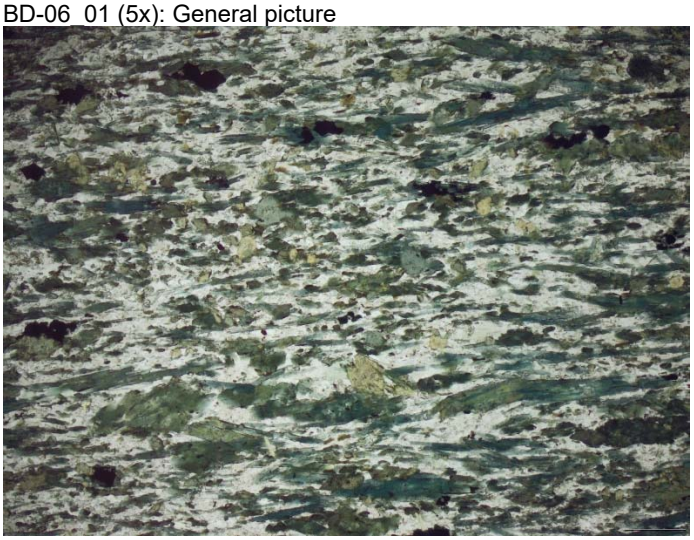

BD-07

Macro description: Andesite with abundant quartz and calcite boudins. It is a common rock close to the tourmalinite units.

Minerals:
55% Quartz: Very fine grained to medium size grains in the boudins.
15% Calcite: In the corners of the boudins, in large crystals (up to 0.5mm)
10% Hornblende: Large crystals broken by foliation
1% Garnet: Euhedral, is present before the chlorite alteration.
10% Chlorite:

General comments:
Amphiboles seem to have been part of the protolith along with some quartz. Some rare plagioclase crystals are also recognizable. Garnet seems to have been broken up and potentially rotated during the foliation. The material that makes up the boudins is a mix of quartz in the core and calcite mostly in the pressure shadows. Calcite seems to be coeval with deformation

Pictures:
BD-07_01 (10x): General picture. Hornblende (on the right) being altered into chlorite that is aligned in the foliation. Biotite inside the hornblende

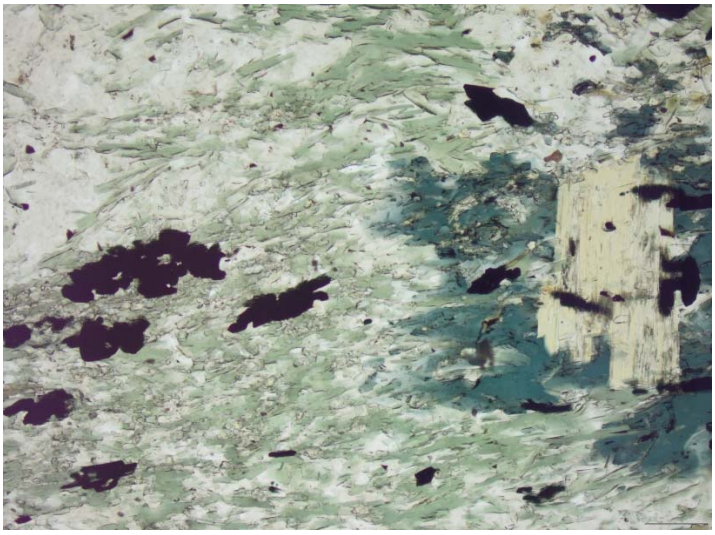

BD-07_02 (10x): Garnet caught in the foliation

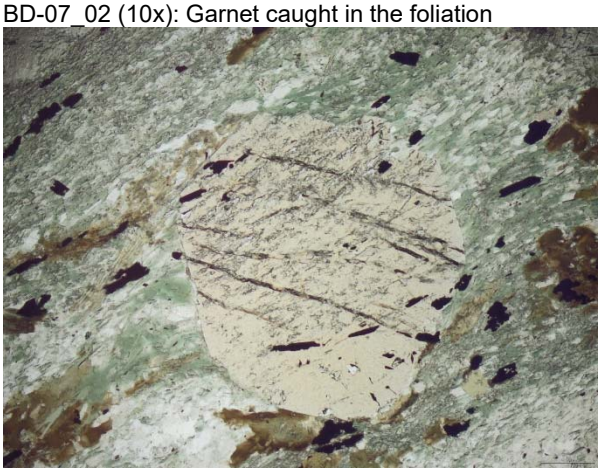

BD-08

Macro description: Shear zone most likely in an andesite. Could be called an mylonite in thin section.

Minerals:
50% Quartz: Can be microcrystalline in the shears and up to 1mm large in the very elongated boudins than can be with biotite and calcite. Can also be on its own.
10% Biotite: in the boudins along with quartz and calcite
10% Sericite: Dispersed through microcrystalline quartz
15% Calcite: Generally in large syn-deformation crystals
10% Pyrite: In bands and disseminated mostly in quartz rich boudins or stratas.

General comments:
The protolith is hard to determine as the sample is very quartz and sericite altered and there probably is only quartz left that was originally present. The general matrix is made up of microcrystalline quartz and sericite alteration and seem to have been the first to be put in place. The boudins are made out of coarse quartz, biotite and calcite which would have to have been present before then shear in order to give them a boudin shape. Microcrystalline quartz and sericite alteration came along a shear which split the boudin and set a layer of microcrystalline quartz and sericite between them.

Pictures:
BD-08_01 (5x): Strong deformation and mineral banding in polarized and analyzed light.

a. Polarized

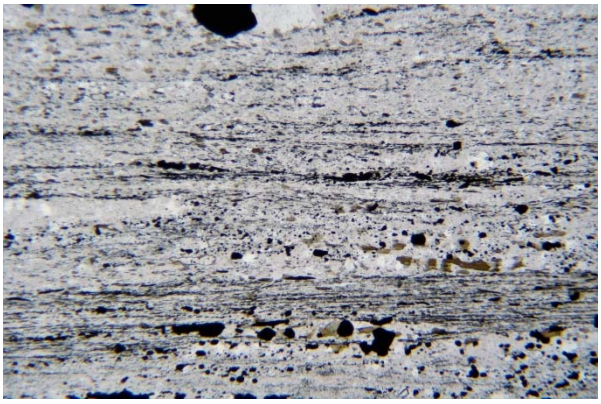

b. Analyzed

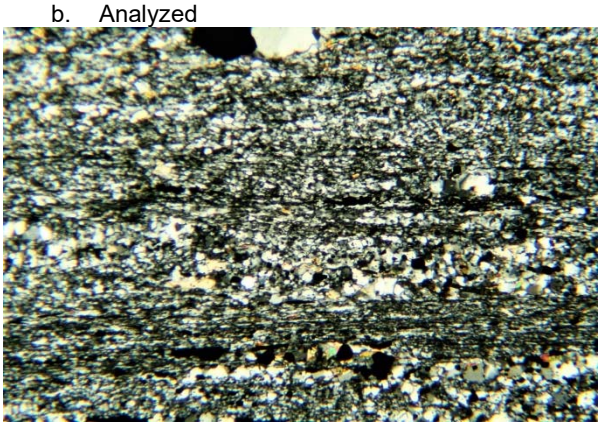

BD-09

Macro description: Tourmaline breccia with disseminated sulfide. There also is a more concentrated sulfide vein at the middle of the thin section that is accompanied by a negative sulfide halo, i.e., there is no sulfide on the first 5 mm around the vein but there is a high concentration in it.

Minerals:
40% Microcrystalline tourmaline: Acts as the matrix.
30% Quartz: As angular clasts in the tourmaline matrix.
10% Pyrite: Disseminated in the tourmaline breccia.
Traces Muscovite: In quartz and tourmaline.

General comments:
The protolith is undetermined. Microcrystalline tourmaline and quartz alteration comprise the matrix of this lithology. Areas are generally segregated in silica pods inside a tourmaline rich medium, but can also mix. Tourmaline, sulfide and traces of coarse muscovite are comprised in the central vein of the thin section and seem to all have been deposited in the same event.

Selected microprobe circles:
BD-09_C1 (10x): A quartz grain with numerous inclusions of pyrite and tourmaline. Polarized.

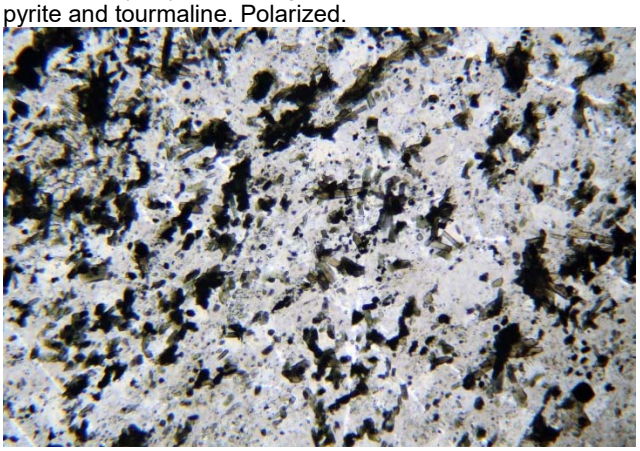

BD-09_C1_EMP1: Microcrystalline tourmaline growing on small grained tourmaline. EMP picture.

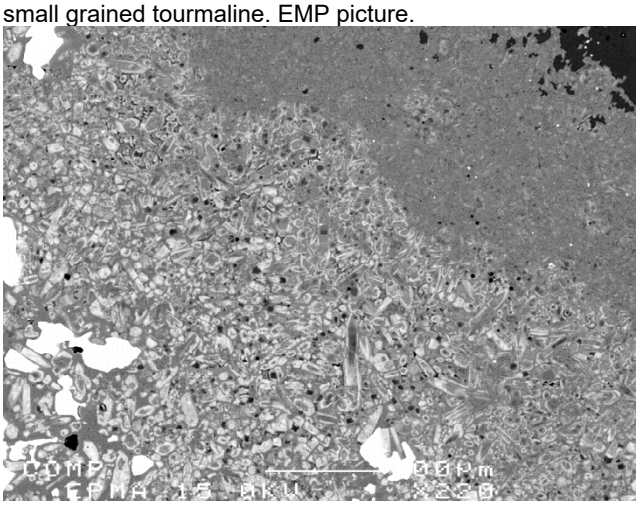

BD-09_C1_EMP2: Close-up of the different tourmaline crystal sizes. EMP picture.

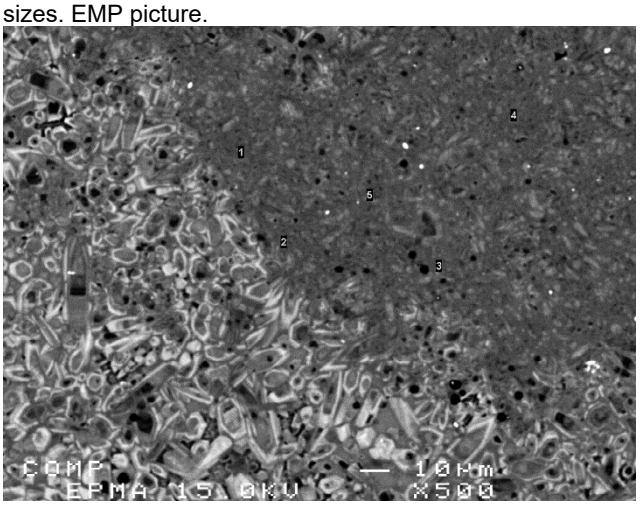

BD-10

Macro description: Sulfide breccia

Minerals:
20% Pyrite:
30% Chalcopyrite:
30% Microcrystalline tourmaline:
10% Fine grained tourmaline:
Traces Matildite:

General comments:
The protolith is undetermined. Pervasive microcrystalline tourmaline alteration seems to be the original matrix. Fine grained tourmaline has grown with the microcrystalline tourmaline rich areas or blobs as an anchor point. Sulfides along with medium grained quartz brecciated through the tourmaline matrix. Pyrite and arsenopyrite have come first, with the rest of the gaps filled by chalcopyrite. A considerable amount of coarse grained muscovite is also associated with this breccia. It is generally located at the border between the sulfides and the microcrystalline tourmaline.

Selected microprobe circles:
BD-10_C2 (5x): Silver-rich (blue) and non silver-rich chalcopyrite in contact with pyrite.

BD-10_C2_EMP1: Silver rich chalcopyrite in a fracture in pyrite along with Matildite. EMP picture.

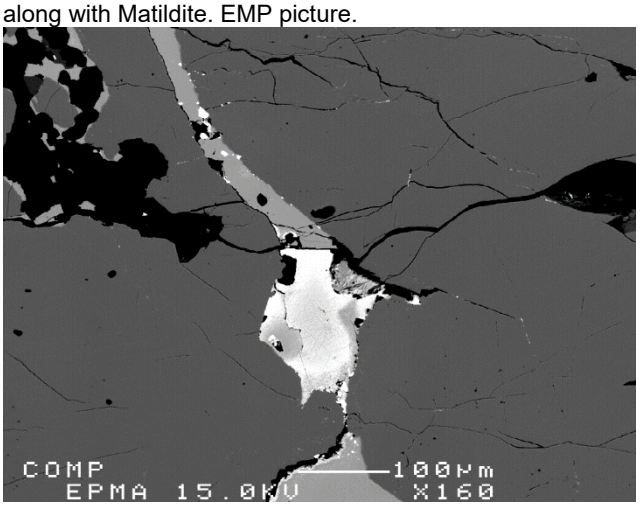

BD-11

Macro description: Typical example of the garnet rich unit.

Minerals:
20% Quartz: Coarse in blobs and disseminated through biotite.
40% Biotite: Fine grained and uniformly dispersed with quartz to form the matrix.
10% Calcite: Disseminated
5% Garnet: Disseminated
5% Magnetite: Disseminated

General comments:
The protolith is undetermined. The observed textures indicate that garnet was not the last mineral emplaced and that tourmaline is deposited after garnet.

Pictures:
BD-11_01 (5x): Fine to coarse tourmaline growing up to where a garnet was broken. Tourmaline comes after garnet in this case. This also shows that garnet is being cut by a late quartz event.

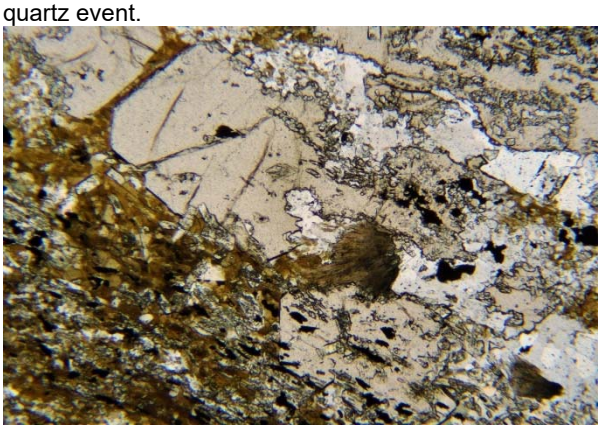

BD-12

Macro description: Garnet-rich unit with important chlorite.

Minerals:
20% Quartz:
20% Sericite:
15% Chlorite:
5% Garnet:
5% Pyrite:
2% Pyrrhotite:
1% Magnetite:
Traces Chalcopyrite:

General comments:
Garnet crystals are fractured and filled by pyrite, chalcopyrite and quartz. Later, biotite, chlorite and epidote cut through the sulfides.

Pictures:
BD-12_01 a) and b) (5x): Pyrite, pyrrhotite and magnetite cutting through a garnet. Biotite, some carbonates and chlorite are cutting through sulfides in the lower left quadrant.
a. Polarized reflected

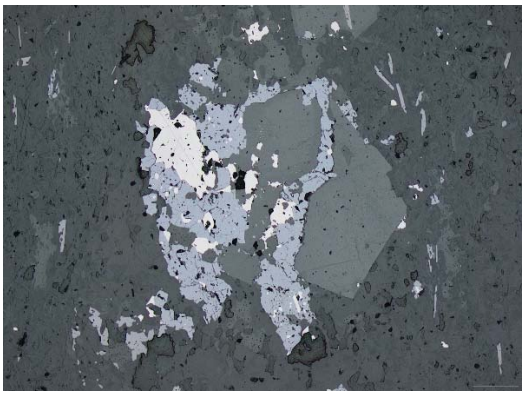

b. Polarized

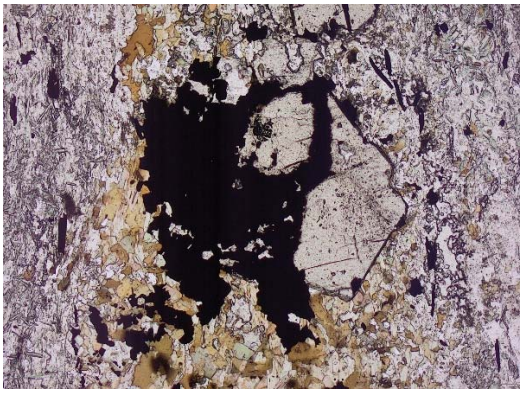

BD-13

Macro Description: Garnet-rich unit.

Minerals:
10% Garnet.
30% Biotite
5% Fine-Medium grain tourmaline
15% Amphibole (actinolite?)
20% Quartz
15% Magnetite
Traces Pyrite

General comments:
Up to a centimeter-wide garnets grown into a foliated biotite and amphibole medium. It appears that garnet crystals have been affected by the foliation and have rotated and were fracture by the event. Fine inclusions of tourmaline and quartz were observed in garnet., indicating that garnet is likely present prior to quartz and tourmaline alteration.

Pictures:
BD-13_01 (5x): 8mm wide garnet caught into deformation. Fractures in the garnet are parallel to the foliation. Earlier hornblende is partly aligned into deformation and chlorite is well crystallized and generally aligned with the foliation.

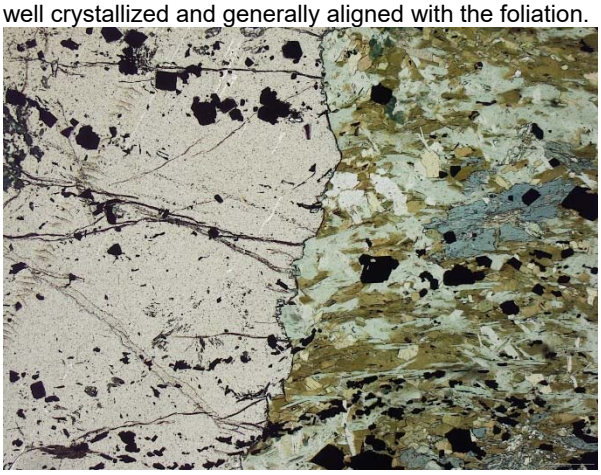

BD-13_C1_EMP1: Garnet crystal with quartz, tourmaline, pyrite and magnetite inclusions. EMP picture.

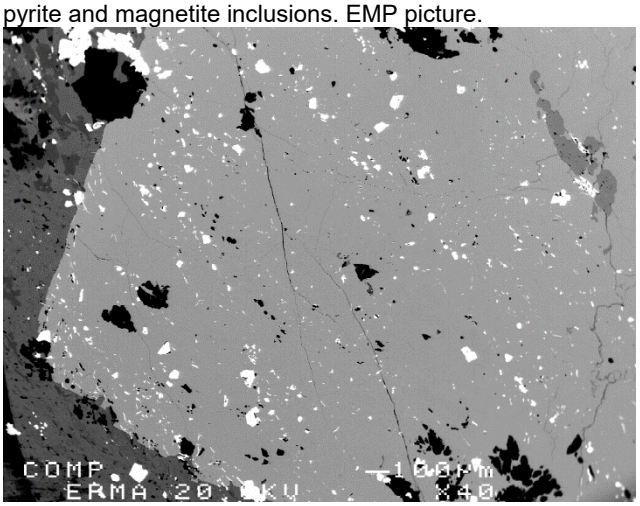

BD-14

Macro description: Chlorite-actinolite vein with garnet in it.

Minerals:
20% Chlorite
40% Tourmaline: Medium grained.
10% Garnet
15% Biotite. Mostly in the chlorite matrix but is common everywhere
2% Muscovite. In the Chlorite matrix

General comments:
Garnet looks like it was on of the early phases in the thin section. It is cut by tourmaline, oxides and seems to have been crushed by the shearing. Garnet is almost only contained in the chlorite vein, which points to this vein being at least as old as the garnet.

Paragenetic sequence:
Garnet: -
Chlorite: -
Tourmaline: --
Magnetite: --
Ilmenite: --

Pictures:
BD-14_01 (5x): 8mm wide garnet crystal in a chlorite vein and cut by a tourmaline rich event.

BD-14_02 (5x): Garnet being cut by opacious minerals along with tourmaline and by albite (blue).

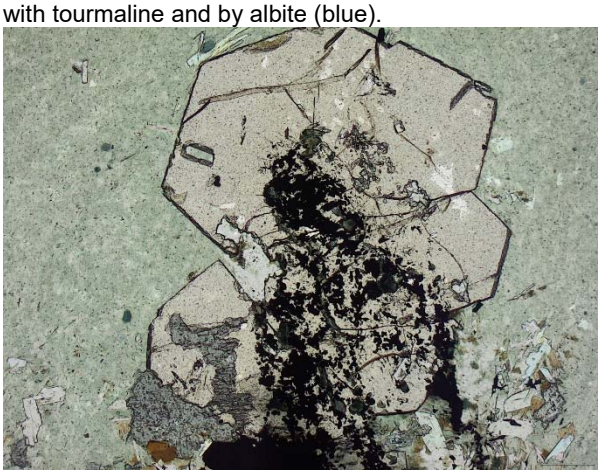

BD-15

Macro Description: Sulfide breccia with abundant sphalerite. Field sample of the main chalcopyrite vein.

Minerals:
25% Chalcopyrite. Cpy is very fracture filling and does not hold a mineral shape in any occurrence. 60% Microcrystalline tourmaline.
10% Sphalerite.
3% Fine-Medium grained tourmaline
2% Muscovite

General comments:
It seems in this thin section that coarser tourmaline could have been deposited prior to the microcrystalline tourmaline. It is grouped into blobs which seem to float in a microcrystalline tourmaline matrix. Chalcopyrite and sphalerite have a very close timing and fill fractures in the microcrystalline tourmaline matrix. The fractures also cut through the blobs of coarser tourmaline.

Pictures:
BD-15_01 (5x): Chalcopyrite breaking the microcrystalline tourmaline, splitting a rose-like patterned pod of tourmaline.

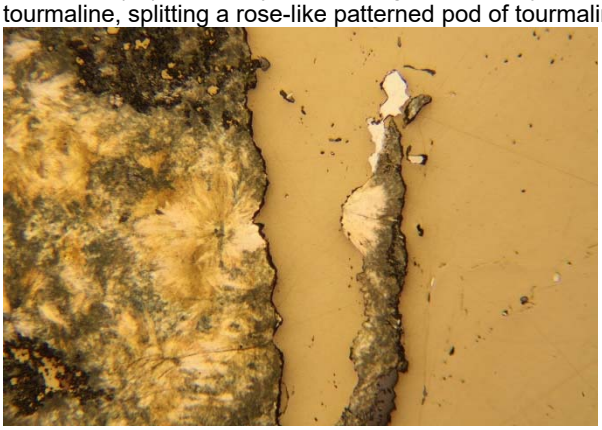

Selected microprobe circles:
BD-15_C1 (5x): Chalcopyrite and sphalerite.

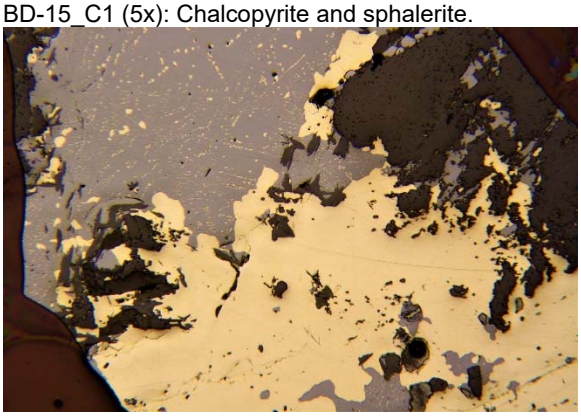

BD-15_C2 (5x): Pyrite floating in chalcopyrite.

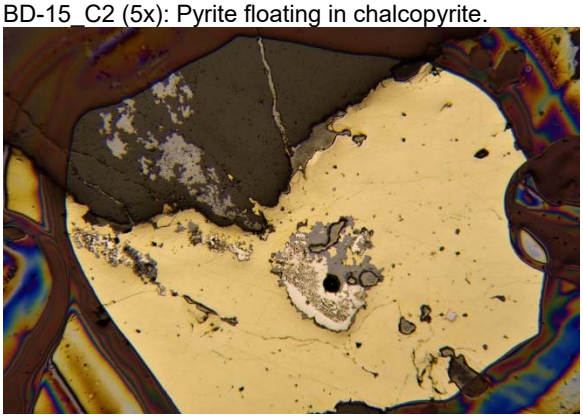

BD-15_C3 (5x): Chalcopyrite and sphalerite with chalcopyrite exsolutions.

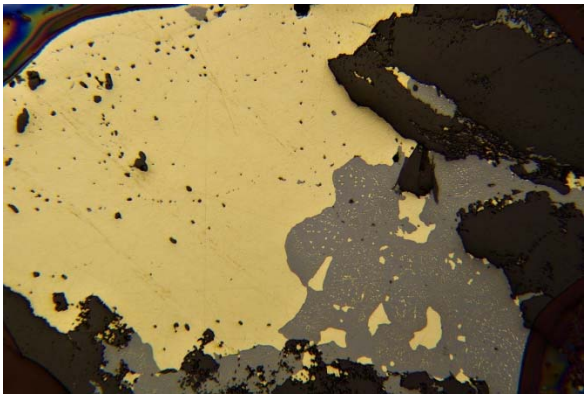

BD-15_C4 (5x): Pyrite floating in chalcopyrite.

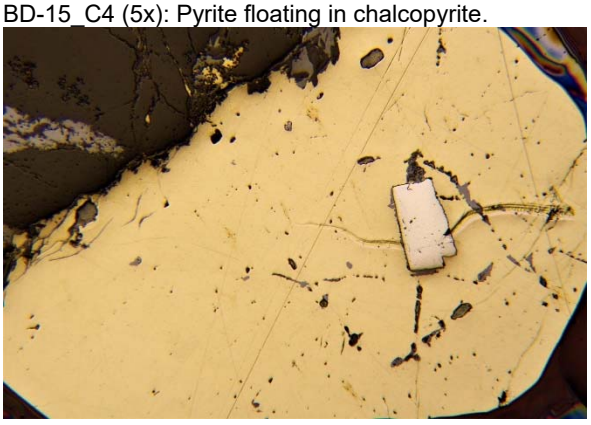

BD-16

Macro Description: Tourmaline breccia unit with angular clasts and pyrite.

Minerals:
15% Microcrystalline tourmaline.
5% Fine-medium grained tourmaline
5%Pyrite.
70% Quartz
1% Sericite

General comments:
Microcrystalline tourmaline sets a network of veins through a equigranular quartz grains. Fine to medium grained tourmaline stems from the microcrystalline tourmaline aggregates. Microcrystalline tourmaline van be seen cross-cutting through pyrite.

Paragenetic sequence:

Quartz	----
Tourmaline	---
PY	--

Pictures:
BD-16_01 (10x): Sharp boundary between very fine grained tourmaline and a quartz clast. Larger and later tourmaline crystals in a fragment enclosed in tourmaline matrix. Polarized.

BD-16_02 a) and b)(10x): Polarized transmitted and polarized reflected light pictures of a pyrite grain that is either cut by or simultaneous as a tourmaline event.

a. Polarized.

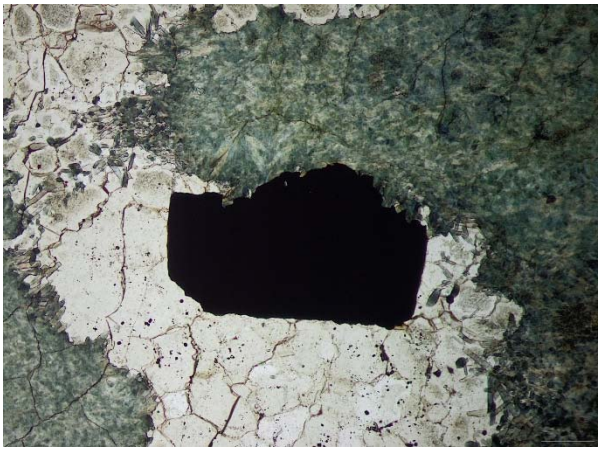

b. Reflected polarized.

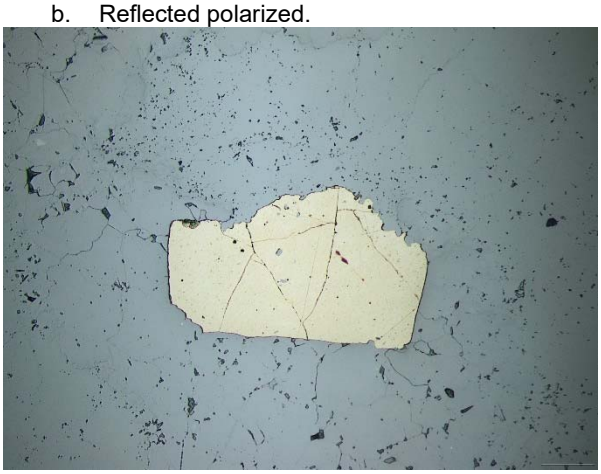

BD-17

Macro Description: Tourmaline veinlet unit presenting a vein and the surrounding tourmaline blob halo.

Minerals:
50% Quartz
15% Microcrystalline tourmaline
10% Fine-medium tourmaline
3% Sericite.
1% Chlorite

General comments:
Tourmaline blob-rich and quartz-rich bands seem to be alternating at either side of the center of the vein. Both the middle vein and the larger blobs on the sides have microcrystalline tourmaline surrounded by coarser tourmaline crystals in their tourmaline rich zones. Only the vein in the middle seems to connect while the other layers seem discontinuous.

Pictures:
BD-17_01 (5x): Calcite and chlorite vein cutting through the tourmaline veinlet.

BD-17_02 (10x): Inward growing medium grained tourmaline in a vein-like portion of the thin section.

BD-18

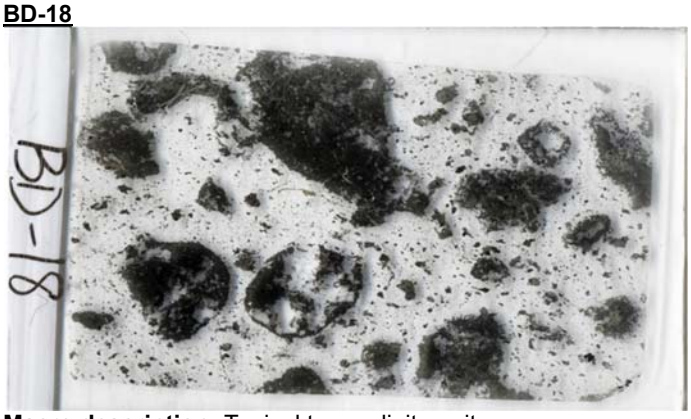

Macro description: Typical tourmalinite unit.

Minerals:
20% Microcrystalline tourmaline.
10% Fine-medium grained tourmaline
60% Quartz.
Traces Pyrite.
Traces Magnetite

General comments:
Tourmaline + quartz blobs surrounded by a very quartz-rich matrix. The tourmaline blobs sometimes show multiple onion-like textures. Most of the blob is comprised of very fine-grained tourmaline, some fine-grained tourmaline and some rare late large tourmaline crystals as pictured in BD-18_C1.

Selected microprobe circles:
BD-18_C2 (10x): Chemically zoned tourmaline analyzed under the WDS microprobe.

BD-18_C2_EM1: Large tourmaline grain showing multiple growth episodes. The brighter portions of the tourmaline crystal are Fe rich while the darker parts are Mg rich.

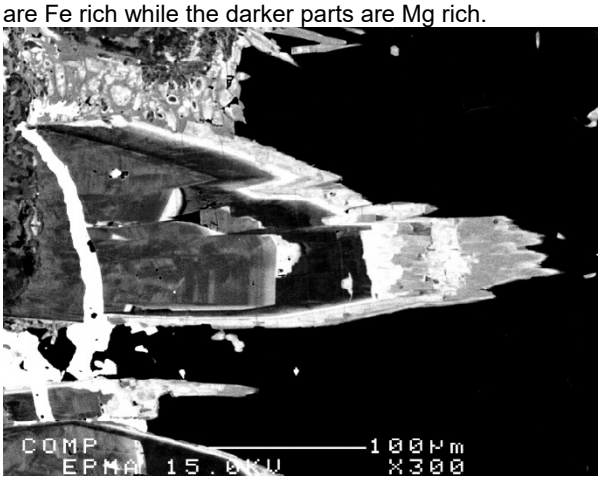

BD-19

Macro description: Sulfide breccia with important arsenopyrite.

Minerals:
40% Microcrystalline tourmaline:
5% Medium grained tourmaline:
10% Muscovite:
20% Pyrite:
10% Chalcopyrite:
2% Sphalerite:
1% Arsenopyrite:

General comments:
This thin section is comprised of a tourmaline vein that was observed on the field that is cut by a sulfide vein. This is the most gold-rich thin section of this set. Pyrite and arsenopyrite can either by floating in chalcopyrite or can be seated with the microcrystalline tourmaline matrix.

Sulfide and muscovite breccia: The sulfides brecciate through the tourmaline matrix and are accompanied by coarse muscovite.

Selected microprobe circles:
BD-19_C1 (5x): Large euhedral arsenopyrite crystal. Reflected polarized.

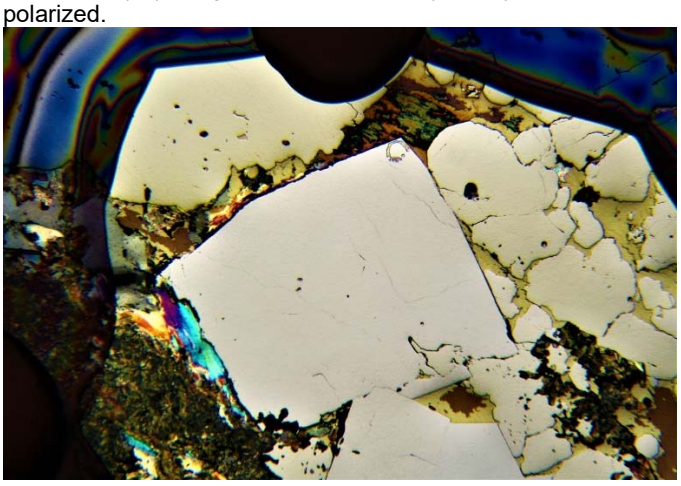

BD-19_C2 (5x): Large euhedral arsenopyrite crystal. Reflected polarized.

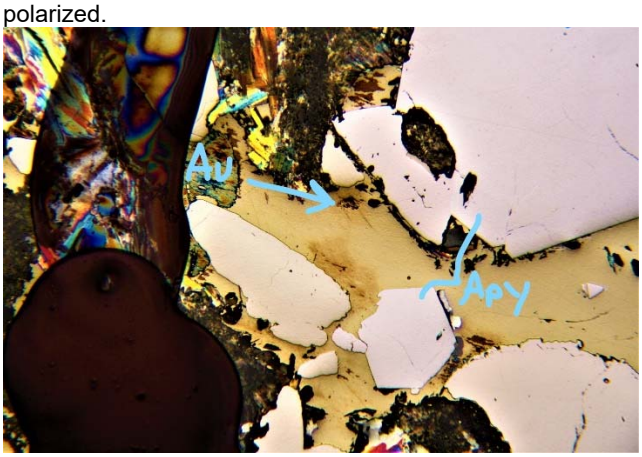

BD-19_C1_01 (40x): Electrum speck in chalcopyrite and at the contact with arsenopyrite. Reflected polarized.

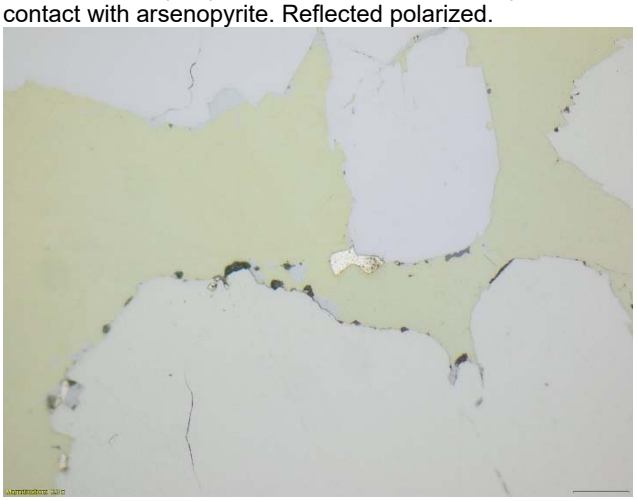

BD-19_C1_02 (40x): Matildite, hessite and electrum specks comprised in sphalerite and at the contact with arsenopyrite. Reflected polarized.

BD-19_C1_03 (40x): 100 µm electrum grain in chalcopyrite and not at the contact with other sulfides. Reflected polarized.

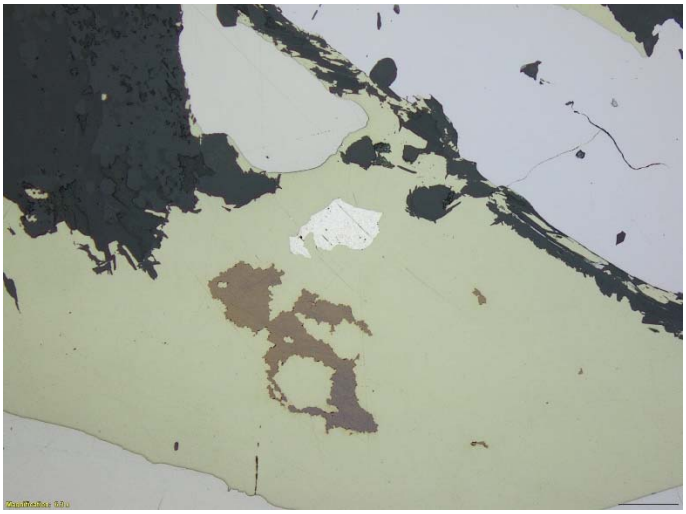

BD-19_C1_EMP1: 100 µm electrum grain in the same context as picture BD-19_C1_03. EMP picture.

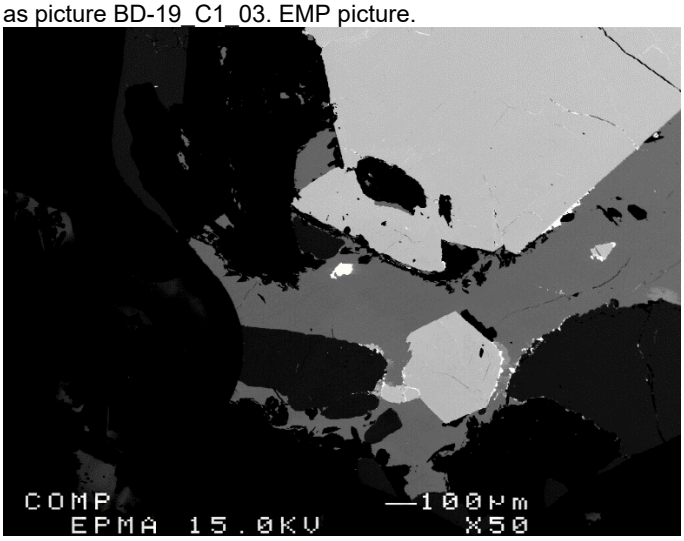

6012: From the thin section collection of “Gaboury, D. (1991) Étude Pétrographique et Géochimique des Roches Hôtes de l’Horizon Aurifère Tourmalinisé Barry-Or, Canton Barry, Québec. Thèse de mémoire de projet de fin d’études, Université du Québec à Chicoutimi”. It is unclear where in the trench this sample was taken from but the zoned tourmaline crystals could provide important information.

Minerals:
20% Muscovite: Very coarse muscovite grouped together in what must have been a vein. Muscovite also cuts through garnet along with chlorite and quartz.
15% Pyrite: Mostly euhedral pyrite generally surrounded by sphalerite.
2% Chalcopyrite: Associated with sphalerite.
5% Tourmaline:
2% Quartz: Fracture filling in garnets.
35% Garnet: Very large garnet crystal, taking up a third of the thin section. Has been cut through by muscovite, chlorite and quartz.
10% Sphalerite: Surrounding the pyrite. Came after pyrite which acted as an anchor point to growing the sphalerite.
0.5% Chlorite: Found generally in large grains in the muscovite rich areas.

General comments:
The tourmaline crystals present important growth zonations that are observable in analyzed light. The crystals can reach up to 1mm in length. Pyrite can be seen as subhedral crystals and as anhedral disseminated crystals. Rare open space-filling chalcopyrite and sphalerite are observed but do not form a network or veins cutting through other minerals.

Pictures:
6012_01 (5x): Nicely zoned tourmaline in another orientation. Analyzed.

6012_02 (5x): Euhedral and anhedral pyrite grains. Reflected polarized.